ESCUELA TÉCNICA SUPERIOR DE INGENIERÍA DE TELECOMUNICACIÓN

UNIVERSIDAD POLITÉCNICA DE CARTAGENA

Proyecto Fin de Carrera

ANÁLISIS DE LOS MODOS DE LA GUÍA COAXIAL RIDGE MEDIANTE EL MÉTODO DE RESONANCIA TRANSVERSA Y "FIELD MATCHING" PARA EL ESTUDIO DE FILTROS DE MICROONDAS

AUTOR: MªÁngeles Ruiz Bernal
DIRECTOR(ES): José Luis Gómez Tornero

Cartagena, Mayo 2006

Autor	MªÁngeles Ruiz Bernal
E-mail del Autor	mariangeles_r_b@hotmail.com
Director(es)	José Luis Gómez Tornero
E-mail del Director	josel.gomez@upct.es
Codirector(es)	
Título del PFC	**Análisis de los modos de la guía "coaxial ridge" mediante el método de resonancia transversa y "Field Matching" para el estudio de filtros de microondas.**
Descriptores	Filtros de Microondas, Filtros de Plano E, Guías de Onda, ridges, Resonadores.

Resumen

Este proyecto fin de carrera propone una nueva configuración de filtros de plano E como alternativa a la configuración estándar que permite una reducción de tamaño y una mejora de la selectividad del filtro incorporando secciones de guía de onda "coaxial-ridge" usadas como resonadores.

La guía de onda "coaxial-ridge" consiste en una guía de onda coaxial con inserciones metálicas (ridges). Al no presentar una estructura canónica, el análisis de los modos electromagnéticos que se pueden propagar en la guía "coaxial-ridge" no es analítico. En este PFC, se pretende desarrollar un método de análisis modal basado en la ecuación de resonancia transversa y el método "field matching". De esta manera, se calcula la constante de propagación, la frecuencia de corte y la distribución de campo de los modos TE y TM de orden superior de esta estructura. El análisis de los modos de la guía "coaxial-ridge" es necesario para poder estudiar de manera rigurosa las discontinuidades en esta tecnología, y por lo tanto para poder caracterizar la respuesta de la nueva configuración de filtro propuesta.

Titulación	Ingeniero de Telecomunicación
Intensificación	
Departamento	Tecnologías de la Información y la Comunicaciones
Fecha de Presentación	Mayo de 2006

ÍNDICE GENERAL

ÍNDICE PARTE I

Capítulo I

INTRODUCCIÓN

1.1. FILTROS DE PLANO E

Los filtros de plano-E con inserciones metálicas fueron originariamente propuestos como circuitos de microondas de bajo coste y producción masiva [1], [2]. La configuración estándar de un filtro de plano-E se basa en un bloque de guía de onda rectangular hueca seccionado en dos mitades entre las que se ubica una inserción inductiva, normalmente un septum metálico, en el plano E de una guía de onda rectangular, separados estos septum aproximadamente media longitud de onda. En la Figura 1-1 se presenta esta configuración estándar.
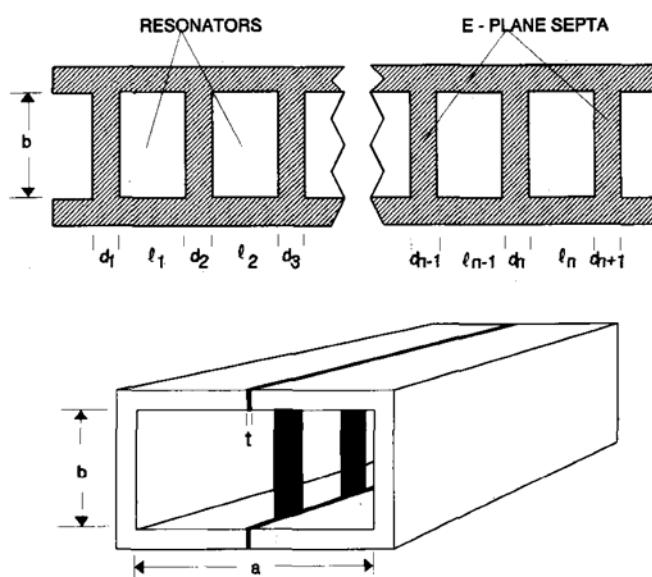

Figura 1-1: Geometría de un filtro de plano-E

Debido a la ausencia de pérdidas por dieléctrico, esta estructura tiene un elevado factor de transmisión y es adecuada para aplicaciones de banda estrecha. Además, estos filtros de plano E son muy fáciles de fabricar ya que se basan en circuitos impresos fabricados mediante procesos fotolitográficos y también presentan la ventaja de no necesidad de puesta a punto.

Sin embargo, a pesar de estas características favorables, los filtros de plano E presentan dos problemas principales: gran tamaño y una banda de rechazo inapropiada para muchas aplicaciones tales como multiplexores.

Este proyecto propone una nueva configuración de filtros de plano E como alternativa a la configuración estándar que permite una reducción de tamaño y una mejora de la selectividad del filtro. Esta mejora se consigue incorporando secciones de guía de onda ridge y coaxial ridge usadas como resonadores en un filtro de plano E como puede ser observado en la Figura 1-2. Debido a que la longitud de onda guiada así como la impedancia característica en la guía de onda ridge y coaxial ridge dependen de la altura de los ridges y de la posición del conductor interno, sin añadir complejidad en su fabricación, esta nueva configuración permite alterar las características de propagación a lo largo de la misma guía.

El argumento dado en [3] es que todas las secciones de guía serán resonantes a una frecuencia fundamental particular, pero no serán simultáneamente resonantes a frecuencias mayores. Esto se debe a que existirán diferentes longitudes de onda en cada una de las distintas secciones del filtro. Por lo tanto, los armónicos espurios de resonancia aparecerán desplazados a mayores frecuencias y la banda de rechazo del filtro será por lo general mejorada.

Es importante destacar que la sección de guía de onda coaxial ridge permite el acoplo paralelo entre sus resonadores lo que resulta en una significante reducción del tamaño total del filtro. Además del acoplo serie esta topología permite un acoplo cruzado entre los resonadores, lo que introduce ceros de transmisión a frecuencias finitas. Este cero de transmisión se debe a que cuando una onda se propaga a través de la guía, esta puede seguir distintos caminos (acoplo serie y acoplo cruzado), tal y como se muestra en la Figura 1-2. Al final de la sección de guía de onda coaxial ridge, las ondas pueden ser sumadas en fase o en oposición de fase. Por lo tanto, el cero de transmisión aparecerá cuando las ondas se resten debido a la oposición de fase. Así mismo dichos ceros de transmisión consiguen mejorar la selectividad de la respuesta del filtro.

Además es importante tener en mente que esta configuración mantiene la simplicidad de fabricación y la producción masiva de los filtros de plano E estándar.
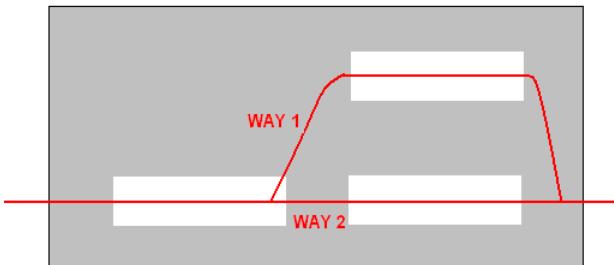
Figure 1-2: Inserción metálica de un filtro de plano E formado por una guía de onda ridge asimétrica y otra coaxial ridge

1.2. MODELADO DE FILTROS DE PLANO E

El esquema generalizado de una inserción metálica de un filtro de plano E se muestra en la Figura 1-3 (a). Este esquema puede ser descompuesto como una conexión en cascada de diferentes secciones de guías de onda tales como guía de onda rectangular, guía de onda reducida, guía de onda ridge y coaxial ridge. La sección de cada uno de los anteriores tipos de guía se muestra en la Figura 1-3 (b).

La sección de una guía de onda entre dos septum metálicos sucesivos forma un resonador y dos resonadores se acoplan a través de los acopladores constituidos por septum metálicos. Este septum metálico es básicamente una sección de guía de onda reducida. Este proyecto propone la incorporación de secciones de guía de onda ridge y coaxial ridge como resonadores en una inserción metálica de plano E, lo que conlleva a alterar las propiedades de propagación de la guía sin añadir complejidad en la fabricación del filtro.

(a)

(b)
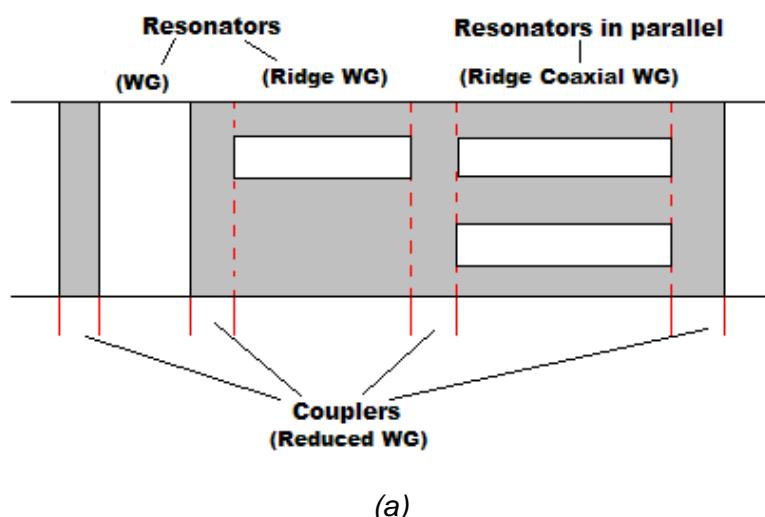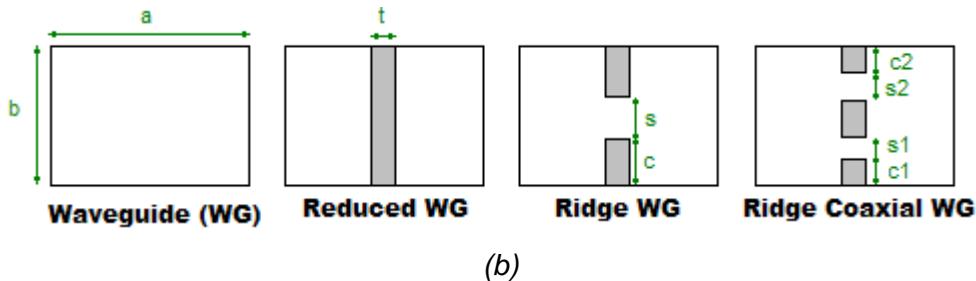
Figure 1-3: Inserción metálica indicando las posibles partes de un filtro de

plano E (a), sección transversal de las diferentes guías de onda (b)

El análisis de un filtro de plano E se basa en la resolución de dos diferentes problemas.

El primero de ellos consiste en determinar la propagación electromagnética en cada sección de guía de onda con el objetivo de obtener la frecuencia de corte y la distribución de campo de los modos de orden superior que pueden existir. Llegados a este punto, cabe destacar que para una guía de onda rectangular y para una guía de onda reducida, la distribución de campo y la frecuencia de corte de los modos es fácilmente obtenible analíticamente [4]. Sin embargo, para las guías de onda ridge y coaxial ridge, debido a que las condiciones de contorno impuestas por las secciones transversales son más complicadas, por lo tanto no se podrá obtener una solución analítica. Para determinar la propagación en estos casos se requiere una solución numérica la cual será el objetivo principal de este proyecto. La técnica de resonancia transversa combinada con el método de "field matching" serán empleados para este propósito implementándose así un método muy preciso para la obtención de la descripción de onda completa de la propagación de los modos de cada estructura en una base ortonormal.

El segundo de los problemas consiste en el uso de la solución del problema anterior para la aplicación del método "Mode Matching" incluyendo los modos de orden superior con el objetivo de obtener la modelado electromagnético de un filtro de plano-E. Para lograr esto se requiere caracterización de las discontinuidades formadas entre las distintas secciones que constituyen el filtro. La resolución de este segundo problema queda como propuesta para futuros trabajos.

Por lo tanto, el principal objetivo de este proyecto consiste en el desarrollo de un método de análisis modal basado en la ecuación de resonancia transversa y el método "field matching" para la realización de un simulador numérico de la propagación electromagnética en una guía de onda Coaxial ridge. Hasta donde es sabido, esta

estructura no ha sido analizada hasta ahora a pesar de que posee interesantes propiedades.

A partir de la guía de onda Coaxial ridge, como casos particulares, otras estructuras útiles pueden ser obtenidas, tales como guía de onda Ridge o guía de onda coaxial rectangular. El análisis de la guía de onda Ridge simétrica y de la guía de onda coaxial ha sido rigurosamente estudiado en muchos trabajos [Referencia], sin embargo la guía de onda Ridge asimétrica no ha sido profundamente investigada hasta ahora por lo que su estudio será también incluido en este proyecto.

1.3. GUÍAS DE ONDA: ESTRUCTURAS DE TRANSMISIÓN

Las guías de onda y muchas de sus variantes son extensamente usadas en sistemas de microondas. Prácticas guías de onda tienen normalmente secciones rectangulares o circulares, cuyas frecuencias de corte y ecuación de campo han sido estudiadas mediante el método de separación de variables. Recientemente, otras formas de guías de onda rectangulares han despertado interés debido a que ofrecen ventajas en términos de mayor ancho de banda, concentración de campo en regiones específicas de la guía, rotación de campo, excitación de modos individuales y acoplo cruzado.

Como ha sido comentado anteriormente, la aplicación más importante de estas estructuras es su incorporación como resonadores en el diseño de filtros de plano E para optimizar la banda de paso y reducir el tamaño total del filtro.

Además, estas estructuras pueden ser también aplicadas a las medidas EMI/EMC [5] lo que permite aprovechar el menor ruido y mayor potencia que aportan frente a otras tecnologías como microstrip. Otras aplicaciones destacables son líneas de transmisión para beam forming networks [6] compatibles con dispositivos de microondas de estado sólido [7,8], transiciones de alta calidad [3]. Además, estas líneas de transmisión tienen además muchas aplicaciones en comunicaciones por satélite, antenas y aplicaciones de modo dual tales como polarizadores o transductores ortomodo.

Muchas de estas estructuras se forman mediante la modificación guías de onda rectangulares o circulares, resultando así las guías de interés en nuestro proyecto: Ridge y Coaxial ridge, las cuales serán brevemente presentadas a continuación.

1.3.1. GUÍA DE ONDA RIDGE

La forma de la sección de una guía de onda Ridge se muestra en la Figura 1- 4 (a). Como puede observarse, consiste en un guía de onda rectangular cargada con unas

inserciones metálicas (ridges) en las paredes inferior y superior de la guía. Propuesta por primera vez en [11], la propagación en la guía de onda ridge ha sido rigurosamente estudiada en [10] y destaca por la combinación de las ventajas de menor frecuencia de corte del modo dominante, mayor ancho de banda libre de modos de orden superior y baja impedancia característica. Estas propiedades han sido aplicadas en una larga variedad de aplicaciones de microondas [14], incluyendo filtros [13], [12], transformadores [18], T-junctions [15] o incluso como líneas de transmisión mejoradas [16], [17].

En este proyecto, las características de la guía de onda Ridge asimétrica van a ser estudiadas en detalle ya que hasta ahora han recibido poco interés. Este estudio puede guiar a resultados interesantes debido a que las características de propagación de esta guía pueden ser controladas por una adecuada selección de la geometría de los ridges sin añadir mayor complejidad al proceso de fabricación. Este estudio será especialmente útil para el diseño de filtros de plano E.

(a)   *(b)*
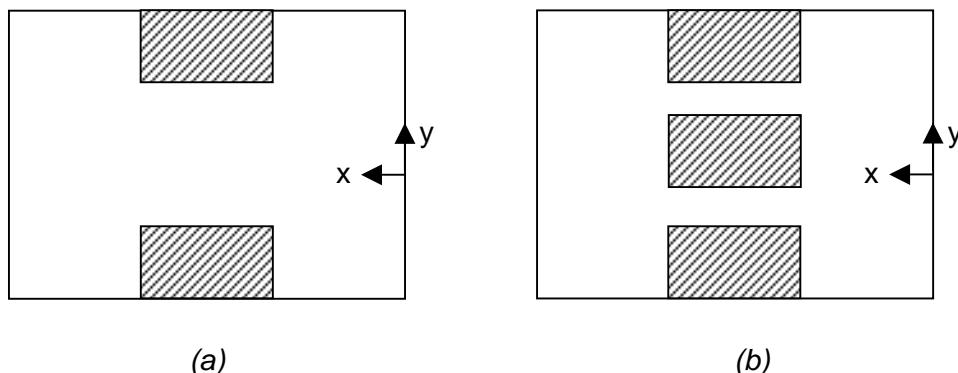
Figura 1-4: Sección transversal de guía de onda Ridge (a) y de ridge coaxial (b)

1.3.2. GUÍA DE ONDA COAXIAL RIDGE

La forma de la sección de una guía de onda coaxial Ridge es mostrada en Figura 1-4 (b). Como se puede observar, consiste en una guía de onda coaxial con ridges en las paredes inferior y superior de la guía.

Entre las diversas geometrías presentadas en las publicaciones, la guía de onda Coaxial ridge ha recibido poca atención. El modo fundamental quasi-estático TEM ha sido rigurosamente estudiado usando una formulación de ecuación integral y el método de Momentos [20]. Sin embargo la solución para los modos de orden superior

no ha aparecido todavía en ninguna publicación. En este proyecto se presentará una solución de onda completa para los modos de orden superior de esta estructura.

Como ha sido comentado anteriormente, esta guía de onda no es una estructura canónica, así que el análisis de los modos electromagnéticos no es analítico. Por lo tanto se requiere una solución numérica para resolver la propagación en esta guía usando la técnica de resonancia transversa y el método "Field Matching".

1.4. TÉCNICA DE RESONANCIA TRANSVERSA Y MÉTODO "FIELD MATCHING"

La elección de un método numérico particular para la determinación de la frecuencia de corte y la distribución de campo en una guía de onda depende de varios factores. Entre ellos se encuentra la geometría de la estructura estudiada pero también la precisión, velocidad, requerimientos de almacenamiento, versatilidad, etc.

Para el desarrollo de este proyecto los métodos elegidos como más adecuados han sido la técnica de resonancia transversa y el método "field matching".

La técnica de resonancia transversa se basa en el hecho de que para guías de onda homogéneas, la distribución de campo de cada modo en la sección transversal es independiente de la frecuencia [19]. Este hecho se deriva como resultado de la separabilidad de las coordenadas de tiempo y espacio en la ecuación de onda y es fundamental en la aproximación modal de la propagación en una guía de onda. El conocimiento de la frecuencia de corte es por tanto suficiente para determinar la constante de propagación a cualquier frecuencia (a partir de la ecuación del vector de Helmoholtz). De esta manera, la estructura relativa del campo será la misma para cada sección trasversal y cada frecuencia. Los campos son por tanto analizados a la frecuencia de corte, asumiendo ondas estacionarias a lo largo de las coordenadas transversales y no propagación a lo largo del eje longitudinal (resonancia transversa, $k_z = 0$). De modo que la dependencia longitudinal del campo puede ser despreciada y la derivada con respecto a ella puede ser tomada como cero. Por lo tanto, el problema tridimensional es reducido a uno de tan sólo dos dimensiones. Este último problema dará la distribución electromagnética de campo para los modos TE y TM en la sección transversal, la cual será validad para otras frecuencias aparte de la de corte.

El concepto de "field-matching" se basa en la división teórica de la sección transversal bajo estudio en regiones discretas. Los campos en cada región (o equivalentemente los vectores potenciales) son por tanto expresados en una base ortonormal. Estas regiones deben tener formas geométricas simples de forma que la aplicación de condiciones de contorno sea fácil. Se aplicará una relación en las

interfaces cumpliéndose que los campos tangenciales deben ser continuos en las superficies comunes. Utilizando las propiedades de ortogonalidad de las bases, esta relación se reduce a un sistema lineal con lo que se pueden obtener unas bases que describen el campo.

Capítulo II

TRABAJO DESARROLLADO

2.1. OBJETIVOS

Los propósitos y objetivos de este proyecto son el desarrollo de una rápida y precisa herramienta de simulación para la predicción de las características electromagnéticas de una guía de onda Coaxial ridge. La incorporación de dicha estructura en la inserción metálica de un filtro de plano E permite investigar las posibilidades de mejora en la banda de rechazo y la reducción de tamaño de los filtros de plano E.

Estas mejorías serán obtenidas gracias al acoplo paralelo y acoplo cruzado entre los resonadores de una sección de guía de onda coaxial ridge. Los resonadores serán acoplados en paralelo lo que dará como resultado una significante reducción del tamaño total de los filtros. Además, el acoplo cruzado entre resonadores introduce ceros de transmisión a frecuencias finitas. Este cero de transmisión y reducción de tamaño son la más atractiva mejoría perseguida por esta nueva configuración de filtros de plano E en los que se incorpora la guía de onda Coaxial ridge, como alternativa a la configuración estándar.

Como principal objetivo de este proyecto, las propiedades de la guía de onda Coaxial ridge necesitan ser estudiadas. La dependencia con la frecuencia de corte y posiblemente otras características de la geometría de la guía han de ser determinadas.

Para conseguir los objetivos y propósitos de este proyecto se llevarán a cabo las siguientes tareas:

- Usar la técnica de resonancia transversa para expresar el vector potencial en cada región de la estructura como una suma de series que respetan las condiciones de contorno impuestas.

- Aplicar el método "field matching" en las discontinuidades y plantear un problema de autovalores cuyas soluciones serán el número de onda de corte de cada modo.

- Implementación en FORTRAN y MATLAB de una rutina numérica que resuelva este problema de autovalores anterior.

- Estudio de convergencia para determinar el número de términos de expansión necesarios para obtener unos resultados precisos.

- Validación del algoritmo implementado mediante una comparativa entre los números de onda obtenidos tras la ejecución del código implementado con los proporcionados por un software comercial basado en el Método de Elementos Finitos.

- Estudios paramétricos variando las dimensiones de la estructura para demostrar la dependencia de las características de propagación de la guía con la geometría de la misma.

- Extracción de conclusiones de estos estudios paramétricos útiles para el diseño de filtros de Plano E.

2.2. MÉTODO USADO

Para la aplicación de la técnica de resonancia transversa, el método "field matching" y en un futuro el método "Mode Matching", es conveniente describir los campos eléctrico y magnético en términos de los vectores potenciales de Hertzian. Dos vectores potenciales son empleadas, uno para los modos TE y otro para los modos TM. Las expresiones que definen el campo eléctrico y magnético en términos de los vectores potenciales son:

$$E = \nabla \times A_h + \frac{1}{j\omega\varepsilon}\nabla \times \nabla \times A_e \qquad\qquad H = \nabla \times A_e - \frac{1}{j\omega\mu}\nabla \times \nabla \times A_h \qquad\qquad (2.2\text{-}1)$$

Suponiendo propagación en el eje z para las ondas electromagnéticas y solución separable para los vectores potenciales, los dos tipos de vectores potenciales magnético y eléctrico pueden ser expandidos como suma de modos:

$$A_h = \sum_{q=1}^{\infty}\sqrt{Z_{hq}}\cdot T_{hq}(x,y)\cdot\left[V_{hq}e^{-j\cdot K_{zhq}\cdot z} + B_{hq}e^{+j\cdot K_{zhq}\cdot z}\right]\hat{z} \qquad (2.2\text{-}2)$$

$$A_e = \sum_{p=1}^{\infty} \sqrt{Y_{ep}} \cdot T_{ep}(x,y) \cdot \left[V_{ep} e^{-j \cdot K_{zep} \cdot z} - B_{ep} e^{+j \cdot K_{zep} \cdot z} \right] \hat{z} \qquad (2.2\text{-}3)$$

donde Z e Y son las impedancia y admitancia de la guía para los modos TE y TM respectivamente y son dadas por las expresiones:

$$Z_{hq} = \frac{\omega\mu}{K_{hq}} = \frac{1}{Y_{hq}} \qquad Y_{ep} = \frac{\omega\mu}{K_{ep}} = \frac{1}{Z_{ep}} \qquad (2.2\text{-}4)$$

2.2.1. CONSIDERACIONES DE SIMETRÍA

Varias consideraciones de simetría derivan de la compresión física del problema y las cuales permiten reducir la complejidad matemática y computacional de la solución numérica.

En una guía de onda que presenta simetría con respecto a un plano, ambos modos TE y TM constan de una parte par y otra impar. La parte par puede ser determinada estudiando una mitad de la estructura y asumiendo una pared magnética en el plano de simetría mientras que para la parte impar se asume una pared eléctrica en el plano de simetría. Por tanto el problema completo es transformado en cuatro subproblemas más pequeños: modos TE pares, modos TE impares, modos TM pares y modos TM impares.

Puesto que nuestro estudio está centrado en la inserción de la guía de onda coaxial ridge en un filtro de plano E, sabemos que esta guía será excitada con el modo TE_{10} de una guía de onda rectangular, el cual es un modo par. Así mismo, debido a las relaciones de continuidad en las superficies de discontinuidad y a la simetría, este modo par será el único que se propague a la región transmitida puesto que es el único excitado en la región incidente. Por tanto podemos reducir el número de modos incluidos en nuestros cálculos asumiendo una pared magnética a lo largo del plano de simetría, de forma que los únicos modos que deben ser calculados son $TE_{2n+1,m}$ y $TM_{2n+1,m}$.

2.2.2. APLICACIÓN DE LA TÉCNICA DE RESONANCIA TRANSVERSA Y EL MÉTODO FIELD MATCHING.

La Figura 2-1 muestra la división teórica de la sección transversal de la guía de onda coaxial ridge en tres regiones de forma geométrica simple.

La distribución de campo de cada modo ($T(x,y)$) en cada región es independiente de la frecuencia, debido a la separabilidad de la ecuación de onda. Por

tanto, los campos serán analizados a la frecuencia de corte donde no hay propagación a lo largo del eje z, solamente propagación transversal.
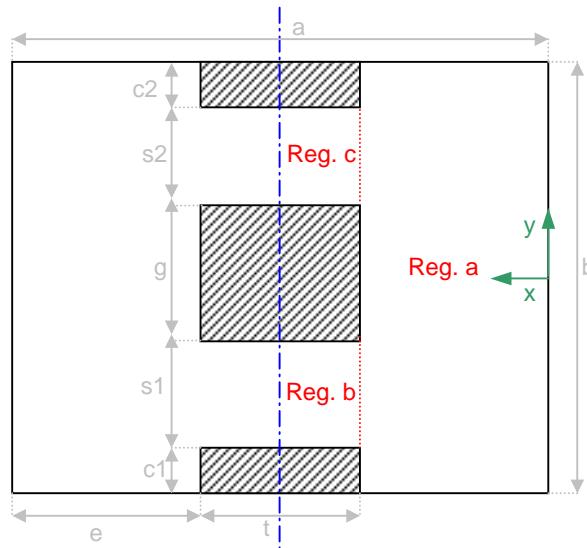

Figure 2-1: Sección transversal de una guía de onda coaxial ridge

Expresando la dependencia transversa del vector potencial magnético en cada región (Figura 2-1) como una suma de series respectando las condiciones de contorno obtenemos las siguientes distribuciones de campo para los modos TE:

Región 1
$$T_{hq}{}^1(x,y) = \sum_{m=0}^{M1} A_{qm}{}^1 \cos\left(K_{xqm}{}^1 x\right) \frac{\cos\left(\dfrac{m\pi}{b}\left(y+\dfrac{b}{2}\right)\right)}{\sqrt{1+\delta_{om}}} \qquad (2.2\text{-}5)$$

Región 2
$$T_{hq}{}^2 = \sum_{m=0}^{M2} A_{qm}{}^2 \frac{1}{K_{xqm}{}^2} \sin\left(K_{xqm}{}^2 \cdot (x-\frac{a}{2})\right) \cdot \frac{\cos\left(\dfrac{m\pi}{s1}\left(y+\dfrac{b}{2}-c1\right)\right)}{\sqrt{1+\delta_{om}}} \qquad (2.2\text{-}6)$$

Región 3
$$T_{hq}{}^3 = \sum_{m=0}^{M3} A_{qm}{}^3 \frac{1}{K_{xqm}{}^3} \sin\left(K_{xqm}{}^3 \cdot (x-\frac{a}{2})\right) \cdot \frac{\cos\left(\dfrac{m\pi}{s2}\left(y-\dfrac{b}{2}+c2+s2\right)\right)}{\sqrt{1+\delta_{om}}} \qquad (2.2\text{-}7)$$

La dependencia transversa del vector potencial eléctrico (modos TM) es determinado de forma similar a este caso magnético.

El siguiente paso consiste en la igualación de las componentes tangenciales (x e y) de los campos eléctrico y magnético en la superficie común para cada modo. De

acuerdo con lo establecido anteriormente, la propagación z de los campos ha sido eliminada. Sin embargo, puesto que la distribución de campo en la sección transversal de cada modo es la misma para las ondas que se propagan y ya que los modos se propagan con una constante k_z distintiva, esta condición tiene que ser satisfecha por cada modo individual separadamente.

Las condiciones de contorno para estas discontinuidades derivadas del campo eléctrico (A) y magnético (B) se expresan a continuación:

$$A : E_1(e) = \begin{cases} E_2(e) \Rightarrow -\left(\dfrac{b}{2} - c1\right) < y < -\left(\dfrac{b}{2} - c1 - s1\right) \\ E_3(e) \Rightarrow \left(\dfrac{b}{2} - c2 - s2\right) < y < \left(\dfrac{b}{2} - c2\right) \\ 0 \Rightarrow otro\_caso \end{cases} \qquad (2.2\text{-}8)$$

$$B : H_1(e) = \begin{cases} H_2(e) \Rightarrow -\left(\dfrac{b}{2} - c1\right) < y < -\left(\dfrac{b}{2} - c1 - s1\right) \\ H_3(e) \Rightarrow \left(\dfrac{b}{2} - c2 - s2\right) < y < \left(\dfrac{b}{2} - c2\right) \end{cases} \qquad (2.2\text{-}9)$$

Partiendo de las anteriores condiciones de contorno se llega al siguiente sistema de tres ecuaciones con tres incógnitas para el vector potencial magnético (modos TE).

$$\left[A^{q1}\right] = -\frac{2}{b} \cdot D_e^{q1} \cdot \left[\left[J_2\right]^T \cdot D_e^{q2} \cdot \left[A^{q2}\right] + \left[J_3\right]^T \cdot D_e^{q3} \cdot \left[A^{q3}\right]\right] \qquad (2.2\text{-}10)$$

$$\left[A^{q2}\right] = -\frac{2}{s1} \cdot D_h^{q2} \cdot \left[J_2\right] \cdot D_h^{q1} \cdot \left[A^{q1}\right] \qquad (2.2\text{-}11)$$

$$\left[A^{q3}\right] = -\frac{2}{s2} \cdot D_h^{q3} \cdot \left[J_3\right] \cdot D_h^{q1} \cdot \left[A^{q1}\right] \qquad (2.2\text{-}12)$$

Sustituyendo (2.2-11) y (2.2-12) en (2.2-10) se obtiene la ecuación característica para el vector potencial magnético:

$$\left[A^{q1}\right] = \frac{4}{b} \cdot D_e^{q1} \cdot \left[\frac{1}{s1} \cdot \left[J_2\right]^T \cdot D_e^{q2} \cdot D_h^{q2} \cdot \left[J_2\right] + \frac{1}{s2} \cdot \left[J_3\right]^T \cdot D_e^{q3} \cdot D_h^{q3} \cdot \left[J_3\right]\right] \cdot D_h^{q1} \cdot \left[A^{q1}\right] \qquad (2.2\text{-}13)$$

$$\underbrace{\left\{\left[D_e^{q1}\right]^{-1} - \frac{4}{b}\left[\frac{1}{s1} \cdot \left[J_2\right]^T \cdot D_e^{q2} \cdot D_h^{q2} \cdot \left[J_2\right] + \frac{1}{s2} \cdot \left[J_3\right]^T \cdot D_e^{q3} \cdot D_h^{q3} \cdot \left[J_3\right]\right] \cdot D_h^{q1}\right\}}_{BigMatrix} \cdot \left[A^{q1}\right] = 0 \qquad (2.2\text{-}14)$$

donde J_2 y J_3 son las matrices J_C de acuerdo con Bornemann para las regiones 2 y 3 respectivamente y cuyas expresiones se muestran a continuación:

$$J_2 = \int\limits_{-\left(\frac{b}{2}-c1\right)}^{-\left(\frac{b}{2}-c1-s1\right)} \cdot \frac{\cos\left(\frac{m\pi}{s1}\left(y+\frac{b}{2}-c1\right)\right)}{\sqrt{1+\delta_{om}}} \cdot \frac{\cos\left(\frac{n\pi}{b}\left(y+\frac{b}{2}\right)\right)}{\sqrt{1+\delta_{on}}} dy \tag{2.2-15}$$

$$J_3 = \int\limits_{\frac{b}{2}-c2-s2}^{\frac{b}{2}-c2} \frac{\cos\left(\frac{m\pi}{s2}\left(y-\frac{b}{2}+c2+s2\right)\right)}{\sqrt{1+\delta_{om}}} \cdot \frac{\cos\left(\frac{n\pi}{b}\left(y+\frac{b}{2}\right)\right)}{\sqrt{1+\delta_{on}}} dy \tag{2.2-16}$$

Respecto a las matrices D son matrices cuyas diagonales tienen el valor que se muestra a continuación:

$$D_e^{q1} = diag\left(\frac{1}{K_{xhn}^{q1}\sin(K_{xhn}^{q1}\cdot e)}\right) \tag{2.2-18}$$

$$D_h^{q1} = diag\left(\cos(K_{xhm}^{q1}\cdot e)\right) \tag{2.2-19}$$

$$D_e^{q2} = diag\left(\cos(K_{xhn}^{q2}\frac{t}{2})\right) \tag{2.2-20}$$

$$D_h^{q2} = diag\left(\frac{K_{xhn}^{q2}}{\sin(K_{xhn}^{q2}\cdot\frac{t}{2})}\right) \tag{2.2-21}$$

$$D_e^{q3} = diag\left(\cos(K_{xhn}^{q3}\frac{t}{2})\right) \tag{2.2-22}$$

$$D_h^{q3} = diag\left(\frac{K_{xhn}^{q3}}{\sin(K_{xhn}^{q3}\cdot\frac{t}{2})}\right) \tag{2.2-23}$$

La ecuación (2.2-14) es un sistema homogéneo lineal indeterminado. Las soluciones no triviales para este sistema existen cuando el determinante de la expresión entre corchetes es cero. Variando la frecuencia, el determinante característico puede ser resuelto para sus autovalores K_c. Para ello una rutina numérica será programada en FORTRAN como será comentado a continuación. Una vez encontrados los números de onda de corte, K_c, los coeficientes A^{q1}, que son los autovectores del problema, pueden ser determinados. Usando entonces las ecuaciones (2.2-11) y (2.2-12) podemos determinar los coeficientes A^{q2} y A^{q3} respectivamente. Con estos resultados podemos obtener una descripción de la distribución de campo correspondiente a cada modo.

Un proceso similar es seguido para el vector potencial eléctrico que guía a una solución de los modos TM.

2.2.3. NORMALIZACIÓN EN POTENCIA

A fin de usar los resultados obtenidos anteriormente para aplicar el método de "Mode Matching" en las discontinuidades, los coeficientes de amplitud A^{q1}, A^{q2}, A^{q3} deben ser normalizados. Con esta normalización, la potencia transferida por cada modo de amplitud la unidad a ambos lados de la discontinuidad será independiente de la forma y el área de la sección transversal, e igual a una constante. Asumimos que la amplitud de potencia de cada modo es igual a la unidad. Atendiendo a las ecuaciones (2.2-3) y (2.2-4), la potencia transferida por un modo con F=1 y B=0 tiene que ser igual a 1W. Esto asegura que los parámetros S de la matriz de dispersión estén entre 0 y 1. La condición de normalización de potencia para el modo TE i-ésimo es:

$$\iint_s \left(\nabla \cdot T_h^i\right)^2 ds = 1 \qquad (2.2\text{-}24)$$

la cual permite calcular un coeficiente de normalización con el que se escalarán los coeficientes de amplitudes hallados anteriormente.

2.3. IMPLEMENTACIÓN DE LA GUÍA DE ONDA RIDGE COAXIAL EN FORTRAN Y MATLAB

A fin de determinar los valores que hacen cero el determinante descrito en (2.2-14) una rutina numérica ha sido implementada haciendo uso de FORTRAN. Combinando este algoritmo con MATLAB se ha implementado una interfaz gráfica de usuario (GUI) la cual permite al usuario la introducción de datos, la dirección de instrucciones y la visualización de los resultados computacionales.
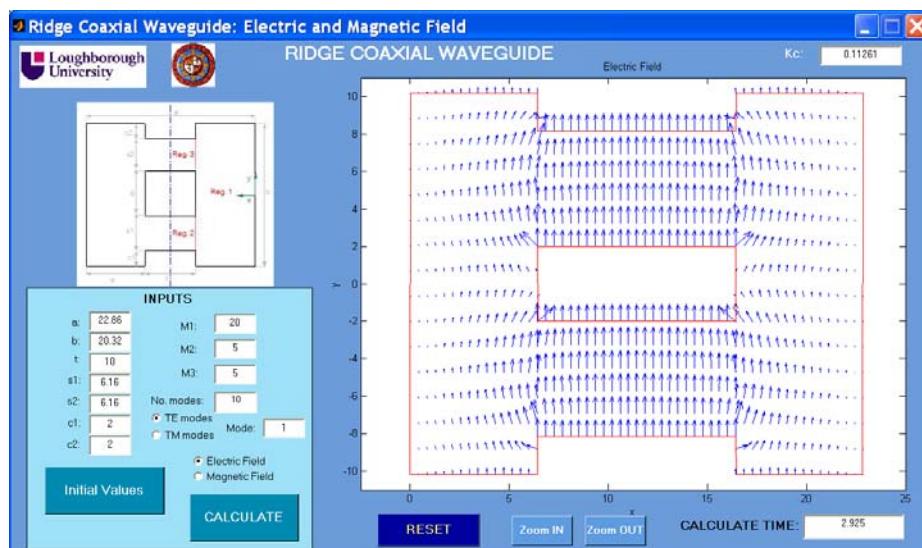

Figura 2-2: Interfaz gráfica de usuario (GUI)

17

Esta interfaz, mostrada en la Figura 2-2, provee una herramienta de simulación muy fácil de usar debido a que es muy visual e intuitiva además de muy rápida. Se ha realizado una comparativa de tiempos entre la herramienta implementada y un software comercial basado en el método de Elementos Finitos (Ansoft HFSS), demostrándose una reducción considerable de tiempo de ejecución de más de sesenta veces inferior.

2.4. ANÁLISIS DE CONVERGENCIA Y VALIDACIÓN

El estudio de convergencia del número de onda de corte, k_c, con respecto a un número creciente de términos de expansión ha sido realizado en este proyecto. Los resultados obtenidos de este análisis son imprescindibles para determinar el número de términos de expansión requerido en cada región a fin de obtener unos resultados precisos, sin sobrecargar la simulación con términos que contribuyan a una extensión innecesaria. Evitar la redundancia es particularmente esencial en los procesos de optimización, donde el coste computacional de cada simulación es crucial para la eficiencia.

Como conclusión extraída de este análisis de convergencia podemos destacar que el número de términos de expansión depende de la región que va a ser descrita. Para regiones más estrechas, un menor número de términos de expansión es requerido debido a que, como es razonable pensar, un área más pequeña necesita menos términos de expansión para ser descrita.

Tras el análisis de convergencia debemos validar la precisión del código implementado y del número de términos de expansión seleccionado. Para llevar a cabo esta validación se ha comparado la frecuencia de corte proporcionada por FORTRAN con la determinada por el software comercial HFSS.

La Tabla 2-1 presenta una comparación entre los dos métodos para los cuatro primeros modos de una guía de onda Coaxial ridge asimétrica. En este caso, 20 términos de expansión han sido utilizados para la dependencia transversa del vector potencial en la región 1, mientras que 3 y 5 términos de expansión han sido utilizados en la región 2 y 3 respectivamente. Como se puede observar el error relativo entre los dos métodos es menor que $8.19 \cdot 10^{-4}$. La buena concordancia encontrada entre el código desarrollado y el software comercial valida la precisión del primero.

TE			TM		
GTR	FEM	Relative Error	GTR	FEM	Relative Error
0.1115929	0.1115029	8.07E-04	0.3509337	0.3507440	5.41E-04
0.1870706	0.1871900	6.38E-04	0.4888783	0.4886350	4.98E-04
0.3253941	0.3254495	1.70E-04	0.5435874	0.5436235	6.64E-05
0.4216279	0.4217941	3.94E-04	0.6246037	0.6240923	8.19E-04

Table 2-1: Comparación entre las cuatro primeras longitudes de onda de corte (rad/mm) obtenidas con GTR y con software comercial FEM

Dimensiones (en mm): a=22.86, b=20.32, c1=c2=2, s1=3.16, s2=9.16, t=10

Las distribuciones de campo de cada modo también han sido comparadas con el mismo software comercial y han sido validadas gracias a la buena analogía encontrada entre ellas. A continuación se muestra esta distribución de campo para los cuatro primeros modos TE cuyos números de onda de corte han sido mostrados en la Tabla anterior.


MODE 1 (Kc= 0.1115929)   MODE 2 (Kc= 0.1870706)

MODE 3 (Kc= 0.3253941)   MODE 4 (Kc= 0.4216279)
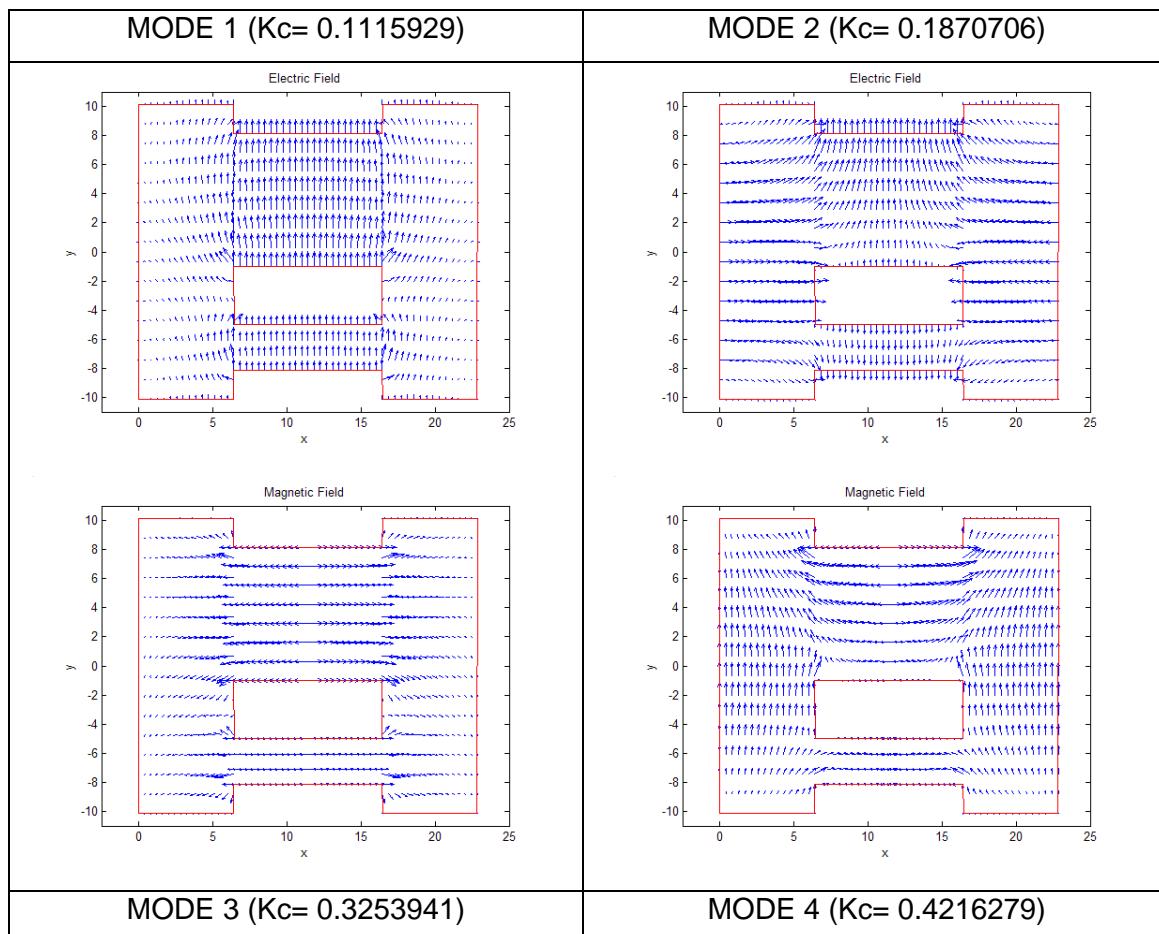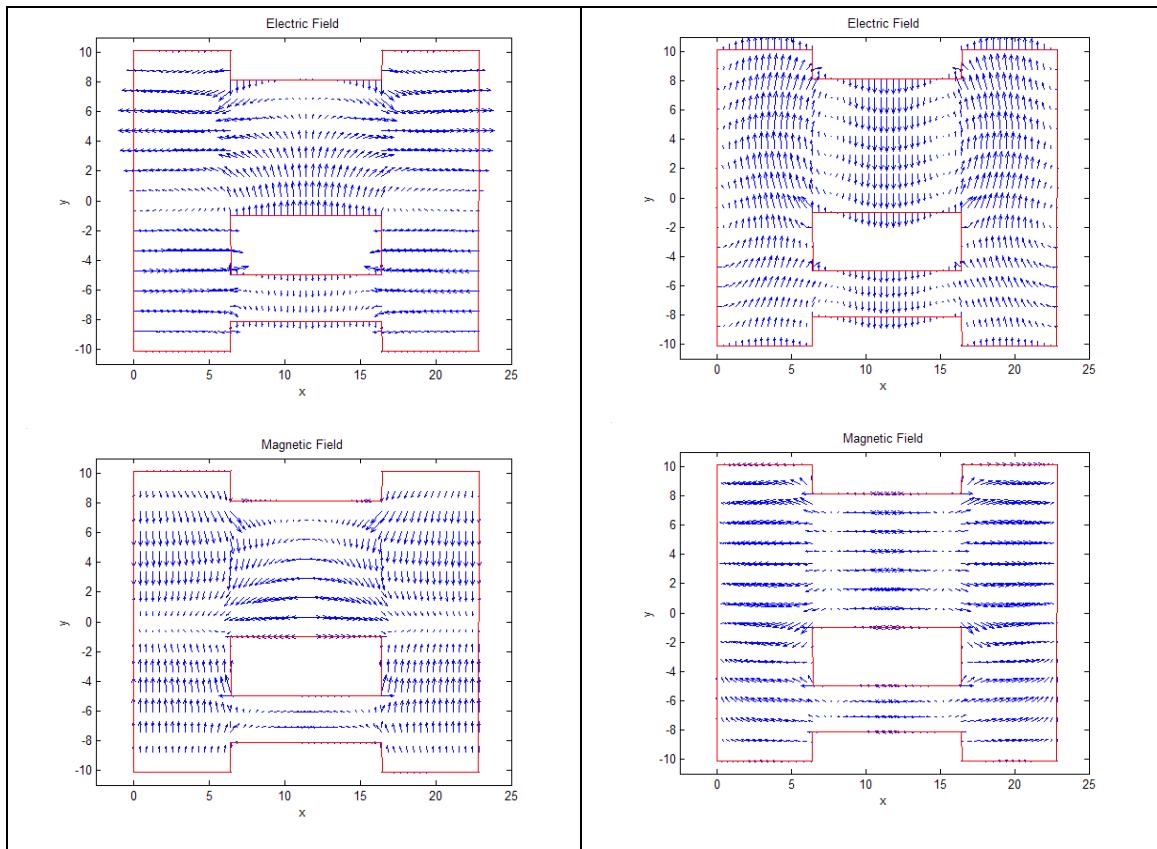
Figura 2-3: Distribución de campo eléctrica y magnética para los cuatro primeros modos TE

2.5. ESTUDIO PARAMÉTRICO

Diversos estudios paramétricos de la variación de las dimensiones de la guía de onda han sido realizados a fin de demostrar la dependencia de la frecuencia de corte con la geometría de la estructura.

Los resultados obtenidos más interesantes serán mostrados a continuación a fin de conocer cómo la variación de cada parámetro afecta a la propagación de los modos en la guía. Estos resultados serán especialmente interesantes en el diseño de filtros de plano E para determinar qué dimensiones son más influyentes a fin de obtener la respuesta requerida del filtro que incorpore secciones de guía de onda ridge y coaxial ridge.

Los parámetros tenidos en cuenta a la hora de realizar estos estudios paramétricos han sido T, S1, S2, C1 y C2 que permiten variar el ancho, el alto y la posición de los GAPs y del conductor interno.

2.5.1. VARIACIÓN DE K_C VS. LA ANCHURA DEL CONDUCTOR INTERNO

La Figura 2-4 muestra el número de onda de corte cuando la altura del conductor interno y de los ridges se mantiene fija y se varía la anchura T. Se observa una pequeña variación tanto para los modos TE y TM para valores inferiores a 1mm. Cuando el valor de T aumenta por encima de 1 mm, el valor de K_c aumenta ligeramente, siendo este incremento más pronunciado para los modos TM como puede ser observado a continuación.


(a)

(b)
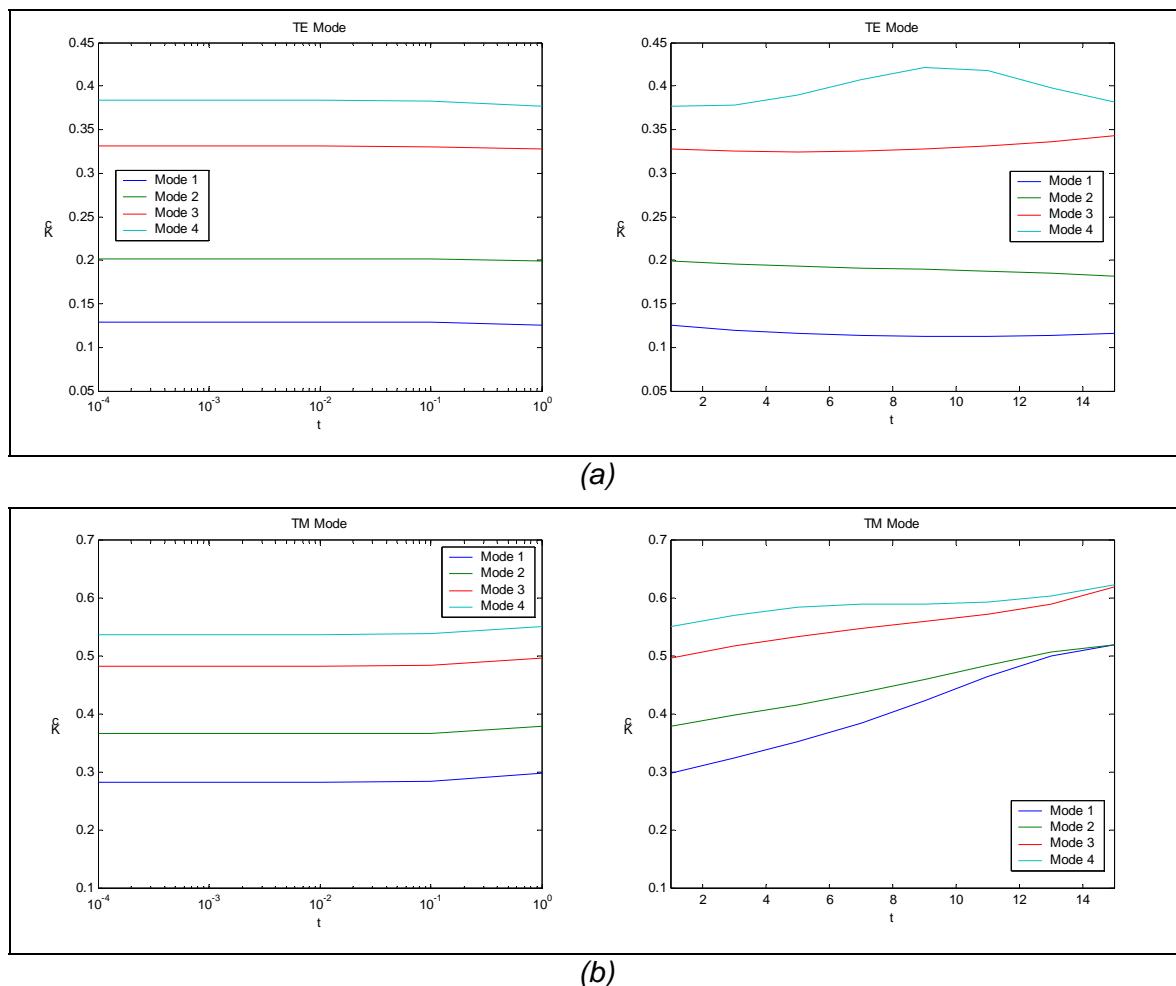
Figure 2-4: K_c vs. para los cuatro primeros modos TE (a) y TM (b)

Dimensiones (en mm): a=22.86, b=20.32, c1=c2=2, s1=s2=6.16, t=10

2.5.2. VARIACION DE K_c VS. POSICION DEL CONDUCTOR INTERNO (VARIANDO S1 AND S2)

La Figura 2-5 muestra el número de onda de corte para una altura del conductor interno fija, g, cuando este es desplazado arriba y abajo sobre el eje y. Para los modos TE se observa una pequeña variación, debido a que la capacidad equivalente total permanece aproximadamente constante. La variación de los modos TM es más pronunciada, presentando un máximo para el primer y tercer modo cuando el conductor interno está justo en el centro de la estructura y un mínimo para los modos segundo y cuarto en la misma posición. Esta variación depende de la distribución de campo de cada modo.


(a)   *(b)*
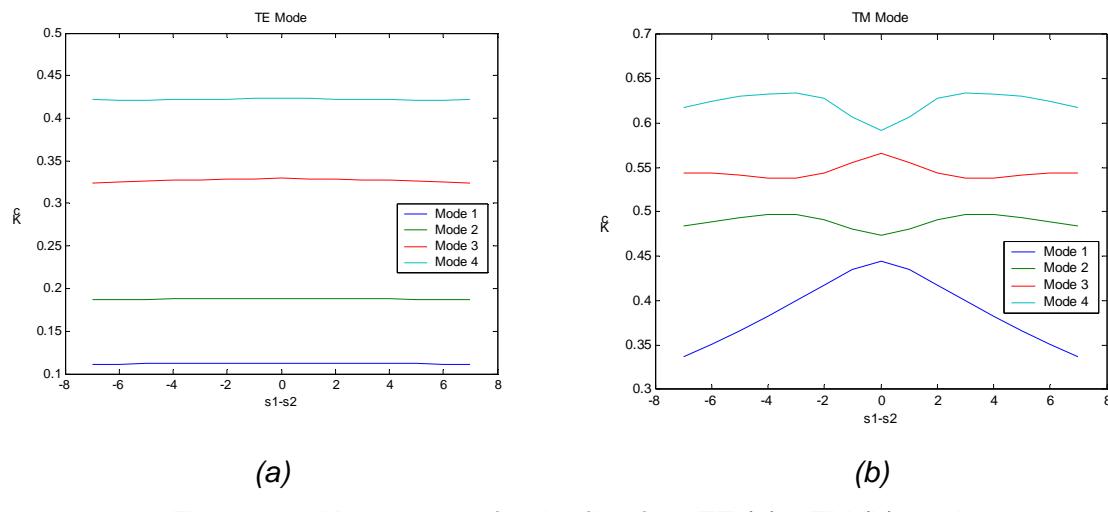
Figura 2-5: K_c vs. s1-s2 for the first four TE (a) y TM (b) modes
Dimensiones (en mm): a=22.86, b=20.32, c1=c2=2, s1+s2=12.32, t=10, g=4

2.5.3. VARIATION KC VS. ALTURA DEL GAP INFERIOR (S1) (CENTRAL CONDUCTOR INCREASING IN HEIGHT)

La Figura 2-6 muestra la variación del número de onda para un GAP superior fijo (S2) cuando el GAP inferior (S1) se modifica debido a la variación de la altura del conductor interno (g). Como se puede observar, cuando se incrementa la altura del GAP inferior el valor de K_c se ve también incrementado. Un comportamiento opuesto se produce para los modos TM pero en este caso la variación es más pronunciada. Estas variaciones se deben a la mayor concentración de campo debajo de los ridges lo que se traduce en un aumento efectivo de la dimensión "a" de la guía.

<div align="center">(a)   (b)</div>
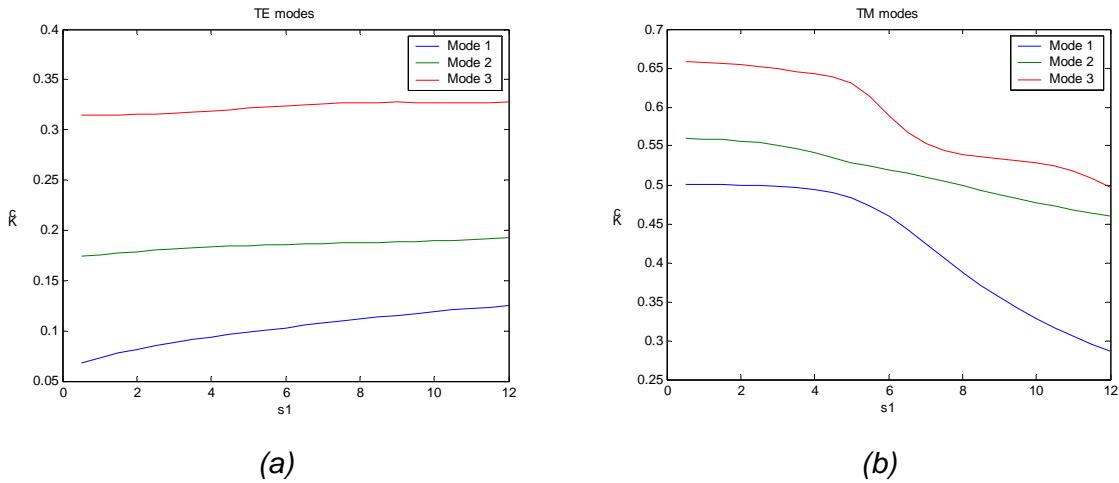
Figura 2-6: K_c vs. s1 para los cuatro primeros modos TE (a) y TM (b)

Dimensiones (en mm): a=22.86, b=20.32, c1=c2=2, s1+g=12.16, s2=4.16, t=10

2.5.4. VARIACIÓN DE K_C VS. LA ALTURA DE LA INSERCIÓN METÁLICA INFERIOR (C1)

La Figura 2-7 presenta la variación del número de onda cuando se varía la altura del ridge inferior (C1) manteniéndose fijos los valores del ridge superior (C2) y del conductor interno (g). Cabe destacar que, tanto para los modos TE como para los TM, el comportamiento observado es prácticamente el mismo que en el apartado anterior debido a que en ambos estudios paramétricos es la altura del GAP inferior la que se está modificando.


<div align="center">(a)   (b)</div>
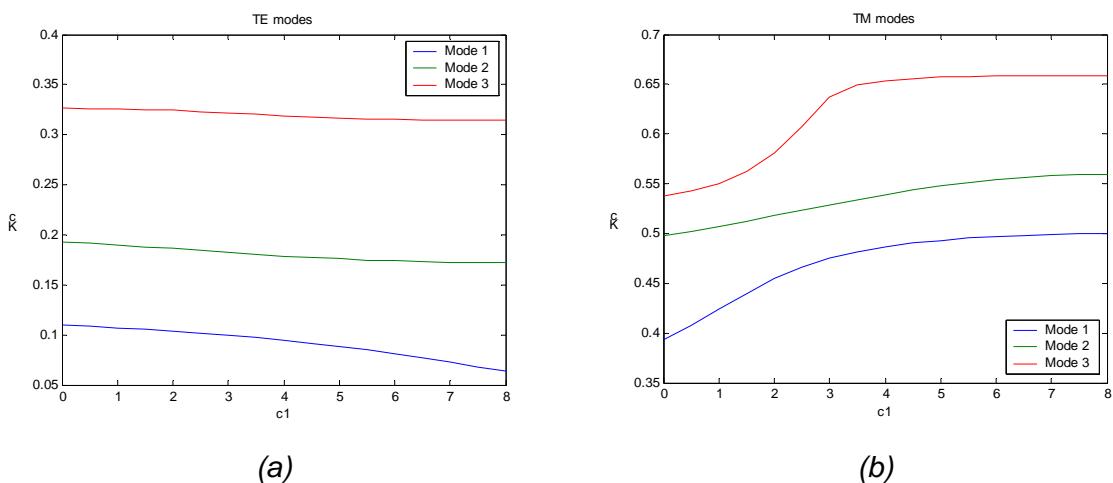
Figura 2-7: K_c vs. c1 para los cuatro primeros modos TE (a) y TM (b)

Dimensiones (en mm): a=22.86, b=20.32, s1+c1=8.16, c2=2, s2=4.16, g=6 t=10

<div align="center">23</div>

Capítulo III

CONCLUSIONES Y LÍNEAS FUTURAS

Esta sección resume el trabajo presentado en este proyecto en relación con los objetivos fijados. Además, se señalarán las contribuciones hechas en este proyecto y se propondrán ideas para futuros trabajos.

3.1. PROGRESO DEL TRABAJO

Como fué señalado en la introducción, el primer objetivo de este proyecto ha sido el desarrollo de una rápida y precisa herramienta de simulación de la guía de onda coaxial ridge. Esta herramienta es necesaria para incorporar la guía de onda coaxial ridge en la inserción metálica de un filtro de plano E a fin de investigar las posibles mejoras de banda de rechazo y de reducción de tamaño del filtro. Además, esta nueva configuración de filtros de plano E permite la aparición de un cero de transmisión a frecuencias finitas. Es importante destacar que esta configuración mantiene la simplicidad de fabricación y la producción masiva del filtro de plano E estándar.

Siguiendo una revisión de publicaciones, la técnica de resonancia transversa y el método "Field Matching" fueron elegidos como más apropiados. Varias formulaciones del problema fueron consideradas [20], [21] y finalmente, se decidió seguir [21] como rutina óptima. Expresando la dependencia transversa del vector potencial en cada región de la estructura como una suma de series respetando unas condiciones de contorno y aplicando el método "Field Matching" en las discontinuidades se formó un problema de autovalores cuyas soluciones son las desconocidas longitudes de onda de corte.

A fin de obtener la solución a este problema de autovalores se implementó una rutina numérica haciendo uso de FORTRAN y MATLAB. El programa desarrollado fue

minuciosamente comparado con resultados publicados y otros softwares disponibles y su validación fue confirmada.

Se llevó a cabo una comparativa de tiempos entre el código implementado y un software comercial basado en el método de Elementos finitos, obteniéndose una considerable reducción de tiempo.

Por último, se realizaron numerosos estudios paramétricos de la variación de las dimensiones de la guía de onda para demostrar la dependencia del número de onda de corte con la geometría de la estructura. De estos estudios paramétricos se extrajeron interesantes conclusiones las cuales fueron enfocadas a establecer qué parámetros son más influyentes en la obtención de una respuesta determinada de un filtro de plano E que incorpore secciones de guía de onda ridge o coaxial ridge. Estas conclusiones se resumen en la siguiente sección.

3.2. CONCLUSIONES DE LOS ESTUDIOS PARAMÉTRICOS ÚTILES PARA EL DISEÑOS DE FILTROS DE PLANO E.

En este apartado se pretenden resumir las conclusiones extraídas de los estudios paramétricos realizados en el proyecto a fin de conocer qué parámetros son más influyentes a la hora de obtener la respuesta requerida de un filtro de plano E que incorpore secciones de ridge o coaxial ridge. Sin embargo nos centraremos exclusivamente en aquellas conclusiones que conciernen al primer modo TE debido a que será el único que se propague por la guía ya que los demás modos están al corte.

No obstante, es importante destacar que para el futuro modelado de las discontinuidades utilizando el método Mode Matching todos los modos de orden superior son necesarios a pesar de que sólo el primer modo de cada sección de guía será transmitido a través de ella.

Las conclusiones a tener en cuenta para futuros trabajos que incluyan guías de onda coaxial ridge son:

- Con respecto a la anchura de los GAPs y del conductor interno (parámetro T) cabe destacar que la variación de K_c para el primer modo TE es muy pequeña en todo el rango de posibles valores de T. Por lo tanto, podemos concluir que el valor de T no es un parámetro crítico para el diseño de filtros de plano E. Valores de T típicamente usados en los filtros de plano E son valores muy pequeños alrededor de 0.1mm.

- En relación a la altura de los GAPs (parámetros S1 y S2) el número de onda de corte, K_c, del primer modo TE aumenta cuando se incrementa dicha altura. La variación de K_c en este caso es más pronunciada que en el estudio paramétrico

anterior, por lo tanto, estos parámetros han de ser considerados para el diseño de filtros de plano E. En dichos filtros estos parámetros se corresponde con la altura de los resonadores.

- Con respecto a la altura del conductor interno (g) cabe destacar que al variar dicho parámetro también se está variando la altura de los GAPs, y por tanto las conclusiones extraídas en el estudio paramétrico anterior son aplicables a este caso también.

- En lo que se refiere a la posición del conductor central, la variación de K_c del primer modo TE es despreciable, concluyéndose por tanto que éste tampoco es un parámetro crítico para el diseño de filtros de plano E.

3.3. SUGERENCIAS PARA FUTUROS TRABAJOS

Como sugerencia para futuros trabajos se plantea la investigación de las ventajas que pueden proporcionar las nuevas configuraciones de filtros de plano E que incorporen guías de onda coaxial ridge y ridge asimétrica. Para ello es necesaria una rápida y precisa herramienta de simulación para los filtros de plano E. A fin de lograr esto, será necesaria la formulación y la programación del método "Mode Matching". Las soluciones de las discontinuidades ridge asimétrico-guía rectangular y coaxial ridge-ridge han de ser combinadas con la propagación a lo largo de secciones de guía de longitud finita a fin de obtener un simulador de estructuras 3D para filtros de plano E.

Una vez que se disponga de la herramienta de simulación anterior se podrá demostrar la mejora incorporada por la novedosa configuración planteada en este proyecto.

Además, un proceso de diseño para este tipo de filtros sería también muy interesante. Junto con la herramienta de simulación, ésta completaría un paquete software CAD. Por tanto, queda propuesto para futuros trabajos el desarrollo de una herramienta CAD para filtros de plano E.

REFERENCIAS

[1] Y. Konoshi and K. Uenakada, "The design of a bandpass filter with inductive strip-planar circuit mounted in waveguide," IEEE Trans. Microwave Theory Tech,, vol. MTT-22, pp. 869-873, Oct. 1974.

[2] Y. Tajima and Y. Sawayama, "Design and anafysis of a waveguidesandwich microwave filter," IEEE Trans. Microwave Theoiy Tech., vol. M'M-22, pp. 839–841, Sept. 1974.

[3] R. Levy, "*New coaxial -to-stripline transformers using rectangular lines*," IRE TRANS. ON MICROWAVE THEORY AND TECHNIQUES, vol. MTT-9, pp. 273–274; May, 1961.

[4] Collin R, *Theory of Guided Waves*, IEEE Press

[5] L. Gruner, "*Characteristics of Crossed Rectangular Coaxial Structures*", IEEE Trans. Microwave Theory and Techniques, pp. 622-627, Vol. 28, No. 6, June 1980

[6] F. Alessandri, M. Mongriardo and R. Sorrentino, "*Computer-Aided Design of Beam Forming Networks for Modern Satellite Antennas*" IEEE Trans. Microwave Theory and Techniques, pp. 1117-1127, Vol 40, No. 6, June 1992

[7] O.R. Cruzan and R.V Garner, "*Characteristic Impedance of Rectangular Coaxial Transmission Lines*," IEEE Transactions on Microwave Theory and Techniques, pp. 488-495, September 1964

[8] F. J. Sansalo:! and E. G. Spencer, *"Low temperature microwave power hmter*," IRE TRANS. ON MICROWAVE THEORY AND TECHNIQUES, vol. MTT-9, pp. 272–273; May, 1961.

[9] R. V. Garver and J. A. Rosado, "*Broad-band TEM diode limiting*," IRE TRANS. ON MICROWAVE THEORY AND TECHNIQUES, vol. MTT-10, pp. 302–310; September, 1962.

[10] George Goussetis, "Waveguide bandpass with improved performance", Ph.D. 2002.

[11] Cohn S, "Properties of Ridge Wave Guide", Proc IRE, Vol 35, August 1947, pp.783-788

[12] Wang C., Zaki K. and Mansour R., "*Modelling of Generalised Double Ridge Waveguide T-Junctions*", IEEE MTT-S International Microwave Symposium Digest, pp. 1185-1188, 1996

[13] Bornemann J., and Arndt F., "Rigorous Design of Evanscent Mode E-plane Finned Waveguide Bandpass Filters", IEEE MTT-S International Microwave Symposium Digest, pp. 603-606, 1989

[14] Helszajn J., *Ridge Waveguide and Passive Microwave Components*, IEE Electromagnetic Waves Series 49, 2001

[15] Wang C., Zaki K. and Mansour R., "Modelling of Generalised Double Ridge Waveguide T-Junctions", IEEE MTT-S International Microwave Symposium Digest, pp. 1185-1188, 1996

[16] Pozar D., *Microwave Engineering*, John Willey&Sons, New York, 1998

[17] Collin R., *Foundations of Microwave Engineering*, 2nd ed., New York: IEEE Press, 2001

[18] Bornemann J. and Arndt F., "*Modal S-Matrix Design of Optimum Stepped Ridged and Finned Waveguide Transformers*", IEEE Transactions on Microwave Theory and Techniques, vol. MTT-35, no. 6, pp. 561-567, June 1987

[19] M. L. Crawford, "Generation of standard EM fields using TEM transmission cells," IEEE Trans. Electromagn. Compat., vol. EMC-16, pp. 189–195, Nov. 1974.

[20] Montgomery J., "On the complete eigenvalue solution of ridged waveguide", IEEE Trans. Microwave Theory and Techniques, MTT-19, 457-555 (1971)

[11] J. Bornemann, "Comparison between different formulations of the Transverse Resonance Field-Matching Technique for the three-dimensional analysis of metal-finned waveguide resonators", International Journal of Numerical Networks, Devices and Fields, Vol. 4, 63-73 (1991)

ESCUELA TÉCNICA SUPERIOR DE INGENIERÍA DE TELECOMUNICACIÓN

UNIVERSIDAD POLITÉCNICA DE CARTAGENA

Proyecto Fin de Carrera

PARTE II

Modal analysis of Ridge Coaxial waveguide using the transverse resonance method and field matching to study microwave filters

AUTOR: MªÁngeles Ruiz Bernal
DIRECTOR(ES): José Luis Gómez Tornero

Cartagena, Mayo 2006

CONTENTS

Chapter I

INTRODUCTION

1.1. E-PLANE FILTERS

Waveguide E-plane filters with all-metal inserts were originally proposed as low-cost mass producible circuits for microwave frequencies [1-1], [1-2], such as bandpass filters. The standard configuration for E-plane filters is to use a split block waveguide housing and place inductive typically all metal septa in the E-plane of a rectangular waveguide, at spacing close to a half wavelength apart. Figure 1-1 present this standard configuration.
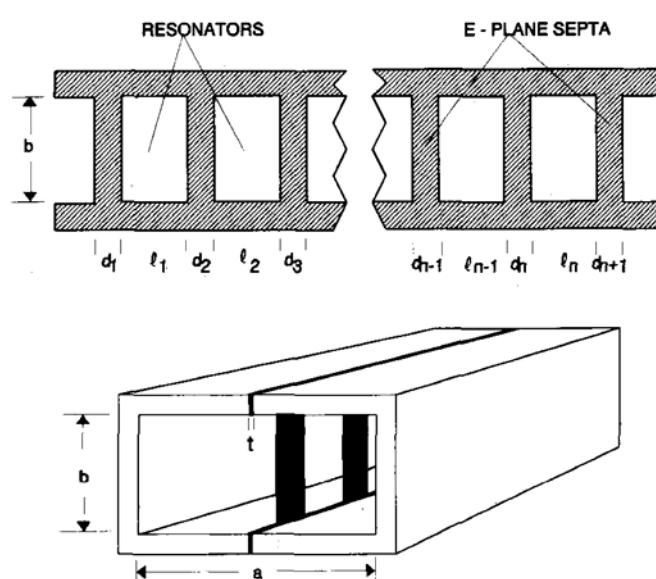
Figure 1-1: E-Plane filter geometry

Because dielectric losses are absent, the structure has a high transmission factor and is suitable for narrow-band applications. Furthermore, these E-plane filters are very easy to build due to the fact that the design is based on printed circuits fabricated with photolithographic process and they also present no need for tuning.

However, despite their favourable characteristics, E-plane filters suffer from bulky size and stopband performance that may often be too low and too narrow for many applications, such as multiplexers.

This project proposes novel E-plane filter configurations as an alternative of the standard configuration with reduced size and improved selectivity. The improvement is achieved incorporating Asymmetric Ridge waveguide and Ridge coaxial waveguide in the all-metal E-plane split-block-housing technology, as it is shown in *Figure 1-2*, in its variation with thin ridges and the inner conductor printed on an all-metal E-plane insert with no further fabrication complexity. Since the guided wavelength as well as the characteristic impedance in Ridge waveguide and Ridged coaxial waveguide propagation varies with the ridges height and the position of the inner conductor, therefore, with no further manufacturing complexity, allows altered propagation characteristics along the same waveguide housing. Based on this remark, sections of Ridge WG and ridge coaxial WG used as resonators in an all-metal E-plane filter may optimise its stopband performance without increasing its manufacturing complexity. The argument in [1-3] was that all the waveguide sections will be resonant at a single fundamental frequency, but not simultaneously resonant at higher frequencies, provided the ridges' gap differs, due to different guide wavelengths in the different filter sections. Hence the spurious harmonic resonance will appear shifted to higher frequencies and the filter's rejection in the stopband will generally be improved.

This novel configuration introduces not only series coupling but also parallel and cross coupling between the resonators of ridge coaxial waveguide filters. Narrow gap resonators are coupled both in series and in parallel. This results in a significant reduction of the total size of the filter. Furthermore, the cross-coupling between the resonators introduces transmission zeros at finite frequencies.

This transmission zero is due to the fact that when the wave is propagated through the guide it can follow two different ways as it is shown in Figure 1-2 (a) y (b). At the end of the section of ridge coaxial WG the waves can be added in phase or in phase opposition, hence a transmission zero appears when the waves are subtracted because of the phase opposition. In Figure 1-2 (c) an example of this transmission zero is depicted.

Furthermore, it is important to keep in mind that this new configuration maintains the fabrication simplicity and mass-producibility of standard E-plane filters.

(a)   (b)

(c)
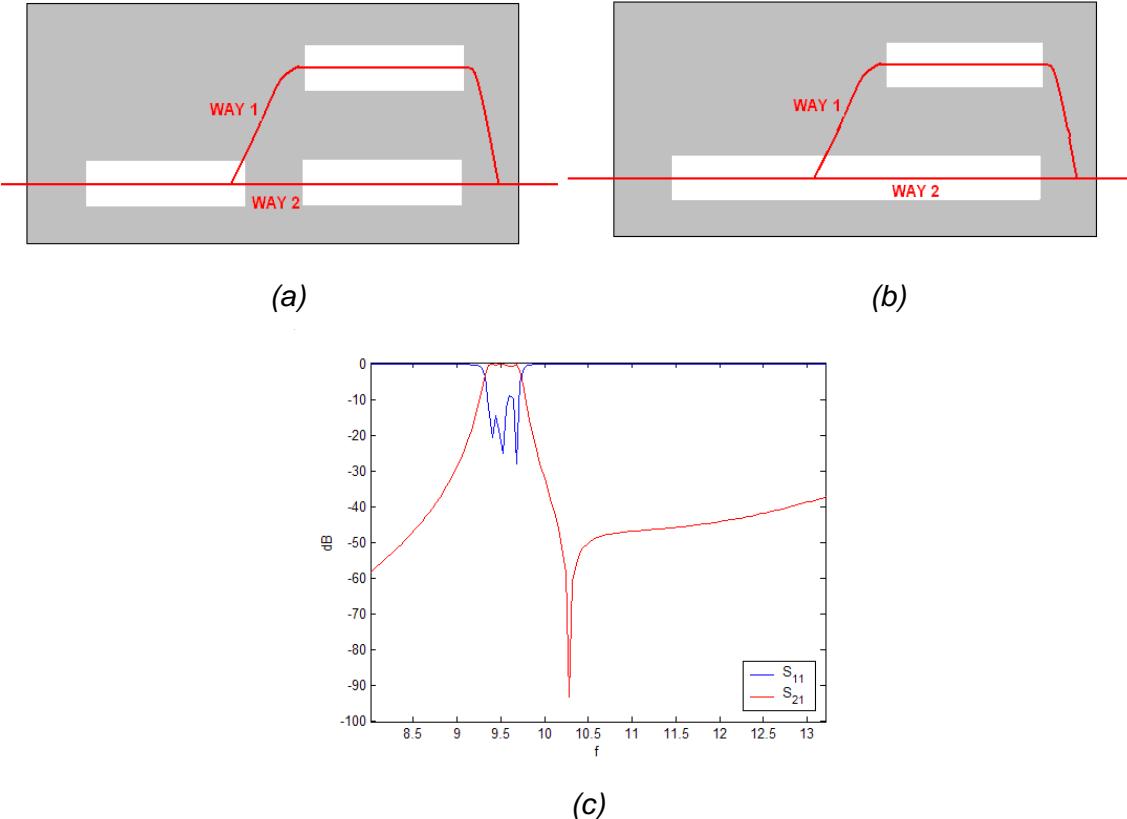
Figure 1-2: Two different configuration of all metal insert of a E-plane filter with a asymmetric Ridge waveguide and a Ridge coaxial waveguide (a) y (b) and a possible response of these filters with transmission zero (c)

1.2. MODELLING OF E-PLANE FILTERS

The generalized layout of an E-plane filter metal insert is shown in Figure 1-3 (a). It can be decomposed into a cascade connection of different waveguide sections such as rectangular waveguide, Reduce waveguide, Ridge waveguide or Ridge coaxial waveguide. The cross-section of these structures is shown in Figure 1-3 (b).

The waveguide section between two subsequent metal septa form a resonator and subsequent resonators are coupled through the couplers realised by the metal septa. The metal septa is basically a Reduce waveguide section. Incorporating Asymmetric Ridge waveguide and Ridge coaxial waveguide in the all-metal E-plane split-block-housing technology as resonators, in its variation with thin ridges and the inner conductor printed on an all-metal E-plane insert with no further fabrication complexity allows altered propagation characteristics along the same waveguide housing.

7

(a)

(b)
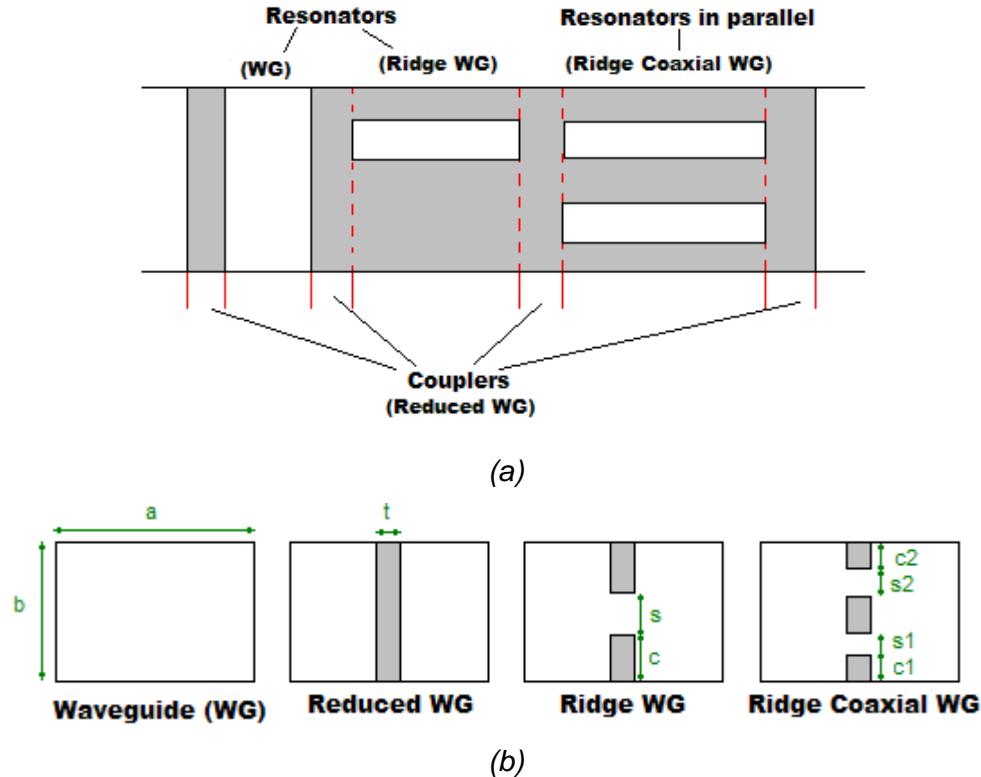
*Figure 1-3: All-metal insert indicating the possible parts of a E-Plane Filter (a),
and Cross section of different waveguides (b)*

The analysis of the E-plane filter is conveniently based on the solution of two different problems.

The first of them is to solve the propagation in each waveguide sections, in order to obtain the cutoff frequency and the field distribution for the higher order modes which can exist. It is important to point out that for the WG and Reduce WG, the field distribution and the cutoff frequency of the modes is easily derived analytically [1-4]. However, for Ridge WG and Ridge Coaxial WG, because the boundary conditions imposed by the cross-section are more complicated, an analytical solution is not obtainable. A numerical solution is therefore required to solve the propagation in these cases. This numerical solution will be studied in this project for the first time. Transverse resonance field matching method is employed for this purpose. Implementation of this method is a very accurate method that returns a full wave description of the propagation in an orthonormal basis of modes of a particular structure. Chapter two includes the theory and formulation of the transverse resonance field matching technique for the electromagnetic modelling of Ridge Coaxial WG and also of the Asymmetric Ridge WG.

The second problem consists of the use of the solution of the first problem for the application of the Mode Matching Method, including higher order modes, in order to obtain the electromagnetic performance of an E-plane filter. To achieve this, the modelling of the discontinuities formed between the different sections is required. The resolution of this second problem is proposed for further works.

Therefore the main objective of this project consists of the development of a modal analysis method based on the transverse resonance equation and "field matching" method for the realisation of a numerical simulator for the EM propagation in the Ridge Coaxial WGTo the author's best knowledge, such structure has not been exploited up to now, even though it possesses interesting properties.

From the Ridge Coaxial WG, as particular cases, other useful structures can be obtained, such a Ridge waveguide and Rectangular Coaxial waveguide. The analysis of symmetric Ridge waveguides and Coaxial waveguides have been rigorously studied in many works, however the analysis of Asymmetric Ridge waveguides has not been investigated profoundly. Due to this a study of the Asymmetric Ridge WG is also presented in this project.

1.3. WAVEGUIDES, TRANSMISSION STRUCTURES

The rectangular hollow conducting waveguides and many of their variations are widely used in microwave systems.

Practical waveguides usually have rectangular or circular cross sections whose cutoff frequencies and field equations have been known for years through the method of separation of variables. Other cross-sectional shapes are possible, but in general few of these have been investigated. Recently, crossed rectangular waveguide shapes have been of interest due to the fact that they may offer some advantages in terms of wider bandwidth, field concentration in specific regions of the guide, field rotation, excitation of individual modes, cross-coupling in dual-mode arrangements, low-cost and low-loss E-plane integrated circuit designs.

Many of those structures are formed by permuting standard rectangular or circular waveguides in certain regions, such as Ridge WG, Coaxial WG and Ridge Coaxial WG. As it was commented, these transmission lines are not canonical structures, so the analysis of the electromagnetic modes is not analytical.

As it was said before the most important application of these structures is that they can be incorporated in the all-metal E-plane split-block-housing technology to allow altered propagation characteristics along the same waveguide housing with no further manufacturing complexity. Based on this remark, sections of ridged coaxial waveguide use of as resonators in an all-metal E-plane filter may optimise its stopband performance with reduced size.

Furthermore, these structures can be applied in the field of EMI/EMC measurements [1-5] allowing to make use of less noise and more power comparing with other technologies such as microstrip, transmission line for beam forming networks [1-6] compatible with solid-state microwave devices [1-8], high quality transitions [1-7], microwave and millimetre wave devices and low-capacitance mounts for varactor diodes [1-9]. They also have many applications in communication satellites, antennas and dual-mode applications, e.g. as polarizers, or orthomode transducers.

1.3.1. RIDGE WAVEGUIDE

The cross-sectional shape of the ridge waveguide is shown in *Figure 1-4*. It consists in a hollow waveguide having a rectangular cross section loaded with ridges at the top and bottom walls. Firstly proposed in [1-10], ridge waveguide propagation has been rigorously studied in [1-19] and is well known to combine the advantages of lower cutoff frequency of the dominant mode, wider bandwidth free from higher modes and low characteristic impedance. These properties have been exploited in a large variety of microwave applications [1-12], including filters [1-11], transformers [1-16], T-junctions [1-13] or even as an improved transmission line [1-14], [1-15].

In this project, the characteristics of the asymmetric Ridge WG are going to be studied in more detail, due to the propagation characteristics of the Ridge WG can be controlled by suitable selection of the geometry of the ridge with no further manufacturing complexity. This study can be useful to design E-Plane filters.
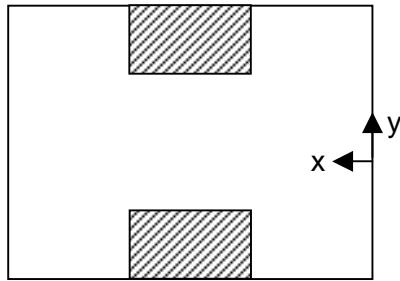
Figure 1-4: Cross section of Ridge Waveguide

1.3.2. COAXIAL WAVEGUIDE

The cross-sectional shape of the rectangular coaxial waveguide is shown in *Figure 1-5.*

It consists in a rectangular transmission line with an inner conductor which can be located in an asymmetric position with respect to the outer conductor.

Coaxial WG have attracted significant attention in the past as TEM cells. The TEM cell is basically a rectangular coaxial line which has been widely used in electromagnetic interference and compatibility measurements, generation of standard electromagnetic fields [1-17] and sensor calibration. Furthermore, this structure has many applications in the design of shielded striplines, varactor mounts, etc.

The Rectangular Coaxial WG has good performances in terms of high quality factor, Q, and power handling capacity, associated with significant size reduction in comparison with rectangular WG. However, manufacturing components having square cross-section are more economical, so this type of coaxial line is predominantly used in feed systems employing a large number of components (e.g., beam forming networks).

Crawford [1-17] has discussed the properties of such lines as well as their advantages, and has described a family of TEM "cells" constructed at the National Bureau of Standards.
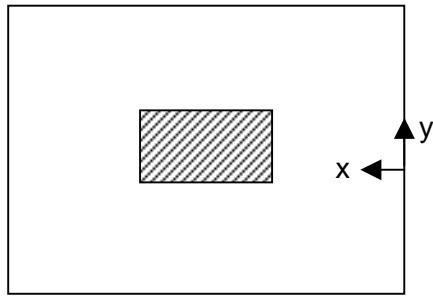
Figure 1-5: Cross section of Coaxial Waveguide

1.3.3. RIDGE COAXIAL WG

The cross section shape of the Ridge Coaxial Waveguide is shown in *Figure 1-6*. The ridge coaxial waveguide is a coaxial rectangular waveguide with metallic insertions at the top and bottom walls.

Among the several geometries reported in the literature, the Ridge Coaxial Waveguide (Ridge Coaxial WG) has received little attention. The fundamental quasi-static TEM mode has been rigorously solved using the integral equation formulation and the Method of Moments [1-18] having zero cutoff frecuency. However any solution of higher order modes for this structure has yet to appear in the literature. In this project we therefore present a rigorous full wave solution of higher order modes of this structure for the first time.

The Ridge Coaxial waveguide is not a canonical structure, so the analysis of the electromagnetic modes is not analytical and a numerical solution is therefore required to solve the propagation in this waveguide. As it was pointed out before, the field matching technique is going to be used for this purpose.

This type of transmission line is useful, for example, as a part of a cascaded transition between a Ridged waveguide and a Coaxial waveguide.
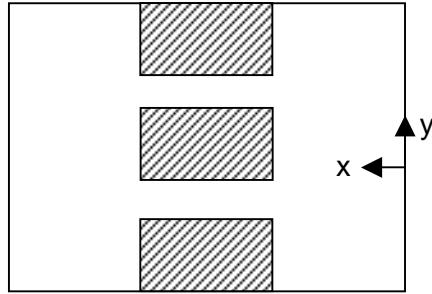
Figure 1-6: Cross section of Ridge Coaxial Waveguide

1.4. OBJETIVES

The aims and objectives of this work are therefore to develop a fast and accurate simulation tool for a prediction of the electromagnetic performance of ridge coaxial waveguide for the incorporation of this structure in an all metal E-plane insert in order to investigate the possibilities of stopband performance improvement and size reduction of all metal E-plane filter.

These improvements are achieved upon introducing parallel coupling between the resonators of ridge coaxial waveguide section. Narrow gap resonators are coupled both in series and in parallel. This results in a significant reduction of the total size of the filter. Furthermore, the topology allows for cross-coupling between the resonators, thus introducing transmission zeros at finite frequencies. This transmission zero is the most attractive improvement pursue with these novel E-plane filter configurations incorporating Ridge Coaxial Waveguide as an alternative of the standard configuration.

In order to reach the point where investigation of this improvement is feasible, the solution of this project has to be used for the application of the Mode Matching Method, including higher order modes, in order to obtain the electromagnetic performance of an E-plane filter. To achieve this, the modelling of the discontinuities formed between the different sections is required. This second problem is proposed for further works.

As a first objective of this project the properties of ridge coaxial waveguide need to be studied. Dependence of cutoff frequencies and possibly other propagation characteristics on the guide's geometry have to be determined.

1.5. OUTLINE OF THIS PROJECT

The aims and objectives described in Section 1.3 will be tackled in several chapters included in this project.

Chapter two includes some literature review to choose Transverse Resonance Field Matching technique as the most appropriate numerical analysis techniques among a large family of methods for solving Maxwell's equations with boundary conditions imposed by a particular physical configuration. The theory and formulation of this technique for the electromagnetic modelling of Ridge Coaxial WG and also of the Asymmetric Ridge WG is also presented. Applying the field matching at the interfaces, the eigenvalue problem will be formed, whose solutions are the unknown cutoff wavenumbers. The power normalisation completes this section.

Chapter three presents a computer algorithm implemented in FORTRAN to solve the Field Matching Method in order to obtain an analytical solution for the propagation characteristics of the Ridge Coaxial WG.

In Chapter four it is presented a graphical user interface (GUI) implemented in MATLAB which links FORTRAN and MATLAB to provide a very fast tool easy to be used. This interface allows the user to enter data, direct instructions and display computational results.

Chapter five presents a convergence analysis in order to know how the implemented algorithm converges to a nominal value with increasing number of expansion terms. This analysis will be useful in future works to determinate how many expansion terms in each region is required in order to obtain accurate results, without overloading the simulation with terms that contribute to a negligible extend.

In Chapter six it is achieved the validation of the accuracy of the developed program comparing it with commercial software. This section presents the cutoff wavenumber obtained by the field matching method based on Generalized Transverse Resonance (GTR) in comparison with cutoff frequencies given by a commercial software based on Finite Elements Method (FEM) (Ansoft HFSS).

Once the results have been validated, Chapter seven presents parametric studies of the variation of the dimensions of the waveguide to demonstrate the dependence of the cutoff wavenumber on the geometry of the structure.

Chapter eight summarizes the conclusions extracted from the parametric study. Since the guided wavelength in ridged coaxial waveguide propagation varies with the geometry

of the structure, these conclusions can be useful to altered propagation characteristics along the same waveguide housing without no further manufacturing complexity.

The conclusions of this work, together with a summary of the contributions and ideas for further work are presented in Chapter nine.

1.6. REFERENCES

[1-1] Y. Konoshi and K. Uenakada, "The design of a bandpass filter with inductive strip-planar circuit mounted in waveguide," IEEE Trans. Microwave Theory Tech,, vol. MTT-22, pp. 869-873, Oct. 1974.

[1-2] Y. Tajima and Y. Sawayama, "Design and anafysis of a waveguidesandwich microwave filter," IEEE Trans. Microwave Theoiy Tech., vol. M'M-22, pp. 839–841, Sept. 1974.

[0-3] Budimir D., Design of E-plane Filters with Improved Stopband Performance, PhD thesis, Department of Electronic and Electrical Engineering, University of Leeds, July 1994

[1-4] Collin R, Theory of Guided Waves, IEEE Press

[1-5] L. Gruner, "Characteristics of Crossed Rectangular Coaxial Structures", IEEE Trans. Microwave Theory and Techniques, pp. 622-627, Vol. 28, No. 6, June 1980

[1-6] F. Alessandri, M. Mongriardo and R. Sorrentino, "Computer-Aided Design of Beam Forming Networks for Modern Satellite Antennas" IEEE Trans. Microwave Theory and Techniques, pp. 1117-1127, Vol 40, No. 6, June 1992

[1-7] R. Levy, "New coaxial -to-stripline transformers using rectangular lines," IRE TRANS. ON MICROWAVE THEORY AND TECHNIQUES, vol. MTT-9, pp. 273–274; May, 1961.

[1-8] F. J. Sansalo:! and E. G. Spencer, "Low temperature microwave power hmter," IRE TRANS. ON MICROWAVE THEORY AND TECHNIQUES, vol. MTT-9, pp. 272–273; May, 1961.

[1-9] R. V. Garver and J. A. Rosado, "Broad-band TEM diode limiting," IRE TRANS. ON MICROWAVE THEORY AND TECHNIQUES, vol. MTT-10, pp. 302–310; September, 1962.

[1-10] Cohn S, "Properties of Ridge Wave Guide", Proc IRE, Vol 35, August 1947, pp.783-788

[1-11] Bornemann J., and Arndt F., "Rigorous Design of Evanscent Mode E-plane Finned Waveguide Bandpass Filters", IEEE MTT-S International Microwave Symposium Digest, pp. 603-606, 1989

[1-12] Helszajn J., Ridge Waveguide and Passive Microwave Components, IEE Electromagnetic Waves Series 49, 2001

[1-13] Wang C., Zaki K. and Mansour R., "Modelling of Generalised Double Ridge Waveguide T-Junctions", IEEE MTT-S International Microwave Symposium Digest, pp. 1185-1188, 1996

[1-14] Pozar D., Microwave Engineering, John Willey&Sons, New York, 1998

[1-15] Collin R., Foundations of Microwave Engineering, 2nd ed., New York: IEEE Press, 2001

[1-16] Bornemann J. and Arndt F., "Modal S-Matrix Design of Optimum Stepped Ridged and Finned Waveguide Transformers", IEEE Transactions on Microwave Theory and Techniques, vol. MTT-35, no. 6, pp. 561-567, June 1987

[1-17] M. L. Crawford, "Generation of standard EM fields using TEM transmission cells," IEEE Trans. Electromagn. Compat., vol. EMC-16, pp. 189–195, Nov. 1974.

[1-18] K. Garb and R. Kastner, "Characteristic Impedance of a Rectangular Double-Ridge TEM Line" IEEE Trans. Microwave Theory and Techniques, pp. 554-557, Vol. 45, No. 4, April 1997

[1-19] Bornemann J., "Comparison between different formulations of the Transverse Resonance Field-Matching Technique for the three-dimensional analysis of metal-finned waveguide resonators", International Journal of Numerical Networks, Devices and Fields, Vol. 4, 63-73 (1991)

<div align="right">

Chapter II

</div>

<div align="right">

Electromagnetic Modelling of Ridge Coaxial WG

</div>

2.1. INTRODUCTION

Most structures used in today's wireless systems are not amenable to closed-form analytical expressions. Modelling tools are therefore essential for the analysis and design of microwave components and subsystems. Numerical methods for passive microwave structures aim to simulate the behaviour of electromagnetic waves in physical geometries consisting of various materials. All such methods derive from Maxwell's equations.

Different physical or mathematical formulations of Maxwell's equations lead to different electromagnetic numerical methods, resulting to a large variety of available modelling techniques [2-1], [2-2].

The choice of a particular numerical method depends on various factors; on the geometry of the structure studied but also the required accuracy, speed, storage requirements, versatility etc. In closed waveguide structures with axial uniformity, it is common to express the propagated electromagnetic waves in terms of orthogonal modes whose cross-sectional shape and electrical properties do not vary along the axis. It is therefore convenient for the physical formulation and efficient for the computational effort required to use the mode-matching method [2-4] for simulating discontinuities between waveguide sections of different cross-section.

The field matching method thus requires thorough description of the field distribution of each mode. As we pointed out before, in hollow rectangular waveguides, the field distribution of the modes is easily derived analytically, but in Ridge Coaxial WG because the boundary conditions imposed by the cross-section are more complicated, an analytical

solution is not obtainable. A numerical solution is therefore required to solve the propagation in Ridge Coaxial WG. Transverse resonance field matching method is employed for this purpose.

The concept of transverse resonance is a rather old one and is equally well applied in equivalent circuits analysis [2-3] or rigorous full wave solutions [1-19]. According to this method, the propagation characteristics for each mode can be analysed at its cutoff frequency, where there is no z-dependence and hence a three dimensional problem is transformed into a two dimensional one. Application of field matching is then from a physical (and mathematical) point of view very similar to mode matching. The cross-section of the waveguide is divided in discrete regions with simple shape. The fields of the standing wave are expressed independently in an orthogonal basis in each region and are matched at common surface.

Section 2.2 includes some literature review to choose Transverse Resonance Field Matching technique as the most appropriate numerical analysis techniques among a large family of methods for solving Maxwell's equations. Section 2.3 gives a brief introduction on the electromagnetic wave modes in terms of vector potentials, which is a more convenient mean of description of these modes for the application of the transverse resonance. The boundary conditions are explained in Section 2.4. Some useful symmetry considerations are summarised in section 2.5. Section 2.6 presents the theory and formulation of the transverse resonance field matching technique for the solution of ridge coaxial waveguide propagation. This section is also completed with the power normalisation of the results in order to use them for mode matching techniques at a discontinuity. In Section 2.7 it is also presented the solution of Asymmetric ridge waveguide as a particular case of Ridge Coaxial WG.

2.2.   FIELD ELECTROMAGNETIC ANALYSIS TECHNIQUE

Several methods have been applied to determine cutoff frequency and the field distribution in a waveguide, some of these methods are: the variational method, finite element method, integral eigenvalue method and the transverse resonance field matching technique.

In Finite difference method, the region of interest is divided into mesh points. A Cartesian lattice (orthogonal and equidistant vertices) is used. The quantity of interest is expressed in terms of its derivatives, which are calculated as finite differences along the

mesh. It is the least analytical method. The mathematical pre-processing is minimal and the method can be applied to a wide range of structures, including those with odd shapes. The major drawback is computational inefficiency, since it requires a large number of mesh points. Another problem of this method is the difficulty of fitting random shaped boundaries (e.g. curved) with a rectangular mesh. This latter problem can be overcome with the finite element method. This is very similar to the finite difference method, although more flexible in setting the mesh.

According to the Variational method, an eigenvalue problem is formed and a parameterised function is assumed to be the eigenfunction in this method. Minimising the eigenvalue equation with respect to its parameters, an upper bound of the eigenvalue is obtained. This method however may call for considerable mathematical insight on the part of the user.

Transverse resonant technique uses the fact that for homogeneously filled waveguides, the cross-sectional distribution of the field for each mode is independent of the frequency [1-19]. This fact is derived as a result of separability of the wave equation for spatial and time coordinates and is fundamental in the mode-approach of waveguide propagation. The knowledge of the cutoff frequency is then sufficient to determine the propagation constant at any frequency (from the vector Helmoholtz equation) since for a given mode, the relative field structure will be the same at every cross-section and every frequency. The fields are therefore analysed at cutoff frequency, assuming standing waves along the transverse coordinates and no propagation along the longitudinal axis (transverse resonance, $k_z = 0$). The longitudinal dependence of the field can thus be neglected and the derivative with respect to it taken as zero. Hence the three-dimensional problem is reduced to two dimensions. The latter will give the cross-sectional distribution of the electromagnetic field for TE and TM modes, which will be valid for frequencies other than cutoff.

The concept of field-matching lies into theoretical division of the cross section under consideration into discrete regions. The fields in each region (or equivalently the vector potentials) are then expressed in an orthonormal basis. The regions should have simple geometrical form (simple boundaries), so that it will be easy to apply the boundary conditions. An interface relation should then be applied, according to which the tangential fields should be continuous at the common surface. Using the orthogonality property of the basis, reduces this relation to a linear system. Hence we can obtain a basis that

describes the field. The Integral eigenvalue method is based on exactly the same physical principal. This formulation is equally well applied in equivalent circuits analysis or rigorous full wave solutions. Furthermore it is the most suitable for the requirements of this work.

2.3.   ELECTROMAGNETIC WAVE MODES

Electromagnetic wave modes are solutions of the field equations in a given coordinate system, and with given boundary conditions. The total field in the specified cross-section may be expressed as a superposition of separate modes. Each mode can be characterized by its electrical and magnetic components. The electrical and magnetic vectors are visualized by so-called field patterns, which qualitatively show the direction and amplitude of these vectors.

For a large variety of structures the electromagnetic wave modes can be distinguished into the following categories:

- TE modes: modes with a magnetic field but no electric field in the direction of the propagation ($H_z \neq 0$, $E_z = 0$).

- TM modes: modes with a electric field but no magnetic field in the direction of the propagation ($H_z = 0$, $E_z \neq 0$).

- TEM modes: modes with no longitudinal electric and magnetic component ($H_z = 0$, $E_z = 0$)

The most fundamental property is that they form an orthogonal basis in which the fields in the waveguide can be expressed. Their orthogonality is the mathematical equivalent of the fact that the modes propagate independently and do not couple.

In the Ridge Coaxial WG case, the fundamental TEM mode has been rigorously solved using the integral equation formulation and the Method of Moments [1-18]. However any solution of higher order modes for this structure has yet to appear in the literature. In this project we therefore present a rigorous full wave solution of higher order modes of Ridge Coaxial WG and Asymmetric Ridge WG.

The knowledge of the modal spectrum is required not only for determining the frequency range of single mode propagation, but also for implementing the subsequent modal analysis, or mode-matching technique of the discontinuities.

In order to apply the transverse resonance field matching technique and mode matching method, is convenient to describe the fields in terms of the Hertzian vector

potentials. Two vector potential functions should then be employed; one for TE and one for TM modes. The expressions that define the magnetic and electric fields in terms of the vector potential functions (*A*) of the TE and TM modes are.

$$\text{TE modes} \begin{cases} E = \nabla \times A_h \\ H = -\dfrac{1}{j\omega\mu} \nabla \times \nabla \times A_h \end{cases} \qquad \text{TM modes} \begin{cases} E = \dfrac{1}{j\omega\varepsilon} \nabla \times \nabla \times A_e \\ H = \nabla \times A_e \end{cases} \qquad (2.3\text{-}1)$$

In general, we can define the electric and magnetic field with the following expressions:

$$E = \nabla \times A_h + \frac{1}{j\omega\varepsilon} \nabla \times \nabla \times A_e \qquad\qquad H = \nabla \times A_e - \frac{1}{j\omega\mu} \nabla \times \nabla \times A_h \qquad (2.3\text{-}2)$$

Supposing z-propagation for electromagnetic wave and separable solution for the vector potentials, the magnetic and electric type of vector potential can be expanded as sum of modes:

$$A_h = \sum_{q=1}^{\infty} \sqrt{Z_{hq}} \cdot T_{hq}(x,y) \cdot \left[V_{hq} e^{-j \cdot K_{zhq} \cdot z} + B_{hq} e^{+j \cdot K_{zhq} \cdot z} \right] \hat{z} \qquad (2.3\text{-}3)$$

$$A_e = \sum_{p=1}^{\infty} \sqrt{Y_{ep}} \cdot T_{ep}(x,y) \cdot \left[V_{ep} e^{-j \cdot K_{zep} \cdot z} - B_{ep} e^{+j \cdot K_{zep} \cdot z} \right] \hat{z} \qquad (2.3\text{-}4)$$

where Z and Y are the waveguide impedance and admittance of TE and TM modes respectively and are given by the expressions:

$$Z_{hq} = \frac{\omega\mu}{K_{hq}} = \frac{1}{Y_{hq}} \qquad\qquad Y_{ep} = \frac{\omega\mu}{K_{ep}} = \frac{1}{Z_{ep}} \qquad\qquad (2.3\text{-}5)$$

For both magnetic and electric type of potentials, the cutoff wavenumbers along each direction are related according to:

$$\left(K_z^i\right)^2 = K_o^2 - \left(K_x^i\right)^2 - \left(K_y^i\right)^2 \qquad\qquad (2.3\text{-}6)$$

The cutoff wavenumber of each mode is specified by the frequency at which the propagation along the z-axis stops, or equivalently, the frequency at which k_z becomes zero (no propagation along z, transverse propagation only). Hence:

$$K_c^2 = K_x^2 + K_y^2 \qquad (2.3\text{-}7)$$

We can define vector function which is directed along the z-axis and satisfies the Helmholtz equation:

$$\nabla^2 A + K^2 A = 0 \qquad (2.3\text{-}8)$$

- **TE modes** can be then derived by a magnetic type of Hertzian potential $\overline{A_h} = A_h \cdot \hat{z}$.

The components of the electric and magnetic field are given by the next expression:

$$E = \nabla \times A_h = \begin{vmatrix} \hat{x} & \hat{y} & \hat{z} \\ \dfrac{\partial}{\partial x} & \dfrac{\partial}{\partial y} & \dfrac{\partial}{\partial z} \\ 0 & 0 & A_h \end{vmatrix} = \dfrac{\partial A_h}{\partial y}\hat{x} - \dfrac{\partial A_h}{\partial x}\hat{y} \Rightarrow \begin{cases} E_x = \dfrac{\partial A_h}{\partial y} \\[2mm] E_y = -\dfrac{\partial A_h}{\partial x} \\[2mm] E_z = 0 \end{cases} \qquad (2.3\text{-}9)$$

$$H = -\dfrac{1}{j\omega\mu}\nabla \times \nabla \times A_h = -\dfrac{1}{j\omega\mu} \cdot \begin{vmatrix} \hat{x} & \hat{y} & \hat{z} \\ \dfrac{\partial}{\partial x} & \dfrac{\partial}{\partial y} & \dfrac{\partial}{\partial z} \\ \dfrac{\partial A_h}{\partial y} & -\dfrac{\partial A_h}{\partial x} & 0 \end{vmatrix} = -\dfrac{1}{j\omega\mu} \cdot \left[\dfrac{\partial^2 A_h}{\partial x \partial z}\hat{x} + \dfrac{\partial^2 A_h}{\partial y \partial z}\hat{y} - \dfrac{\partial^2 A_h}{\partial x^2}\hat{z} - \dfrac{\partial^2 A_h}{\partial y^2}\hat{z} \right]$$

$$\begin{cases} H_x = -\dfrac{1}{j\omega\mu} \cdot \dfrac{\partial^2 A_h}{\partial x \partial z} \\[3mm] H_y = -\dfrac{1}{j\omega\mu} \cdot \dfrac{\partial^2 A_h}{\partial y \partial z} \\[3mm] H_z = \dfrac{1}{j\omega\mu} \cdot \left[\dfrac{\partial^2 A_h}{\partial x^2} + \dfrac{\partial^2 A_h}{\partial y^2} \right] \xrightarrow{\ (1)\ } = -\dfrac{1}{j\omega\mu} \cdot \left[K_0^2 \cdot A_h + \dfrac{\partial^2 A_h}{\partial z^2} \right] \end{cases} \qquad (2.3\text{-}10)$$

- **TM modes** can be then derived by a electric type of Hertzian potential $\overline{A_e} = A_e \cdot \hat{z}$.

The components of the electric and magnetic field are given by the next expression:

$$H = \nabla \times A_e = \begin{vmatrix} \hat{x} & \hat{y} & \hat{z} \\ \dfrac{\partial}{\partial x} & \dfrac{\partial}{\partial y} & \dfrac{\partial}{\partial z} \\ 0 & 0 & A_e \end{vmatrix} = \dfrac{\partial A_e}{\partial y}\hat{x} - \dfrac{\partial A_e}{\partial x}\hat{y} \Rightarrow \begin{cases} H_x = \dfrac{\partial A_e}{\partial y} \\ H_y = -\dfrac{\partial A_e}{\partial x} \\ H_z = 0 \end{cases} \qquad (2.3\text{-}11)$$

$$E = \dfrac{1}{j\omega\varepsilon}\nabla \times \nabla \times A_e = \dfrac{1}{j\omega\varepsilon}\cdot\begin{vmatrix} \hat{x} & \hat{y} & \hat{z} \\ \dfrac{\partial}{\partial x} & \dfrac{\partial}{\partial y} & \dfrac{\partial}{\partial z} \\ \dfrac{\partial A_e}{\partial y} & -\dfrac{\partial A_e}{\partial x} & 0 \end{vmatrix} = \dfrac{1}{j\omega\varepsilon}\cdot\left[\dfrac{\partial^2 A_e}{\partial x \partial z}\hat{x} + \dfrac{\partial^2 A_e}{\partial y \partial z}\hat{y} - \dfrac{\partial^2 A_e}{\partial x^2}\hat{z} - \dfrac{\partial^2 A_e}{\partial y^2}\hat{z} \right]$$

$$\begin{cases} E_x = \dfrac{1}{j\omega\varepsilon}\cdot\dfrac{\partial^2 A_e}{\partial x \partial z} \\[2mm] E_y = \dfrac{1}{j\omega\varepsilon}\cdot\dfrac{\partial^2 A_e}{\partial y \partial z} \\[2mm] E_z = -\dfrac{1}{j\omega\varepsilon}\cdot\left[\dfrac{\partial^2 A_e}{\partial x^2} + \dfrac{\partial^2 A_e}{\partial y^2} \right] \xrightarrow{\;(1)\;} = \dfrac{1}{j\omega\varepsilon}\cdot\left[K_0^2\cdot A_e + \dfrac{\partial^2 A_e}{\partial z^2} \right] \end{cases} \qquad (2.3\text{-}12)$$

(1) $\nabla^2 A + K^2 A = 0 \Rightarrow \dfrac{\partial^2 A}{\partial x^2} + \dfrac{\partial^2 A}{\partial y^2} + \dfrac{\partial^2 A}{\partial z^2} + K^2 A = 0 \Rightarrow \dfrac{\partial^2 A}{\partial x^2} + \dfrac{\partial^2 A}{\partial y^2} = -\left(K^2 A + \dfrac{\partial^2 A}{\partial z^2} \right)$

2.4.   BOUNDARY CONDITIONS

Boundary conditions at electric and magnetic surfaces can be derived by the appropriate behaviour of the tangential fields.

Electric wall

An electric wall is a surface where the tangential components of the electric fields are zero. Ideal metallic surfaces (infinite conductivity) are electric surfaces.

The boundary conditions for the magnetic and electric potential vectors for the TE and TM modes respectively are obtained as follows:

$$E \times \hat{n} = 0 \Rightarrow (\nabla \times A_h) \times \hat{n} = 0 \Rightarrow \left(\dfrac{\partial A_h}{\partial y}\hat{x} - \dfrac{\partial A_h}{\partial x}\hat{y} \right) \times \hat{n} = 0 \qquad (2.4\text{-}1)$$

$$E \times \hat{n} = 0 \Rightarrow (\nabla \times \nabla \times A_e) \times \hat{n} = 0 \Rightarrow \left[\dfrac{\partial^2 A_e}{\partial x \partial z}\hat{x} + \dfrac{\partial^2 A_e}{\partial y \partial z}\hat{y} + \left(K_0^2 A_e + \dfrac{\partial^2 A_e}{\partial z^2} \right)\hat{z} \right] \times \hat{n} = 0 \quad (2.4\text{-}2)$$

where $\hat{n}$ is the unity vector perpendicular to the surface.

<u>Magnetic wall</u>

A magnetic wall is a surface on which the tangential fields of the magnetic field are zero. A material with such a property does not exist, but this concept is useful in order to analyse odd modes.

The boundary conditions for the magnetic and electric potential vectors for the TE and TM modes respectively are obtained as follows:

$$H \times \hat{n} = 0 \Rightarrow (\nabla \times \nabla \times A_h) \times \hat{n} = 0 \Rightarrow \left[\frac{\partial^2 A_h}{\partial x \partial z} \hat{x} + \frac{\partial^2 A_h}{\partial y \partial z} \hat{y} + \left(K_0^2 A_h + \frac{\partial^2 A_h}{\partial z^2} \right) \hat{z} \right] \times \hat{n} = 0 \quad (2.4\text{-}3)$$

$$H \times \hat{n} = 0 \Rightarrow (\nabla \times A_e) \times \hat{n} = 0 \Rightarrow \left(\frac{\partial A_e}{\partial y} \hat{x} - \frac{\partial A_e}{\partial x} \hat{y} \right) \times \hat{n} = 0 \quad (2.4\text{-}4)$$

2.5.   SYMMETRIC CONSIDERATIONS

It is interesting to make some remarks concerning the geometrical and electromagnetic symmetries of waveguides. Such symmetry considerations derive from physical insight of the problem and can prove to be very useful in reducing the mathematical and computational complexity of the numerical solution.

From circuit theory we know that the analysis of a symmetrical circuit can be expressed as a superposition of even and odd mode solutions [2-5]. Even mode in this case implies that equal potentials apply at each end of the circuit; hence there is an open circuit along the line of symmetry. Odd-mode implies opposite potentials at each end of the circuit; hence there is a short circuit along the line of symmetry. The transfer matrix of a network can then be given in terms of the even and odd mode admittances.

This idea can be extended to distributed 3D structures such as waveguides. In waveguides a short circuit is represented by a metallic wall (also referred to as electric wall). This is well understood since the tangential electric field along such a surface is zero and hence the equivalent voltage is zero. By analogy, an open circuit is represented by a magnetic wall; for zero tangential magnetic field, the equivalent current is also zero [2-6]. Hence an even and odd analysis of symmetrical distributed microwave structures can in principle be made assuming magnetic and electric wall along the symmetry plane. This of course assumes that the excitation is symmetric.

Alternatively we can employ the standing wave model for the transverse dependence of the fields in order to visualise even and odd analysis of waveguides. Assume that the waveguide under investigation contains a geometrical symmetry plane

containing the axial (z) and a transverse (y) axis. Then, provided the excitation is symmetrical, equations (2.3-8)is satisfied by either a symmetrical or an antisymmetrical potential function with respect to this transverse direction, which for simplicity we can equally assume to be H_z and E_z for TE and TM modes respectively. It is straightforward to see that symmetrical E_z and antisymmetrical H_z correspond to electric wall at the symmetry plane, while antisymmetrical E_z and symmetrical H_z correspond to magnetic wall at the symmetry plane.

In conclusion we can say that both TE and TM set of modes in a waveguide that possess a symmetry with respect to a plane consist of an odd and an even part. The even part can be derived studying half the structure and assuming a magnetic wall at the symmetry plane while the odd part in a similar manner assuming an electric wall along the symmetry plane. The overall problem is transformed into four smaller subproblems: odd TE modes, even TE modes, odd TM modes and even TM modes.

One important simplification derives from the above. Assume that an even mode is incident to a discontinuity that preserves the same geometrical symmetry. Due to the continuity relations at the surface discontinuity and same symmetry, these even modes will only be coupled in the transmitted region, as well as the only modes excited at the incidence region. Hence we can reduce the number of modes included in our calculation by a factor of two (include only even modes), or alternatively, assume an equivalent structure of half physical size with a magnetic wall along the symmetry plane.

Apart from symmetry considerations, another useful simplification that derives from physical insight of discontinuity problems is the following: the fundamental mode of rectangular waveguides has component of the electric field only along the E-plane (thus its name). This is the plane parallel to the short dimension of the waveguide. However the field distribution of E_y does not depend on the y spatial coordinate but only on x and z. Hence if an obstacle lies along the E-plane isotropically, and therefore does not introduce new boundary conditions on the field so far as the y-coordinate is concerned, the entire scattered field must also be independent from y. Furthermore it immediately follows that this field must have only a single component of electric field, directed along the y-axis. To see this, suppose the x and z components existed. Then, since the electric field must be normal to all metallic surfaces, each would have to vanish on the walls of the waveguide at y=-b/2 and y=b/2. However, since the field is independent of y, these boundary conditions can be satisfied only if each of these components is identically zero everywhere [2-7].

Extensive use of both these conclusions is made during the application of the mode matching technique for E-plane structures. Even mode analysis is exclusively applied, while in standard E-plane filters $TE_{2n+1,0}$ analysis suffices.

Dealing with ridge coaxial waveguide this is not valid any more, as there is variation of the structure as we move along y. Hence we have to include all the $TE_{2n+1,m}$ and $TM_{2n+1,m}$.

2.6.   TRANSVERSE RESONANCE FIELD MATCHING

Taking into account the symmetric considerations commented in the previous section, ,as it is shown in Figure 2-1, the Ridge Coaxial WG has the symmetric shape in the right and left hand side to y axis at x=a/2, so only one half of the structure needs to be analysed.
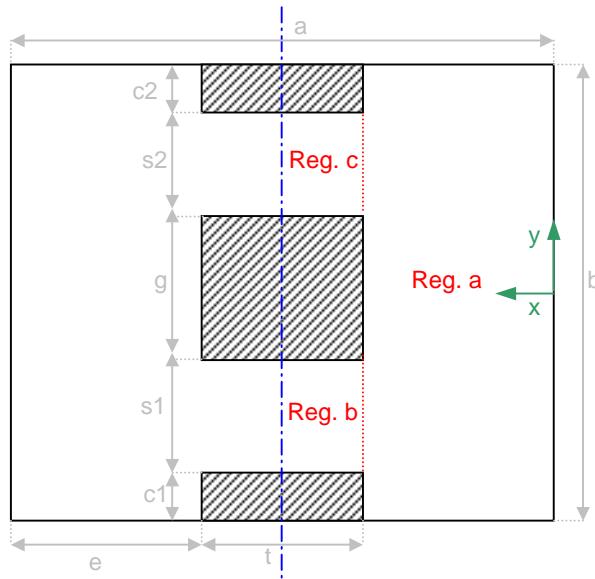
Figure 2-1: Cross section of the RCWG

This will lead to matching unknown fields on two common surfaces and hence to a simplified problem. In order to account for all possible cases, along the symmetry plane we should consider both an electric and a magnetic wall [2-8], [1-19]. [1-19] furthermore, suggests the use of an electric wall along the y-symmetry. However we will not use this symmetry in this work, in order to allow for asymmetrical geometries.

In ridge coaxial waveguide the boundary conditions imposed by the cross section are complicated, so it is advantageous to split up the cross section into three rectangular

regions with simple shapes and to match the field at the respective boundaries between each region.

Hence referring to a Ridge Coaxial WG (Figure 2-1), the optimal choice of regions is:

- Region 1 will be from x= 0 to x= e (trough region)
- Region 2 will be from x=e to x=a/2 and from y=-b/2+c1 to y=-b/2+c1+s1 (lower gap region).
- Region 3 will be from x=e to x=a/2 and from y=b/2-c1-s1 to y=b/2-c1 (upper gap region).

Therefore the difficulty of the structure has been reduced, so the Ridge Coaxial Waveguide can be analyzed step by step, studying the field distribution of the different regions separately and then applying the field matching technique at the common surfaces.

It is interesting to make some remarks concerning the characteristics of waveguides. Such considerations derive from physical insight of the problem and can justify the calculation of the TE and TM modes separately without any coupling each other. These considerations are, on one hand, that there is no discontinuity along the axial axis (z) due to the fact that the obstacles lie along this axis isotropically and, on the other hand, the waveguides under study are homogeneous, there is no dielectric inside.

Taking into account all the considerations explained above, the procedure will be described in the following sections starting with TE modes. For those interested readers, we have provided a series of appendices which expand on a deeper development of the mathematical equation contained below.

2.6.1. FIELD DISTRIBUTION

The field distribution of each mode ($T(x,y)$) is independent of the frequency (due to the separability of the wave equation). We therefore analyse the fields at cutoff frequency where $K_z=0$ and no spatial variation along z exists ($\frac{\partial}{\partial z} = 0$), so there is no propagation along z, transverse propagation only.

Now we can rewrite

$$\nabla \times \nabla \times A = \overbrace{\frac{\partial^2 A}{\partial x \partial z}}^{0}\hat{x} + \overbrace{\frac{\partial^2 A}{\partial y \partial z}}^{0}\hat{y} + \left(K_c^2 A + \overbrace{\frac{\partial^2 A}{\partial z^2}}^{0}\right)\hat{z} = K_c^2 A \hat{z} \qquad (2.6\text{-}1)$$

At cutoff: $K_0 = K_c$

    We are now ready to derive the expressions for the transverse dependence of the electric and magnetic Hertzian type of potentials in each region. As it was pointed out before, we consider the magnetic wall symmetry plane along x=a/2, considering thus odd modes. The magnetic type of vector potential (TE modes) for the three regions is derived from the two dimensional Helmholtz equation, satisfying the appropriate boundary conditions.

    The transverse dependence for the vectors potential will be determined bellow. Appendix 1 provides further explanation of this mathematical development.

REGION 1

The magnetic type of vector potential for this region is:

$$T_{hq}{}^1(x, y) = \sum_{m=0}^{M1}\left[A_{qm}{}^1 e^{+j \cdot K_{xqm}{}^1 \cdot x} + B_{qm}{}^1 e^{-j \cdot K_{xqm}{}^1 \cdot x}\right]\frac{\cos\left(\frac{m\pi}{b}\left(y + \frac{b}{2}\right)\right)}{\sqrt{1 + \delta_{om}}} \qquad (2.6\text{-}2)$$

The boundary condition to be satisfied in this case is:

$$E_y(x = 0) = 0 \qquad\qquad (2.6\text{-}3)$$

    Hence, the transverse dependence for the magnetic type of vector potential is determined by:

$$T_{hq}{}^1(x, y) = \sum_{m=0}^{M1} A_{qm}{}^1 \cos\left(K_{xqm}{}^1 x\right)\frac{\cos\left(\frac{m\pi}{b}\left(y + \frac{b}{2}\right)\right)}{\sqrt{1 + \delta_{om}}} \qquad (2.6\text{-}4)$$

Where the cutoff wavenumber is:

$$\left(K_{xhm}{}^{q1}\right)^2 = \left(K_0\right)^2 - \left(K_{zqm}\right)^2 - \left(\frac{m\pi}{b}\right)^2 \qquad (2.6\text{-}5)$$

In our case $K_{zqm} = 0$ so $K^2{}_{cutoff} = K^2{}_x + K^2{}_y$

REGION 2

The magnetic type of vector potential for this region is:

$$T_{hq}{}^2(x,y) = \sum_{m=0}^{M2}\left[A_{qm}{}^2 e^{+j\cdot K_{xqm}{}^2\cdot x} + B_{qm}{}^2 e^{-j\cdot K_{xqm}{}^2\cdot x}\right]\frac{\cos\left(\dfrac{m\pi}{s1}\left(y+\dfrac{b}{2}-c1\right)\right)}{\sqrt{1+\delta_{om}}} \quad (2.6\text{-}6)$$

The boundary condition to be satisfied in this case is:

$$H_z\left(x=\frac{a}{2}\right) = H_y\left(x=\frac{a}{2}\right) = 0 \qquad (2.6\text{-}7)$$

$$T_{hq}{}^2 = \sum_{m=0}^{M2} A_{qm}{}^2 \frac{1}{K_{xqm}{}^2}\sin\left(K_{xqm}{}^2\cdot(x-\frac{a}{2})\right)\cdot\frac{\cos\left(\dfrac{m\pi}{s1}\left(y+\dfrac{b}{2}-c1\right)\right)}{\sqrt{1+\delta_{om}}} \qquad (2.6\text{-}8)$$

Where the cutoff wavenumber is:

$$\left(K_{xhm}{}^{q2}\right)^2 = \left(K_0\right)^2 - \left(K_{zqm}\right)^2 - \left(\frac{m\pi}{s1}\right)^2 \qquad (2.6\text{-}9)$$

REGION 3

Region 3 has the same shape and the same boundary condition than region 2 so we only show the final result:

$$T_{hq}{}^3 = \sum_{m=0}^{M3} A_{qm}{}^3 \frac{1}{K_{xqm}{}^3}\sin\left(K_{xqm}{}^3\cdot(x-\frac{a}{2})\right)\cdot\frac{\cos\left(\dfrac{m\pi}{s2}\left(y-\dfrac{b}{2}+c2+s2\right)\right)}{\sqrt{1+\delta_{om}}} \qquad (2.6\text{-}10)$$

Where the cutoff wavenumber is:

$$\left(K_{xhm}{}^{q3}\right)^2 = \left(K_0\right)^2 - \left(K_{zqm}\right)^2 - \left(\frac{m\pi}{s2}\right)^2 \qquad (2.6\text{-}11)$$

Similarly the transverse dependence for the electric type of vector potential (TM modes) is determined in a similar way to the magnetic case (TE modes). The electric type of vector potential for each region is shown below:

REGION 1

$$T_{ep}{}^1(x, y) = \sum_{l=1}^{M1} B_{pl}{}^1 \frac{1}{K_{xel}{}^{p1}} \sin\left(K_{xel}{}^{p1}x\right)\sin\left(\frac{l\cdot\pi}{b}\left(y+\frac{b}{2}\right)\right)$$

(2.6-12)

REGION 2

$$T_{ep}{}^2 = \sum_{l=1}^{M2} B_{pl}{}^2 \cos\left(K_{xel}{}^{p2}\cdot(x-\frac{a}{2})\right)\cdot\sin\left(\frac{l\cdot\pi}{s1}\left(y+\frac{b}{2}-c1\right)\right)$$

(2.6-13)

REGION 3

$$T_{ep}{}^3 = \sum_{l=1}^{M3} B_{pl}{}^3 \cos\left(K_{xel}{}^{p3}\cdot(x-\frac{a}{2})\right)\cdot\sin\left(\frac{l\pi}{s2}\left(y-\frac{b}{2}+c2+s2\right)\right)$$

(2.6-14)

Where the cutoff wavenumber are:

Region 1: $\left(K_{xel}{}^{p1}\right)^2 = \left(K_0\right)^2 - \left(K_{zpl}\right)^2 - \left(\frac{l\cdot\pi}{b}\right)^2$ (2.6-15)

Region 2: $\left(K_{xel}{}^{p2}\right)^2 = \left(K_0\right)^2 - \left(K_{zpl}\right)^2 - \left(\frac{l\cdot\pi}{s1}\right)^2$ (2.6-16)

Region 3: $\left(K_{xel}{}^{p3}\right)^2 = \left(K_0\right)^2 - \left(K_{zpl}\right)^2 - \left(\frac{l\cdot\pi}{s2}\right)^2$ (2.6-17)

In our case $K_{zpl} = 0$ so $K^2{}_{cutoff} = K^2{}_x + K^2{}_y$

2.6.2. FIELD MATCHING

The next step is to match the tangential components (x- and y- components) of the electric and magnetic fields at the common surface for every mode. According to the assumptions stated above, we annihilate the z-propagation of the fields. However, since the cross section field distribution of each mode is the same for propagating waves, and since each mode propagates with an distinctive constant k_z, this condition has to be satisfied for every single mode separately.

The boundary condition for this discontinuity derived by the electric (A) and magnetic (B) field is:

$$A : E_1(e) = \begin{cases} E_2(e) \Rightarrow -\left(\dfrac{b}{2} - c1\right) < y < -\left(\dfrac{b}{2} - c1 - s1\right) \\[2ex] E_3(e) \Rightarrow \left(\dfrac{b}{2} - c2 - s2\right) < y < \left(\dfrac{b}{2} - c2\right) \\[2ex] 0 \Rightarrow other\_case \end{cases} \qquad (2.6\text{-}18)$$

$$B : H_1(e) = \begin{cases} H_2(e) \Rightarrow -\left(\dfrac{b}{2} - c1\right) < y < -\left(\dfrac{b}{2} - c1 - s1\right) \\[2ex] H_3(e) \Rightarrow \left(\dfrac{b}{2} - c2 - s2\right) < y < \left(\dfrac{b}{2} - c2\right) \end{cases} \qquad (2.6\text{-}19)$$

As it was shown in Section 2.2.1, the field matching condition leads to an equivalent matching of both types the vector potentials and their derivatives with respect to x.

For TE modes we see that the magnetic field matching is equivalent to vector potential matching and the electrical field matching is equivalent to the matching of the derivative of the magnetic potential with respect to x.

So:

$$A : \left.\frac{\partial T_{hq}^{\,1}}{\partial x}\right|_{x=e} = \begin{cases} \left.\dfrac{\partial T_{hq}^{\,2}}{\partial x}\right|_{x=e} \Rightarrow -\left(\dfrac{b}{2} - c1\right) < y < -\left(\dfrac{b}{2} - c1 - s1\right) & \text{A1} \\[2ex] \left.\dfrac{\partial T_{hq}^{\,3}}{\partial x}\right|_{x=e} \Rightarrow \left(\dfrac{b}{2} - c2 - s2\right) < y < \left(\dfrac{b}{2} - c2\right) & \text{A2} \\[2ex] 0 \Rightarrow other\_case & \text{A3} \end{cases} \qquad (2.6\text{-}20)$$

$$B : T_{hq}^{\,1}(x = e) = \begin{cases} T_{hq}^{\,2}(x = e) \Rightarrow -\left(\dfrac{b}{2} - c1\right) < y < -\left(\dfrac{b}{2} - c1 - s1\right) & \text{B1} \\[2ex] T_{hq}^{\,3}(x = e) \Rightarrow \left(\dfrac{b}{2} - c2 - s2\right) < y < \left(\dfrac{b}{2} - c2\right) & \text{B2} \end{cases} \qquad (2.6\text{-}21)$$

Now, the electric and magnetic field matching are going to be solved according to the common surface among the three regions.

From **A** it is obtained:

$$\left.\frac{\partial T_{hq}^{\,1}}{\partial x}\right|_{x=e} = \left.\frac{\partial T_{hq}^{\,2}}{\partial x}\right|_{x=e} + \left.\frac{\partial T_{hq}^{\,3}}{\partial x}\right|_{x=e} \qquad (2.6\text{-}22)$$

$$-\sum_{m=0}^{M1} A_{qm}{}^{1} \cdot K_{xhm}{}^{q1} \sin\left(K_{xhm}{}^{q1} \cdot e\right) \frac{\cos\left(\dfrac{m\pi}{b}(y+\dfrac{b}{2})\right)}{\sqrt{1+\delta_{om}}} =$$

$$\sum_{m=0}^{M2} A_{qm}{}^{2} \cos\left(K_{xhm}{}^{q2}\, \frac{t}{2}\right) \cdot \frac{\cos\left(\dfrac{m\pi}{s1}(y+\dfrac{b}{2}-c1)\right)}{\sqrt{1+\delta_{om}}} + \sum_{m=0}^{M3} A_{qm}{}^{3} \cos\left(K_{xhm}{}^{q3}\, \frac{t}{2}\right) \cdot \frac{\cos\left(\dfrac{m\pi}{s2}(y-\dfrac{b}{2}+c2+s2)\right)}{\sqrt{1+\delta_{om}}}$$

The orthogonality property of the cosine function is now to be used; we multiply both sides of the relation (2.6-22) with the appropriate cosine function $\dfrac{\cos\left(\dfrac{n\pi}{b}(y+\dfrac{b}{2})\right)}{\sqrt{1+\delta_{on}}}$

and integrate over its period $y \in \left[-\dfrac{b}{2}, \dfrac{b}{2}\right]$.

$$-\sum_{m=0}^{M1} A_{qm}{}^{1} \cdot K_{xqm}{}^{1} \sin\left(K_{xqm}{}^{1} \cdot e\right) J_{1} = \sum_{m=0}^{M2} A_{qm}{}^{2} \cos\left(K_{xqm}{}^{2}\, \frac{t}{2}\right) \cdot J_{2} + \sum_{m=0}^{M3} A_{qm}{}^{3} \cos\left(K_{xqm}{}^{3}\, \frac{t}{2}\right) \cdot J_{3} \quad (2.6\text{-}23)$$

where,

$$J_{1} = \int_{-\frac{b}{2}}^{\frac{b}{2}} \frac{\cos\left(\dfrac{m\pi}{b}(y+\dfrac{b}{2})\right)}{\sqrt{1+\delta_{om}}} \cdot \frac{\cos\left(\dfrac{n\pi}{b}(y+\dfrac{b}{2})\right)}{\sqrt{1+\delta_{on}}} dy \qquad (2.6\text{-}24)$$

$$J_{2} = \int_{-\left(\frac{b}{2}-c1\right)}^{-\left(\frac{b}{2}-c1-s1\right)} \cdot \frac{\cos\left(\dfrac{m\pi}{s1}(y+\dfrac{b}{2}-c1)\right)}{\sqrt{1+\delta_{om}}} \cdot \frac{\cos\left(\dfrac{n\pi}{b}(y+\dfrac{b}{2})\right)}{\sqrt{1+\delta_{on}}} dy \qquad (2.6\text{-}25)$$

$$J_{3} = \int_{\frac{b}{2}-c2-s2}^{\frac{b}{2}-c2} \frac{\cos\left(\dfrac{m\pi}{s2}\left(y-\dfrac{b}{2}+c2+s2\right)\right)}{\sqrt{1+\delta_{om}}} \cdot \frac{\cos\left(\dfrac{n\pi}{b}\left(y+\dfrac{b}{2}\right)\right)}{\sqrt{1+\delta_{on}}} dy \qquad (2.6\text{-}26)$$

The results of these J_{i} are outlined in Appendix 2.

So:

$$A_{qn}^{1} = -\frac{2}{b} \cdot \frac{1}{K_{xhn}^{q1} \sin(K_{xhn}^{q1} \cdot e)} \cdot \left[\sum_{m=0}^{M2} A_{qm}^{2} \cos(K_{xhm}^{q2}\, \frac{t}{2}) \cdot J_{2} + \sum_{m=0}^{M3} A_{qm}^{3} \cos(K_{xhm}^{q3}\, \frac{t}{2}) \cdot J_{3} \right] \qquad (2.6\text{-}27)$$

Rearrange in matrix form to obtain:

$$\left[A^{q1} \right] = -\frac{2}{b} \cdot D_e^{q1} \cdot \left[\left[J_2 \right]^T \cdot D_e^{q2} \cdot \left[A^{q2} \right] + \left[J_3 \right]^T \cdot D_e^{q3} \cdot \left[A^{q3} \right] \right] \qquad (1) \qquad (2.6\text{-}28)$$

where,

$$D_e^{q1} = diag\left(\frac{1}{K_{xhn}^{q1} \sin(K_{xhn}^{q1} \cdot e)} \right) \qquad (2.6\text{-}29)$$

$$D_e^{q2} = diag\left(\cos(K_{xhn}^{q2} \frac{t}{2}) \right) \qquad (2.6\text{-}30)$$

$$D_e^{q3} = diag\left(\cos(K_{xhn}^{q3} \frac{t}{2}) \right) \qquad (2.6\text{-}31)$$

In ap

From **B1** obtain:

$$T_{hq}^1 (x = e) = T_{hq}^2 (x = e) \qquad (2.6\text{-}32)$$

Now we multiply B1 on both sides with $\dfrac{\cos\left(\dfrac{n\pi}{s1}(y + \dfrac{b}{2} - c1) \right)}{\sqrt{1 + \delta_{on}}}$ and integrate over

$$y \in \left[-\left(\frac{b}{2} - c1 \right), -\left(\frac{b}{2} - c1 - s1 \right) \right]$$

$$-\sum_{m=0}^{M2} A_{qm}^{\ 2} \frac{1}{K_{xhm}^{\ 2}} \sin\left(K_{xhm}^{\ q2} \frac{t}{2} \right) \cdot J_4 = \sum_{m=0}^{M1} A_{qm}^{\ 1} \cos\left(K_{xhm}^{\ q1} e \right) J_5 \qquad (2.6\text{-}33)$$

where,

$$J_4 = \int_{-\left(\frac{b}{2}-c1\right)}^{-\left(\frac{b}{2}-c1-s1\right)} \frac{\cos\left(\dfrac{m\pi}{s1}\left(y + \dfrac{b}{2} - c1 \right) \right)}{\sqrt{1 + \delta_{om}}} \cdot \frac{\cos\left(\dfrac{n\pi}{s1}\left(y + \dfrac{b}{2} - c1 \right) \right)}{\sqrt{1 + \delta_{on}}} dy = \frac{s1}{2} \delta_{mn} \qquad (2.6\text{-}34)$$

and

$$J_5 = \int_{-\left(\frac{b}{2}-c1\right)}^{-\left(\frac{b}{2}-c1-s1\right)} \frac{\cos\left(\dfrac{m\pi}{b}\left(y + \dfrac{b}{2} \right) \right)}{\sqrt{1 + \delta_{om}}} \cdot \frac{\cos\left(\dfrac{n\pi}{s1}\left(y + \dfrac{b}{2} - c1 \right) \right)}{\sqrt{1 + \delta_{on}}} dy = J_2 \qquad (2.6\text{-}35)$$

So

$$-A_{qn}^{2}\frac{1}{K_{xhn}^{q2}}\sin\left(K_{xhn}^{q2}\frac{t}{2}\right)\frac{s1}{2}=\sum_{m=0}^{M1}A_{qm}^{1}\cos\left(K_{xhm}^{q1}e\right)J_{2}\Rightarrow$$

$$\Rightarrow A_{qn}^{2}=-\frac{2}{s1}\cdot\frac{K_{xhn}^{q2}}{\sin\left(K_{xhn}^{q2}\frac{t}{2}\right)}\sum_{m=0}^{M1}A_{qm}^{1}\cos\left(K_{xhm}^{q1}e\right)J_{2} \qquad (2.6\text{-}36)$$

Rearrange in matrix form to obtain:

$$\boxed{\left[A^{q2}\right]=-\frac{2}{s1}\cdot D_{h}^{q2}\cdot\left[J_{2}\right]\cdot D_{h}^{q1}\cdot\left[A^{q1}\right]} \qquad (2.6\text{-}37)$$

where,

$$D_{h}^{q1}=diag\left(\cos(K_{xhm}^{q1}\cdot e)\right) \qquad (2.6\text{-}38)$$

$$D_{h}^{q2}=diag\left(\frac{K_{xhn}^{q2}}{\sin(K_{xhn}^{q2}\cdot\frac{t}{2})}\right) \qquad (2.6\text{-}39)$$

From **B2** obtain:

$$T_{hq}^{1}(x=e)=T_{hq}^{3}(x=e) \qquad (2.6\text{-}40)$$

Multiply B2 on both sides with $\dfrac{\cos\left(\dfrac{n\pi}{s2}(y-\dfrac{b}{2}+c2+s2)\right)}{\sqrt{1+\delta_{on}}}$ and integrate over

$$y\in\left[\left(\frac{b}{2}-c2-s2\right),\left(\frac{b}{2}-c2\right)\right]$$

$$-\sum_{m=0}^{M3}A_{qm}^{3}\frac{1}{K_{xhm}^{q3}}\sin\left(K_{xhm}^{q3}\frac{t}{2}\right)\cdot J_{6}=\sum_{m=0}^{M1}A_{qm}^{1}\cos\left(K_{xhm}^{q1}e\right)J_{7} \qquad (2.6\text{-}41)$$

where,

$$J_{6}=\int_{\left(\frac{b}{2}-c2-s2\right)}^{\left(\frac{b}{2}-c2\right)}\frac{\cos\left(\frac{m\pi}{s2}\left(y-\frac{b}{2}+c2+s2\right)\right)}{\sqrt{1+\delta_{om}}}\cdot\frac{\cos\left(\frac{n\pi}{s2}\left(y-\frac{b}{2}+c2+s2\right)\right)}{\sqrt{1+\delta_{on}}}dy=\frac{s2}{2}\delta_{mn} \qquad (2.6\text{-}42)$$

and

$$J_{7}=\int_{\left(\frac{b}{2}-c2-s2\right)}^{\left(\frac{b}{2}-c2\right)}\frac{\cos\left(\frac{m\pi}{b}\left(y+\frac{b}{2}\right)\right)}{\sqrt{1+\delta_{om}}}\cdot\frac{\cos\left(\frac{n\pi}{s2}\left(y-\frac{b}{2}+c2+s2\right)\right)}{\sqrt{1+\delta_{on}}}dy=J_{3} \qquad (2.6\text{-}43)$$

So,

$$-A_{qn}{}^3 \frac{1}{K_{xhn}{}^{q3}} \sin\left(K_{xhn}{}^{q3}\frac{t}{2}\right)\frac{s2}{2} = \sum_{m=0}^{M1} A_{qm}{}^1 \cos\left(K_{xhm}{}^{q1}e\right)J_3 \Rightarrow$$

$$\Rightarrow A_{qn}{}^3 = -\frac{2}{s2}\cdot\frac{K_{xhn}{}^{q3}}{\sin\left(K_{xhn}{}^{q3}\frac{t}{2}\right)}\sum_{m=0}^{M1} A_{qm}{}^1 \cos\left(K_{xhm}{}^{q1}e\right)J_3 \tag{2.6-44}$$

Rearrange in matrix form to obtain:

$$\boxed{\left[A^{q3}\right] = -\frac{2}{s2}\cdot D_h^{q3}\cdot\left[J_3\right]\cdot D_h^{q1}\cdot\left[A^{q1}\right]} \tag{2.6-45}$$

where,

$$D_h^{q3} = diag\left(\frac{K_{xhn}^{q3}}{\sin(K_{xhn}^{q3}\cdot\frac{t}{2})}\right) \tag{2.6-46}$$

To sum up, we have gotten the following expressions:

$$\left[A^{q1}\right] = -\frac{2}{b}\cdot D_e^{q1}\cdot\left[\left[J_2\right]^T\cdot D_e^{q2}\cdot\left[A^{q2}\right]+\left[J_3\right]^T\cdot D_e^{q3}\cdot\left[A^{q3}\right]\right] \tag{2.6-47}$$

$$\left[A^{q2}\right] = -\frac{2}{s1}\cdot D_h^{q2}\cdot\left[J_2\right]\cdot D_h^{q1}\cdot\left[A^{q1}\right] \tag{2.6-48}$$

$$\left[A^{q3}\right] = -\frac{2}{s2}\cdot D_h^{q3}\cdot\left[J_3\right]\cdot D_h^{q1}\cdot\left[A^{q1}\right] \tag{2.6-49}$$

Substituting (2.6-48) and (2.6-49) into (2.6-47) we end to the characteristic equation for the magnetic type of vector potential (for the case of the magnetic wall symmetry):

$$\left[A^{q1}\right] = \frac{4}{b}\cdot D_e^{q1}\cdot\left[\frac{1}{s1}\cdot\left[J_2\right]^T\cdot D_e^{q2}\cdot D_h^{q2}\cdot\left[J_2\right]+\frac{1}{s2}\cdot\left[J_3\right]^T\cdot D_e^{q3}\cdot D_h^{q3}\cdot\left[J_3\right]\right]\cdot D_h^{q1}\cdot\left[A^{q1}\right] \tag{2.6-50}$$

$$\boxed{\left\{\underbrace{\left[D_e^{q1}\right]^{-1} - \frac{4}{b}\cdot\left[\frac{1}{s1}\cdot\left[J_2\right]^T\cdot D_e^{q2}\cdot D_h^{q2}\cdot\left[J_2\right]+\frac{1}{s2}\cdot\left[J_3\right]^T\cdot D_e^{q3}\cdot D_h^{q3}\cdot\left[J_3\right]\right]\cdot D_h^{q1}}_{BigMatrix}\right\}\cdot\left[A^{q1}\right] = 0} \tag{2.6-51}$$

Equation (2.6-51) is a homogeneous linear indeterminate system. Nontrivial solutions for this system exist as long as the determinant of the expression in brackets is zero. By varying frequency, we may solve the characteristic determinant for its eigenvalues k_c. A numerical routine is required for this purpose. This numerical routine will

be program in FORTRAN as it is explained in Chapter 3. After having found the cutoff wavenumbers kc, we can determine the coefficients A^{q1} which is the eigenvector of the problem. Using equation then (2.6-48) and (2.6-49) we can determine the coefficients A^{q2} and A^{q3} respectively. Hence we will have obtained a description of the field distribution of the corresponding mode.

Similar is the procedure followed for the electric type of Hertzian potential which guides to a solution for the TM modes.

From the field expression we see that the magnetic field matching is equivalent to the matching of the derivative of the magnetic potential with respect to x and the electrical field matching is equivalent to vector potential matching.

$$A : T_{ep}^{\ 1}(x=e) = \begin{cases} T_{ep}^{\ 2}(x=e) \Rightarrow -\left(\dfrac{b}{2}-c1\right) < y < -\left(\dfrac{b}{2}-c1-s1\right) & \text{A1} \\[4mm] T_{ep}^{\ 3}(x=e) \Rightarrow \left(\dfrac{b}{2}-c2-s2\right) < y < \left(\dfrac{b}{2}-c2\right) & \text{A2} \\[4mm] 0 \Rightarrow other\_case & \text{A3} \end{cases}$$
(2.6-52)

$$B : \left.\dfrac{\partial T_{pl}^{\ 1}}{\partial x}\right|_{x=e} = \begin{cases} \left.\dfrac{\partial T_{pl}^{\ 2}}{\partial x}\right|_{x=e} \Rightarrow -\left(\dfrac{b}{2}-c1\right) < y < -\left(\dfrac{b}{2}-c1-s1\right) & \text{B1} \\[4mm] \left.\dfrac{\partial T_{pl}^{\ 3}}{\partial x}\right|_{x=e} \Rightarrow \left(\dfrac{b}{2}-c2-s2\right) < y < \left(\dfrac{b}{2}-c2\right) & \text{B2} \end{cases}$$
(2.6-53)

From **A1** and **A2** obtain:

$$T_{pl}^{\ 1}(x=e) = T_{pl}^{\ 2}(x=e) + T_{pl}^{\ 3}(x=e) \qquad (2.6-54)$$

Now multiply on both sides with $\sin\left(\dfrac{n\pi}{b}(y+\dfrac{b}{2})\right)$ and integrate over $y \in \left[-\dfrac{b}{2},\dfrac{b}{2}\right]$

$$\sum_{l=1}^{M1} B_{pl}^{\ 1} \cdot \frac{1}{K_{xel}^{\ p1}} \sin\left(K_{xel}^{\ p1}\cdot e\right) J_1 = \sum_{l=1}^{M2} B_{pl}^{\ 2}\cos\left(K_{xel}^{\ p2}\frac{t}{2}\right)\cdot J_2 + \sum_{l=1}^{M3} B_{pl}^{\ 3}\cos\left(K_{xel}^{\ p3}\frac{t}{2}\right)\cdot J_3 \qquad (2.6-55)$$

where,

$$J_1 = \int_{-\frac{b}{2}}^{\frac{b}{2}} \sin\left(\frac{l\cdot\pi}{b}(y+\frac{b}{2})\right)\sin\left(\frac{n\pi}{b}(y+\frac{b}{2})\right)dy \qquad (2.6\text{-}56)$$

$$J_2 = \int_{-\left(\frac{b}{2}-c1\right)}^{-\left(\frac{b}{2}-c1-s1\right)} \sin\left(\frac{l\cdot\pi}{s1}(y+\frac{b}{2}-c1)\right)\cdot\sin\left(\frac{n\pi}{b}(y+\frac{b}{2})\right)dy \qquad (2.6\text{-}57)$$

$$J_3 = \int_{\frac{b}{2}-c2-s2}^{\frac{b}{2}-c2} \sin\left(\frac{l\cdot\pi}{s2}\left(y-\frac{b}{2}+c2+s2\right)\right)\cdot\sin\left(\frac{n\pi}{b}\left(y+\frac{b}{2}\right)\right)dy \qquad (2.6\text{-}58)$$

The results of these J_i are outlined in Appendix 3.

So:

$$B_{pn}^1 = \frac{2}{b}\cdot\frac{K_{xen}^{p1}}{\sin(K_{xen}^{p1}\cdot e)}\cdot\left[\sum_{l=1}^{M2}B_{qm}^2\cos(K_{xel}^{p2}\frac{t}{2})\cdot J_2 + \sum_{l=1}^{M3}B_{pl}^3\cos(K_{xel}^{p3}\frac{t}{2})\cdot J_3\right] \qquad (2.6\text{-}59)$$

Rearrange in matrix form to obtain:

$$\boxed{\left[B^{p1}\right] = \frac{2}{b}\cdot D_e^{p1}\cdot\left[\left[J_2\right]^T\cdot D_e^{p2}\cdot\left[B^{p1}\right] + \left[J_3\right]^T\cdot D_e^{p3}\cdot\left[B^{p1}\right]\right]} \qquad (2.6\text{-}60)$$

where,

$$D_e^{p1} = diag\left(\frac{K_{xen}^{p1}}{\sin(K_{xen}^{p1}\cdot e)}\right) \qquad (2.6\text{-}61)$$

$$D_e^{p2} = diag(\cos(K_{xel}^{p2}\frac{t}{2})) \qquad (2.6\text{-}62)$$

$$D_e^{p3} = diag(\cos(K_{xel}^{p3}\frac{t}{2})) \qquad (2.6\text{-}63)$$

From **B1** obtain:

$$\left.\frac{\partial T_{ep}^1}{\partial x}\right|_{x=e} = \left.\frac{\partial T_{ep}^2}{\partial x}\right|_{x=e} \qquad (2.6\text{-}64)$$

$$\sum_{l=1}^{M1}B_{pl}^{\ 1}\cdot\cos\left(K_{xel}^{\ p1}\cdot e\right)\sin\left(\frac{l\pi}{b}(y+\frac{b}{2})\right) = \sum_{l=1}^{M2}B_{pl}^{\ 2}K_{xel}^{\ p2}\sin\left(K_{xel}^{\ p2}\frac{t}{2}\right)\cdot\sin\left(\frac{l\pi}{s1}(y+\frac{b}{2}-c1)\right)$$

Multiply B1 on both sides with $\sin\left(\dfrac{n\pi}{s1}(y + \dfrac{b}{2} - c1)\right)$ and integrate over

$$y \in \left[-\left(\frac{b}{2} - c1\right), -\left(\frac{b}{2} - c1 - s1\right) \right]$$

$$\sum_{l=1}^{M2} B_{pl}{}^2 K_{xel}{}^{p2} \sin\left(K_{xel}{}^{p2}\frac{t}{2}\right) \cdot J_4 = \sum_{l=1}^{M1} B_{pl}{}^1 \cos\left(K_{xel}{}^{p1}e\right) J_5 \qquad (2.6\text{-}65)$$

where,

$$J_4 = \int_{-\left(\frac{b}{2}-c1\right)}^{-\left(\frac{b}{2}-c1-s1\right)} \sin\left(\frac{l\pi}{s1}\left(y + \frac{b}{2} - c1\right)\right) \cdot \sin\left(\frac{n\pi}{s1}\left(y + \frac{b}{2} - c1\right)\right) dy = \frac{s1}{2}\delta_{ln} \qquad (2.6\text{-}66)$$

and

$$J_5 = \int_{-\left(\frac{b}{2}-c1\right)}^{-\left(\frac{b}{2}-c1-s1\right)} \sin\left(\frac{l\pi}{b}\left(y + \frac{b}{2}\right)\right) \cdot \sin\left(\frac{n\pi}{s1}\left(y + \frac{b}{2} - c1\right)\right) dy = J_2 \qquad (2.6\text{-}67)$$

So

$$B_{qn}{}^2 K_{xen}{}^{p2} \sin\left(K_{xen}{}^{p2}\frac{t}{2}\right)\frac{s1}{2} = \sum_{l=1}^{M1} B_{pl}{}^1 \cos\left(K_{xel}{}^{p1}e\right) J_2 \Rightarrow$$

$$\Rightarrow B_{pn}{}^2 = \frac{2}{s1} \cdot \frac{1}{K_{xen}{}^{p2} \sin\left(K_{xen}{}^{p2}\dfrac{t}{2}\right)} \sum_{l=1}^{M1} B_{pl}{}^1 \cos\left(K_{xel}{}^{p1}e\right) J_2 \qquad (2.6\text{-}68)$$

Rearrange in matrix form to obtain:

$$\boxed{\left[B^{p2}\right] = \frac{2}{s1} \cdot D_h^{p2} \cdot [J_2] \cdot D_h^{p1} \cdot \left[B^{p1}\right]} \qquad (2.6\text{-}69)$$

where,

$$D_h^{p1} = diag\left(\cos\left(K_{xel}^{p1}\cdot e\right)\right) \qquad (2.6\text{-}70)$$

$$D_h^{p2} = diag\left(\frac{1}{K_{xen}^{p2} \sin\left(K_{xen}^{p2}\cdot\dfrac{t}{2}\right)}\right) \qquad (2.6\text{-}71)$$

From **B2** obtain:

$$\left.\frac{\partial T_{ep}^1}{\partial x}\right|_{x=e} = \left.\frac{\partial T_{ep}^3}{\partial x}\right|_{x=e} \qquad (2.6\text{-}72)$$

$$\sum_{l=1}^{M1} B_{pl}{}^1 \cdot \cos\!\left(K_{xel}{}^{p1}\cdot e\right)\sin\!\left(\frac{l\pi}{b}(y+\frac{b}{2})\right) = \sum_{l=1}^{M3} B_{pl}{}^3 K_{xel}{}^{p3} \sin\!\left(K_{xel}{}^{p3}\frac{t}{2}\right)\cdot\sin\!\left(\frac{l\pi}{s2}(y-\frac{b}{2}+c2+s2)\right)$$

Multiply B2 on both sides with $\sin\!\left(\dfrac{n\pi}{s2}(y-\dfrac{b}{2}+c2+s2)\right)$ and integrate over

$$y \in \left[\left(\frac{b}{2}-c2-s2\right),\left(\frac{b}{2}-c2\right)\right]$$

$$\sum_{l=1}^{M3} B_{pl}{}^3 K_{xel}{}^{p3} \sin\!\left(K_{xel}{}^{p3}\frac{t}{2}\right)\cdot J_6 = \sum_{l=1}^{M1} B_{pl}{}^1 \cos\!\left(K_{xel}{}^{p1}e\right)J_7 \qquad (2.6\text{-}73)$$

where,

$$J_6 = \int_{\left(\frac{b}{2}-c2-s2\right)}^{\left(\frac{b}{2}-c2\right)} \sin\!\left(\frac{l\pi}{s2}\!\left(y-\frac{b}{2}+c2+s2\right)\right)\cdot\sin\!\left(\frac{n\pi}{s2}\!\left(y-\frac{b}{2}+c2+s2\right)\right)dy = \frac{s2}{2}\delta_{\ln} \qquad (2.6\text{-}74)$$

and

$$J_7 = \int_{\left(\frac{b}{2}-c2-s2\right)}^{\left(\frac{b}{2}-c2\right)} \sin\!\left(\frac{l\pi}{b}\!\left(y+\frac{b}{2}\right)\right)\cdot\sin\!\left(\frac{n\pi}{s2}\!\left(y-\frac{b}{2}+c2+s2\right)\right)dy = J_3 \qquad (2.6\text{-}$$

75)

So,

$$B_{pn}{}^3 K_{xen}{}^{p3} \sin\!\left(K_{xen}{}^{p3}\frac{t}{2}\right)\frac{s2}{2} = \sum_{l=1}^{M1} B_{pl}{}^1 \cos\!\left(K_{xel}{}^{p1}e\right)J_3 \Rightarrow$$

$$\Rightarrow B_{pn}{}^3 = \frac{2}{s2}\cdot\frac{1}{K_{xen}{}^{p3}\sin\!\left(K_{xen}{}^{p3}\frac{t}{2}\right)}\sum_{l=1}^{M1} B_{pl}{}^1 \cos\!\left(K_{xel}{}^{p1}e\right)J_3 \qquad (2.6\text{-}$$

76)

Rearrange in matrix form to obtain:

$$\boxed{\left[B^{q3}\right] = \frac{2}{s2}\cdot D_h^{p3}\cdot\left[J_3\right]\cdot D_h^{p1}\cdot\left[B^{p1}\right]} \qquad (2.6\text{-}77)$$

where,

$$D_h^{p3} = diag \left(\frac{1}{K_{xen}^{p3} \sin(K_{xen}^{p3} \cdot \frac{t}{2})} \right) \qquad (2.6\text{-}78)$$

To sum up, we have gotten the following expressions:

$$[B^{p1}] = \frac{2}{b} \cdot D_e^{p1} \cdot \left[[J_2]^T \cdot D_e^{p2} \cdot [B^{p2}] + [J_3]^T \cdot D_e^{p3} \cdot [B^{p3}] \right] \qquad (2.6\text{-}79)$$

$$[B^{p2}] = \frac{2}{s1} \cdot D_h^{p2} \cdot [J_2] \cdot D_h^{p1} \cdot [B^{p1}] \qquad (2.6\text{-}80)$$

$$[B^{p3}] = \frac{2}{s2} \cdot D_h^{p3} \cdot [J_3] \cdot D_h^{p1} \cdot [B^{p1}] \qquad (2.6\text{-}81)$$

Substituting (2.6-80) and (2.6-81) into (2.6-79) we end to the characteristic equation for the electric type of vector potential (for the case of the magnetic wall symmetry):

$$[B^{p1}] = \frac{4}{b} \cdot D_e^{p1} \cdot \left[\frac{1}{s1} \cdot [J_2]^T \cdot D_e^{p2} \cdot D_h^{p2} \cdot [J_2] + \frac{1}{s2} \cdot [J_3]^T \cdot D_e^{p3} \cdot D_h^{p3} \cdot [J_3] \right] \cdot D_h^{p1} \cdot [B^{p1}] \qquad (2.6\text{-}82)$$

$$\underbrace{\left\{ [D_e^{p1}]^{-1} - \frac{4}{b} \left[\frac{1}{s1} \cdot [J_2]^T \cdot D_e^{p2} \cdot D_h^{p2} \cdot [J_2] + \frac{1}{s2} \cdot [J_3]^T \cdot D_e^{p3} \cdot D_h^{p3} \cdot [J_3] \right] \cdot D_h^{p1} \right\}}_{BigMatrix} \cdot [B^{p1}] = 0 \qquad (2.6\text{-}83)$$

As in the previous case for the TE modes, equation (2.6-83) is a homogeneous linear NxN system. After having found the cutoff wavenumbers kc, we can determine the amplitude coefficients for each region using the equations (2.6-79), (2.6-80) and (2.6-81).

2.6.3. POWER NORMALISATION

In order to use the results obtained from the previous procedure for mode matching techniques at a discontinuity, we should normalize the coefficients A of equations (2.6-47), (2.6-47) and (2.6-47) so that the power transferred by each mode of a unity amplitude at both sides of the discontinuity is independent of the cross-sectional shape and area, and equal to a constant. Assume each mode power amplitude equal to unity. Referring to equations (2.3-3) and (2.3-4), the power transferred by a mode with F= 1 and B= 0 (same as F= 0 and B= 1 for backwards propagating mode), have to be equal to 1W. This will ensure that the S-parameters of the scattering matrix later on are between 0 and 1.

As we saw in section 2.2.2, in the case of a Ridge Coaxial WG, the transverse dependence of the distribution of the Hertzian potential for a single TE_q or TM_p mode is expressed in an orthogonal basis as truncated series. One series gives the distribution of the vector potential in the trough region and the others in the gap regions The field matching at the common surface produces a relation between the coefficients of the three series.

For the ith propagating TE mode, the power normalization condition is:

$$\iint_s (\nabla \cdot T_h^i)^2 \, ds = 1 \qquad (2.6\text{-}84)$$

It can be expanded in this case as following:

$$\iint_{s1} (\nabla \cdot T_h^{1q})^2 \, ds + \iint_{s2} (\nabla \cdot T_h^{2q})^2 \, ds + \iint_{s3} (\nabla \cdot T_h^{3q})^2 \, ds = 1 \qquad (2.6\text{-}85)$$

Where,

$$\iint_{s1}\left[\left(\frac{\partial T_h^{1q}}{\partial x}\right)^2 + \left(\frac{\partial T_h^{1q}}{\partial x}\right)^2\right] x\,dy + \iint_{s2}\left[\left(\frac{\partial T_h^{2q}}{\partial x}\right)^2 + \left(\frac{\partial T_h^{2q}}{\partial x}\right)^2\right] x\,dy + \iint_{s3}\left[\left(\frac{\partial T_h^{3q}}{\partial x}\right)^2 + \left(\frac{\partial T_h^{3q}}{\partial x}\right)^2\right] x\,dy = 1$$

Upon analytical integration of these integrals in the case of magnetic type of Hertzian potential, we obtain the following expressions:

$$\int_{-\frac{b}{2}}^{\frac{b}{2}}\int_0^e \left(\frac{\partial T_h^{1q}}{\partial x}\right)^2 dx\,dy = \sum_{m=1}^{M1} \left(A_m^{1q} \cdot K_{xhm}^{1q}\right)^2 \cdot \left(\frac{b}{4}\right)\left(e - \frac{\sin\left(2 \cdot K_{xhm}^{1q} \cdot e\right)}{2 \cdot K_{xhm}^{1q}}\right) \qquad (2.6\text{-}86)$$

$$\int_{-\frac{b}{2}}^{\frac{b}{2}}\int_0^e \left(\frac{\partial T_h^{1q}}{\partial y}\right)^2 dx\,dy = \sum_{m=0}^{M1} \left(A_m^{1q} \cdot \frac{m \cdot \pi}{b}\right)^2 \cdot \left(\frac{b}{4(1+\delta_{om})}\right)\left(e + \frac{\sin\left(2 \cdot K_{xhm}^{1q} \cdot e\right)}{2 \cdot K_{xhm}^{1q}}\right) \qquad (2.6\text{-}87)$$

$$\int_{-(\frac{b}{2}-c1)}^{-(\frac{b}{2}-c1-s1)}\int_e^{a/2} \left(\frac{\partial T_h^{2q}}{\partial x}\right)^2 dx\,dy = \sum_{m=1}^{M2} \left(A_m^{2q}\right)^2 \cdot \left(\frac{s1}{8}\right)\left(t + \frac{\sin\left(K_{xhm}^{2q} \cdot t\right)}{K_{xhm}^{2q}}\right) \qquad (2.6\text{-}88)$$

$$\int_{-(\frac{b}{2}-c1)}^{-(\frac{b}{2}-c1-s1)}\int_e^{a/2} \left(\frac{\partial T_h^{2q}}{\partial y}\right)^2 dx\,dy = \sum_{m=0}^{M2} \left(A_m^{2q} \cdot \frac{m \cdot \pi}{s1 \cdot K_{xhm}^{2q}}\right)^2 \cdot \left(\frac{s1}{8(1+\delta_{om})}\right)\left(t - \frac{\sin\left(K_{xhm}^{2q} \cdot t\right)}{K_{xhm}^{2q}}\right) \qquad (2.6\text{-}89)$$

$$\int_{(\frac{b}{2}-c2-s2)}^{(\frac{b}{2}-c2)}\int_e^{a/2} \left(\frac{\partial T_h^{3q}}{\partial x}\right)^2 dx\,dy = \sum_{m=1}^{M3} \left(A_m^{3q}\right)^2 \cdot \left(\frac{s2}{8}\right)\left(t + \frac{\sin\left(K_{xhm}^{3q} \cdot t\right)}{K_{xhm}^{3q}}\right) \qquad (2.6\text{-}90)$$

$$\int_{(\frac{b}{2}-c2-s2)}^{(\frac{b}{2}-c2)} \int_{e}^{a/2} \left(\frac{\partial T_h^{3q}}{\partial y}\right)^2 dxdy = \sum_{m=0}^{M3} \left(A_m^{3q} \cdot \frac{m \cdot \pi}{s2 \cdot K_{xhm}^{3q}}\right)^2 \cdot \left(\frac{s2}{8(1+\delta_{om})}\right) \left(t - \frac{\sin(K_{xhm}^{3q} \cdot t)}{K_{xhm}^{3q}}\right) \qquad (2.6\text{-}91)$$

In a similar way, for TM modes de power normalisation condition is: $\iint_{s} \left(\nabla \cdot T_e^i\right)^2 ds = 1$

And it can be expanded:

$$\iint_{s1} \left(\nabla \cdot T_e^{1p}\right)^2 ds + \iint_{s2} \left(\nabla \cdot T_e^{2p}\right)^2 ds + \iint_{s3} \left(\nabla \cdot T_e^{3p}\right)^2 ds = 1 \qquad (2.6\text{-}92)$$

Where,

$$\iint_{s1} \left[\left(\frac{\partial T_e^{1p}}{\partial x}\right)^2 + \left(\frac{\partial T_e^{1p}}{\partial x}\right)^2\right] xdy + \iint_{s2} \left[\left(\frac{\partial T_e^{2p}}{\partial x}\right)^2 + \left(\frac{\partial T_e^{2p}}{\partial x}\right)^2\right] xdy + \iint_{s3} \left[\left(\frac{\partial T_e^{3p}}{\partial x}\right)^2 + \left(\frac{\partial T_e^{3p}}{\partial x}\right)^2\right] xdy = 1$$

The corresponding integrals of the electric type of Hertzian potentials have the following analytical solution:

$$\int_{-\frac{b}{2}}^{\frac{b}{2}} \int_{0}^{e} \left(\frac{\partial T_e^{1p}}{\partial x}\right)^2 dxdy = \sum_{l=1}^{M1} \left(B_l^{1p}\right)^2 \cdot \left(\frac{b}{4}\right) \left(e + \frac{\sin(2 \cdot K_{xel}^{1p} \cdot e)}{2 \cdot K_{xel}^{1p}}\right) \qquad (2.6\text{-}93)$$

$$\int_{-\frac{b}{2}}^{\frac{b}{2}} \int_{0}^{e} \left(\frac{\partial T_e^{1p}}{\partial y}\right)^2 dxdy = \sum_{l=1}^{M1} \left(B_l^{1p} \cdot \frac{l \cdot \pi}{b \cdot K_{xel}^{1p}}\right)^2 \cdot \left(\frac{b}{4}\right) \left(e - \frac{\sin(2 \cdot K_{xel}^{1p} \cdot e)}{2 \cdot K_{xel}^{1p}}\right) \qquad (2.6\text{-}94)$$

$$\int_{-(\frac{b}{2}-c1)}^{-(\frac{b}{2}-c1-s1)} \int_{e}^{a/2} \left(\frac{\partial T_e^{2p}}{\partial x}\right)^2 dxdy = \sum_{l=1}^{M2} \left(B_l^{2p} K_{xel}^{2p}\right)^2 \cdot \left(\frac{s1}{8}\right) \left(t - \frac{\sin(K_{xel}^{2p} \cdot t)}{K_{xel}^{2p}}\right) \qquad (2.6\text{-}95)$$

$$\int_{-(\frac{b}{2}-c1)}^{-(\frac{b}{2}-c1-s1)} \int_{e}^{a/2} \left(\frac{\partial T_e^{2p}}{\partial y}\right)^2 dxdy = \sum_{l=1}^{M2} \left(B_l^{2p} \cdot \frac{l \cdot \pi}{s1}\right)^2 \cdot \left(\frac{s1}{8}\right) \left(t + \frac{\sin(K_{xel}^{2p} \cdot t)}{K_{xel}^{2p}}\right) \qquad (2.6\text{-}96)$$

$$\int_{(\frac{b}{2}-c2-s2)}^{(\frac{b}{2}-c2)} \int_{e}^{a/2} \left(\frac{\partial T_e^{3p}}{\partial x}\right)^2 dxdy = \sum_{l=1}^{M3} \left(B_l^{3p} K_{xel}^{3p}\right)^2 \cdot \left(\frac{s2}{8}\right) \left(t - \frac{\sin(K_{xel}^{3p} \cdot t)}{K_{xel}^{3p}}\right) \qquad (2.6\text{-}97)$$

$$\int\limits_{(\frac{b}{2}-c2-s2)}^{(\frac{b}{2}-c2)} \int\limits_{e}^{a/2} \left(\frac{\partial T_e^{3p}}{\partial y}\right)^2 dxdy = \sum_{l=1}^{M3} \left(B_l^{3p}\cdot\frac{l\cdot\pi}{s2}\right)^2 \cdot \left(\frac{s2}{8}\right)\left(t + \frac{\sin\left(K_{xel}^{3p}\cdot t\right)}{K_{xel}^{3p}}\right) \qquad (2.6\text{-}98)$$

2.7. PARTICULAR CASE: ASYMMETRIC RIDGE WG

In the absence of the inner conductor (g = 0, s2=0), the transmission line of Figure 2-1 becomes a Ridge WG, as we can see in Figure 2-2. Ridged waveguide propagation has been rigorously studied in [2-11]. In this section the Field Matching Method is applied to the Asymmetric Ridge WG due to it can have diverse advantages with respect to the symmetric Ridge WG, as the propagation characteristics of the Ridge WG can be controlled by suitable selection of the geometry of the ridges.
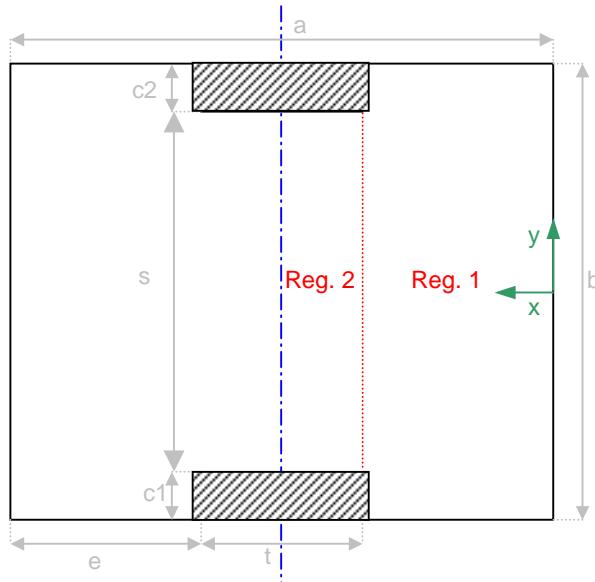
Figure 2-2: Cross section of Ridge Waveguide

Following the same procedure than in the case of a Ridge Coaxial WG, due to the x-symmetry of the structure, as it was explained before, the analysis can be carried out assuming only half of the structure's cross-section, from x=0 to x=a/2 (Figure 2-2). In this particular case, the cross section will be divided in two regions instead of three. The optimal choice of regions is:

- Region 1 will be from x= 0 to x= e (trough region)
- Region 2 will be from x=e to x=a/2 (gap region).

The field distributions for the TE and TM modes of these two regions are given by the same expressions that describe the field distributions of the Ridge Coaxial WG in Region 1 for TE (2.6-4) and TM (2.6-12) modes and Region 2 for TE (2.6-8) and TM (2.6-13) modes.

Appling the field matching for the TE modes between these two regions, we obtain the following homogeneous linear system:

$$\left[A^{q1}\right] = -\frac{2}{b}\cdot D_e^{q1}\cdot\left[J_2\right]^T\cdot D_e^{q2}\cdot\left[A^{q2}\right] \qquad (2.7\text{-}1)$$

$$\left[A^{q2}\right] = -\frac{2}{s1}\cdot D_h^{q2}\cdot\left[J_2\right]\cdot D_h^{q1}\cdot\left[A^{q1}\right] \qquad (2.7\text{-}2)$$

where,

$$D_e^{q1} = diag\left(\frac{1}{K_{xhn}^{q1}\sin(K_{xhn}^{q1}\cdot e)}\right) \quad D_h^{q1} = diag(\cos(K_{xhm}^{q1}\cdot e)) \qquad (2.7\text{-}3) \text{ and } (2.7\text{-}4)$$

$$D_e^{q2} = diag(\cos(K_{xhn}^{q2}\frac{t}{2})) \qquad D_h^{q2} = diag\left(\frac{K_{xhn}^{q2}}{\sin(K_{xhn}^{q2}\cdot\frac{t}{2})}\right) \qquad (2.7\text{-}5) \text{ and } (2.7\text{-}6)$$

Substituting (2.5-2) into (2.5-1) we end to the characteristic equation for the magnetic type of vector potential (for the case of the magnetic wall symmetry):

$$\left[A^{q1}\right] = \frac{4}{b\cdot s1}\cdot D_e^{q1}\cdot\left[J_2\right]^T\cdot D_e^{q2}\cdot D_h^{q2}\cdot\left[J_2\right]\cdot D_h^{q1}\cdot\left[A^{q1}\right] \qquad (2.7\text{-}7)$$

$$\underbrace{\left\{\left[D_e^{q1}\right]^{-1} - \frac{4}{b\cdot s1}\cdot\left[J_2\right]^T\cdot D_e^{q2}\cdot D_h^{q2}\cdot\left[J_2\right]\cdot D_h^{q1}\right\}}_{BigMatrix}\cdot\left[A^{q1}\right] = 0 \quad (2.7\text{-}8)$$

Similar is the procedure followed for the electric type of Hertzian potential. The field matching equations can be rearranged until we finally obtain

$$\left[B^{p1}\right] = \frac{4}{b\cdot s1}\cdot D_e^{p1}\cdot\left[J_2\right]^T\cdot D_e^{p2}\cdot D_h^{p2}\cdot\left[J_2\right]\cdot D_h^{p1}\cdot\left[B^{p1}\right] \qquad (2.7\text{-}9)$$

$$\underbrace{\left\{\left[D_e^{p1}\right]^{-1} - \frac{4}{b\cdot s1}\cdot\left[J_2\right]^T\cdot D_e^{p2}\cdot D_h^{p2}\cdot\left[J_2\right]\cdot D_h^{p1}\right\}}_{BigMatrix}\cdot\left[B^{p1}\right] = 0 \quad (2.7\text{-}10)$$

Furthermore, for the power normalisation the same expressions (2.6-86)-(2.6-89) for TE modes and (2.6-93)-(2.6-96) are used in order to normalise the amplitude coefficient A1 and A2 due to in this particular case, only two regions describe the structure.

The above described mathematical formulation of the cross-section field distribution for the Ridge Coaxial WG and Asymmetric Ridge WG has been implemented as computer

algorithm. MATLAB [2-9] and FORTRAN [2-10] have been used for this purpose. The program has been written in FORTRAN to speed its execution time and MATLAB was used to check the obtained results step by step. In order to ensure the accuracy of this tool, comparison of the cutoff frequency obtained by this method with results obtained with commercial software is essential and presented hereafter. Furthermore, as formulated in the previous section, the number of expansion terms for the fields in the gaps and trough region can vary. A convergence analysis to determine the number of expansion terms required for acceptable accuracy avoiding redundancy is also presented.

2.8.   REFERENCES

[2-1] Sorrentino R., *Numerical Methods for Passive Microwave and Millimeter Wave Structures*, IEEE Press, 1989

[2-2] Itoh T., *Numerical Techiques for Microwave and Millimeter-Wave Passive Structures*, Wiley Interscience, 1989

[2-3] S.B. Cohn, "*Properties of Ridge Wave Guide*", Proc IRE, Vol 35, August 1947, pp.783-788

[2-4] Uher, Bornemann, Rosenberg, *Waveguide Components for Antenna Feed Systems: Theory and CAD*, 1993, Artech House

[2-5] Hunter I., *Theory and Design of Microwave Filters*, IEE Press, London 2001

[2-6] Collin R., *Foundations of Microwave Engineering*, 2nd editions, IEEE Press, New York 2001

[2-7] J. Schwinger , *Discontinuities in waveguides* , Gordon and Breach Sc. Publ., New York, 1968

[2-8] J.P. Montgommery, "*On the complete eigenvalue solution of ridged waveguide*", IEEE Trans. Microwave Theory and Techniques, MTT-19, 457-555 (1971)

[2-9] MATLAB, Mathworks Inc.

[2-10] DIGITAL Visual FORTRAN

[2-12] George Goussetis, "Waveguide bandpass with improved performance", Ph.D. 2002.

Chapter III

Implementation of Ridge Coaxial WG in FORTRAN

In order to solve the homogeneous linear system described in (2.6-51) we are going to implement a computer algorithm using FORTRAN.

Cutoff wavenumbers will be obtained by mapping the whole range of wavenumber of interest. To search for the nontrivial solution of (2.6-51), the determinant of Bigmatrix has to be equal to zero. A group of eigenvalues that satisfy the characteristic equation can be obtained. Each eigenvalue corresponds to a cutoff wavenumber for a higher order TE mode in the Ridge coaxial waveguide.

After having found the cutoff wavenumbers kcs, we can determine the amplitude coefficients for each region, which are the eigenvectors of the problem, using the equations (2.6-47), (2.6-48) and (2.6-49). In order to use the results obtained from the previous procedure for mode matching techniques at a discontinuity, we have to achieve a power normalisation of the amplitude coefficients A1, A2 and A3.

Figure 3-1 outlines the flow chart of the subroutine RidgeTE(Q,Kcs,A1,A2,A3), which will return all the elements needed for the application of mode-matching technique for a ridged coaxial waveguide, where Q is the number of cuttoff wavenumbers to be found, Kcs is a vector where the found cuttoff wavenumbers will be stored., while A1, A2 and A3 will return the normalised amplitudes of the expansion terms for each mode in each region.

As it can be observed in the flow chart, this subroutine is built at the call of other subroutines and functions which are going to be brief explained below.

- **FUNCTION *DET_CHAR_MATTE(Kc)***

    This function will compute the value of the characteristic determinant for RIDGE COAXIAL WG propagation for TE even modes (magnetic symmetry) according to the formulation proposed by Bornemann. The characteristic matrix is built at the call of CHAR_MAT and then LU decomposition is applied.

- **SUBROUTINE *CHAR_MATTE(Kc,DUM)***

    This function will compute the characteristic matrix for Ridge Coaxial WG propagation for TE odd modes according to the formulation proposed by Bornemann. To build this matrix is necessary to call PmatrTE2 and PmatrTE3.

- **SUBROUTINE *PmatrTE2(Plm)***

    This subroutine builds the J_2 matrix (equation (2.6-25)) for a given Ridge Coaxial WG structure according to Bornemann Jc for Region 2 Dimensions are given in mm. Subroutine PmatrTE3 is used for Region 3 to build the J_3 matrix given by equation (2.6-26).

- **SUBROUTINE *CHECK_ROOTTE(KcSTART,KcSTOP)***

    This subroutine takes as an input the space where two values of the characteristic determinant change sign. It returns KcLOW=-1 if there is a pole in this space, or else a closer approximation to the root. If the KcLOW returns -10, it means that more than one time the sign changes within the given space. The method used actually sees whether the derivatives towards the point of changing sign lead to zero or to greater absolute values. In the latter case returns -1 (no root but pole), while in the first case the procedure is repeated in order to specify a shorter interval.

- **FUNCTION *NORMALTE(x)***

    This function returns the integral over a cross section of the square gradient of the transverse dependence of the vector potential. In order to normalise with respect to power, this quantity should be equal to one. Hence a normalisation coefficient x needs to be specified.

- **SUBROUTINE *BUILTTE(Kc,A1,A2,A3)***

This subroutine will solve the homogeneous linear system for a given Kc (the linear system of the characteristic Bigmatrix) in order to solve for the coefficients A1, A2 and A3 of the expansion terms in each region trough and gaps respectively.

Identical functions and subroutines have been built for TM modes to solve the homogeneous linear system described in (2.6-83) so they are not going to be explained in detail here.

Other important consideration concerning this developed program is that the dimensions of the structure must be read in the main function of the program. This function is in charge of the call to the subroutine RidgeTE for the TE modes and also the subroutine RidgeTM for the TM modes.

These dimensions are read from files and as it will be shown in chapter 4 these files will be made by MATLAB using a practical interface built for this purpose.
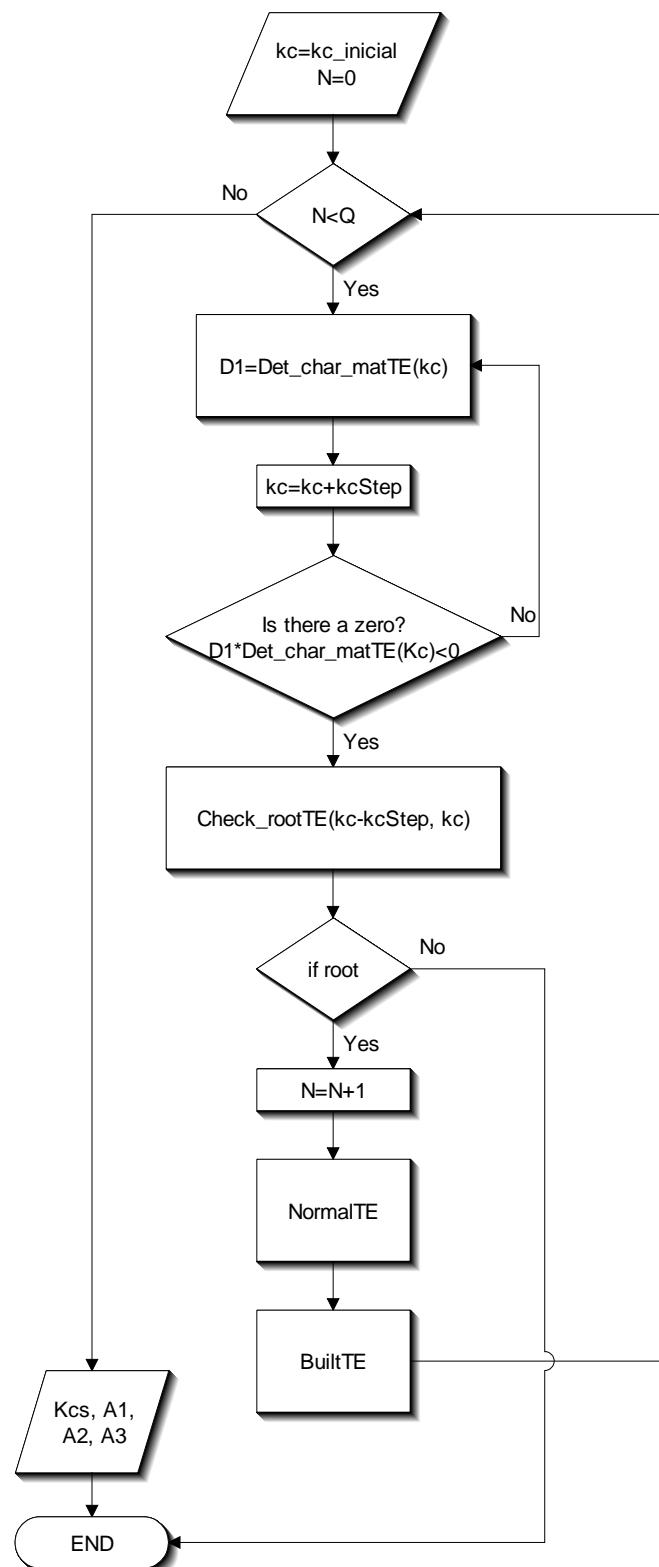
Figure 3-1. Flow chart of the subroutine RidgeTE

Chapter IV

Simulation in Matlab

MATLAB has been used to implement a graphic-user-interface (GUI), which allows the user to enter data, direct instructions and display computational results.

The computer program implemented in FORTRAN which was explained in the previous chapter, even though it is useful to calculate the elements needed for the application of mode-matching technique for a ridged coaxial waveguide, it is awkward to be used for an user in order to perform a better study of this structure. For this reason in order to provide a software easy to use and comfortable to specify the dimensions of the structure a practical interface has been developed in MATLAB. This interface allows to represent the electric and magnetic field distribution of each mode and can be useful to achieve parametric studies

This interface links FORTRAN and MATLAB to provide a very fast tool which is also easy to be used due to the fact that it is very visual and intuitive hence no further explanation is needed to be able to work with it. When an user introduces the dimensions of the waveguide in the interface, MATLAB writes them in files and calls FORTRAN which will read these files and solve the EM propagation for the given structure. After that FORTRAN will write the results in another file which will be read by MATLAB. With these results MATLAB will be able to represent the field distribution of each mode at cutoff.

In Figure 4-1 it is shown this graphical-user-interface (GUI) and a window provided by FORTRAN which contains a list of all the cutoff wavenumber for the specified number of required modes.

Another important characteristic of this interface is that it is general so not only Ridge Coaxial waveguide can be represented but also Ridge waveguide or Rectangular coaxial waveguide as particular cases.

It is interesting to make some remarks concerning the time needed to calculate the results and therefore the speed of this new tool. Such considerations offer an important point of view to compare our implemented code with a commercial software based on Finite Elements Method (Ansoft HFSS).

Table 4-1 gives the time required for both FORTRAN and HFSS on a Pentium VI, 2.4GHz and 512MB RAM for the simulation of a Ridge Coaxial WG when 20 modes are calculated.

Fortran	HFSS
6 sec.	372 sec. (6 min 12 seg)

Table 4-1: Time comparison

As can be observed, a considerable reduction of time is achieved with our implemented code, due to the time required by FORTRAN is more than 60 times lower.
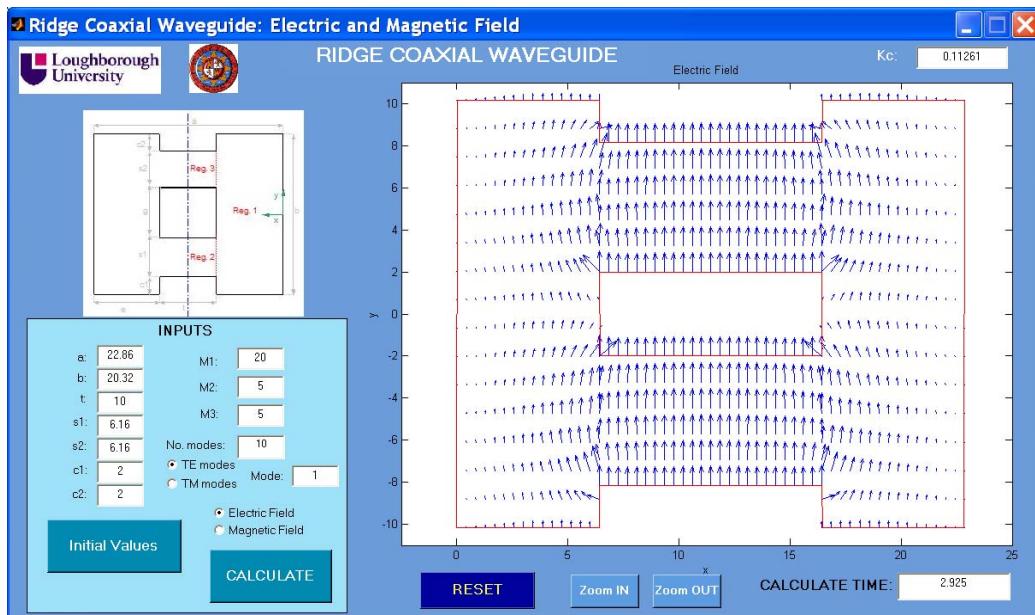
(a)
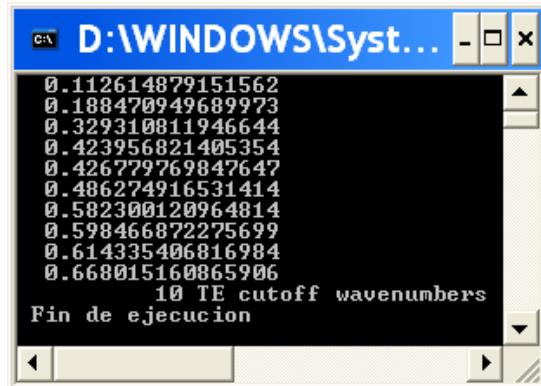
(b)

Figure 4-1: Graphical Interface (a) and list of all the cutoff wavenumbers (b)

Chapter V

Study of Convergence

A convergence analysis, generally in numerical analysis applications, is the one that investigates how an algorithm converges to a nominal value with increasing number of calculations or terms. In this section, the convergence of the cutoff wavenumber with increasing number of expansion terms is presented. Results obtained by this analysis will be useful in future works, where the solution of ridge waveguide and ridge coaxial waveguide can be used for the simulation of more complex structure. At that stage it will be useful to know how many expansion terms in each region is required in order to obtain accurate results, without overloading the simulation with terms that contribute to a negligible extend. Avoidance of redundancy is particularly essential in optimisation procedures, where the computational cost of each simulation is crucial for the efficiency.

The following subsections present the convergence to the cutoff wavenumber of the first order mode for different cases both ridge waveguide and ridge coaxial waveguide. This study of convergence is achieved by means of different tables with increasing number of expansion terms M1, M2 and M3 for the trough and gaps regions and this convergence is also plotted for an easier visualization of the results.

5.1. RIDGE WG

The study of convergence will be investigated trough different cases where the dimensions of the waveguide will be varied. It is reasonable to suppose that for narrower regions, a smaller value of M1 and M2 might suffice due to the fact that smaller areas can be described with less expansion terms.

Another important point to keep in mind is that the convergence under study is a relative convergence which means that there is a relationship between the number of expansion terms in each region. Therefore the number of expansion terms imposed for a region makes the expansion terms of the other region conditional on it.

5.1.1. BIGGER GAP

For this first convergence analysis, the dimensions of the waveguide under study are described in Table 5-1. The choice of these values is not random. It is important to point out that the selected value of the width of the ridges (T parameter) is 0.1mm which is a typical value used for the incorporation of this structure in a E-plane Filter which is one of the most important application of this structures, as it was said in the introduction.
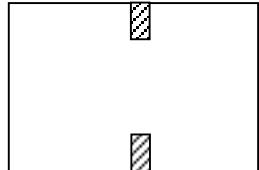
A=22.86	
B=10.16	
C1=2	
S1=6.16	
T=0.1	

Table 5-1: Dimensions of the Ridge WG in mm

Figure 5-1 shows the convergence analysis for the cutoff wavenumber of the first order TE and TM mode with increasing number of expansion terms M1 and M2 for the trough and gap region. This convergence is also plotted in each case.

TE		
M1	**M2**	**Kc (mode 1)**
2	1	0.1370382
4	2	0.1280003
6	3	0.1291708
8	4	0.1289010
10	5	0.1290258
12	6	0.1290228
14	7	0.1291148
16	8	0.1290425
18	9	0.1291585
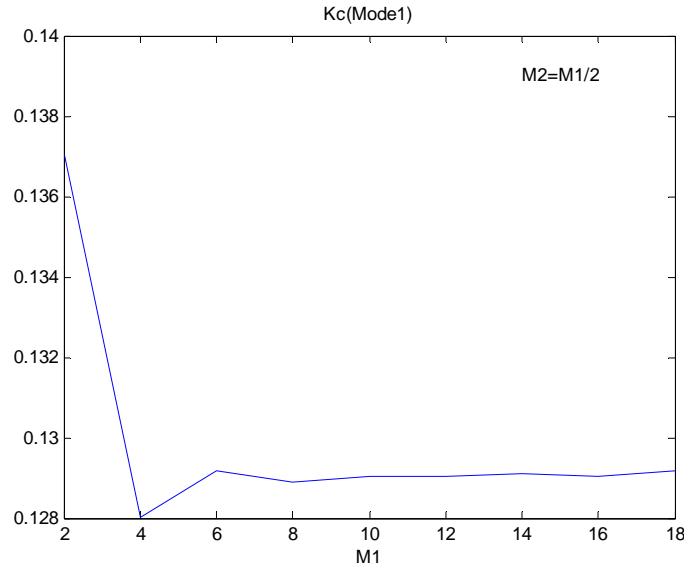
(a)

TM		
M1	**M2**	**Kc (mode 1)**
2	1	0.3408302
4	2	0.3696122
6	3	0.3652372
8	4	0.3679191
10	5	0.3671921
12	6	0.3674320
14	7	0.3673635
16	8	0.3673735
18	9	0.3672535
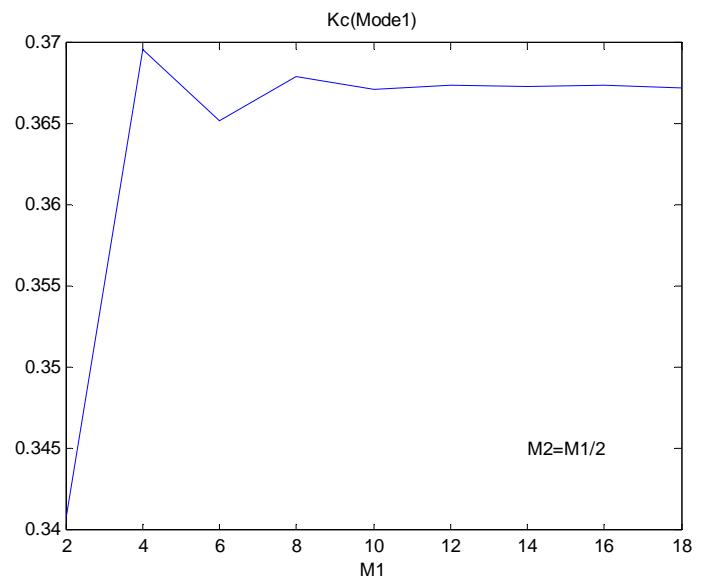
(b)

Figure 5-1: Convergence analysis for fundamental mode of ridge waveguide for TE (a) and TM (b) with dimensions as in Table 5-1

Very good results are observed for M1=10 and M2=5, indicating these values for further analysis. Note that for higher ridges narrower gaps are obtained, a smaller value of M2 might suffice. In any case, a convergence analysis can determine the required number of expansion terms as we will show in the following subsection.

5.1.2. SMALLER GAP

In this case the ridges are higher that is to say that the gap is smaller and therefore M2 should take a small value as it was commented before. The dimensions of the Ridge Waveguide in this case are given in Table 5-2.

A=22.86	
B=10.16	
C1=3	
S1=4.16	
T=0.1	

Table 5-2: Dimensions of the RIDGE WG in mm

TE		
M1	**M2**	**Kc (mode 1)**
3	1	0.1180807
6	2	0.1174843
9	3	0.1185982
12	4	0.1185903
15	5	0.1184472
18	6	0.1184639
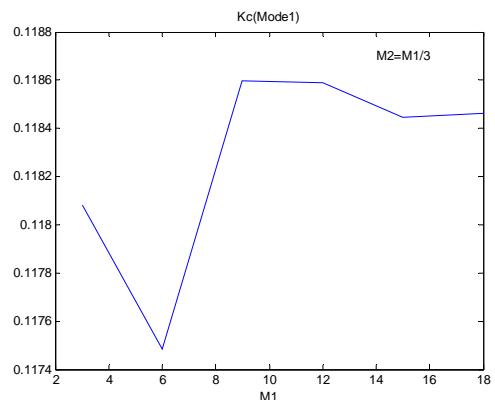
(a)

TM		
M1	**M2**	**Kc (mode 1)**
3	1	0.3884657
6	2	0.3935175
9	3	0.3919907
12	4	0.3923751
15	5	0.3920575
18	6	0.3920586
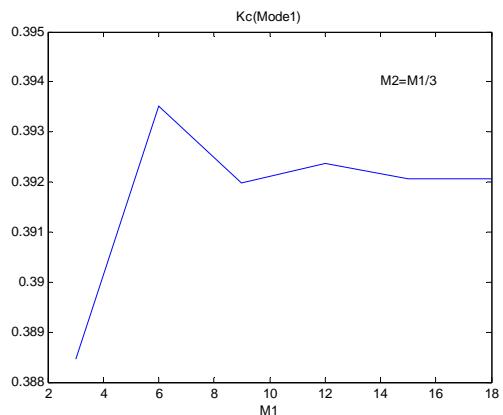
(b)

Figure 5-2: Convergence analysis for fundamental mode of ridge waveguide for TE (a) and TM (b) with dimensions as in Table 5-2

In this case very good results are observed for M1=9 and M2=3. As was to be expected, less number of expansion terms is needed to describe a smaller GAP.

5.2. RIDGE COAXIAL WG

To analyse the convergence for the Ridge Coaxial WG we will achieve the study of different cases. As it was explained for the Ridge WG, the selected value of the width of the ridges is 0.1mm for the first convergence analysis but for the second one it will be increased up to 10mm. It is reasonable to suppose that for wider regions, a bigger number of expansion terms will be needed due to the fact that bigger areas will be described.

5.2.1. THINER GAP

Figure 5-3 shows the convergence analysis for the cutoff wavenumber of the first order TE and TM mode with increasing number of expansion terms M1 M2 and M3 for the trough and gaps region respectively. The dimensions are given in Table 5-3. It is important to remember that the first mode in a coaxial line is the fundamental TEM but it is not studied in this project.

A=22.86	
B=20.32	
C1=C2=2	
S1=S2=6.16	
T=0.1	

Table 5-3: Dimensions of the RCWG in mm

TE			
M1	**M2**	**M3**	**Kc (mode 1)**
4	1	1	0.1370382
8	2	2	0.1280003
12	3	3	0.1291708
16	4	4	0.1289010
20	5	5	0.1290258
24	6	6	0.1290228
28	7	7	0.1291148
32	8	8	1.5316501

(a)
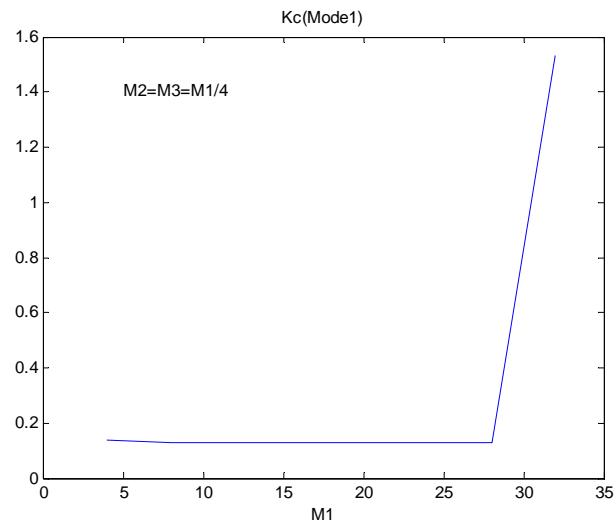
TM			
M1	**M2**	**M3**	**Kc (mode 1)**
4	1	1	0.265471
8	2	2	0.285755
12	3	3	0.283252
16	4	4	0.285051
20	5	5	0.284275
24	6	6	0.284650
28	7	7	0.284376
32	8	8	1.559424
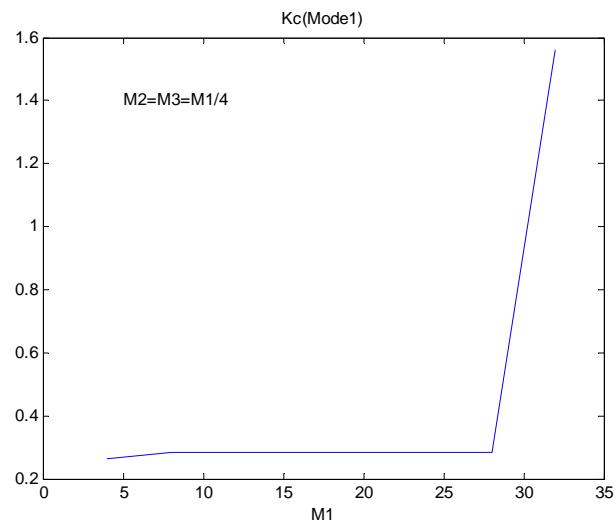
(b)

Figure 5-3: Convergence analysis for fundamental mode of ridge coaxial waveguide for TE (a) and TM (b) with dimensions as in Table 5-3

A good convergence is obtained for M1=16 and M2=M3=4 indicating these values for further analysis. Note that in this symmetric case the values for M2 and M3 are the same due to identical areas must be described by the same number of expansion terms. In an asymmetric case we have to choose a suitable number of expansion terms for each gap according to their areas.

5.2.2. WIDER GAP

Even though 10mm is not a practical value for the width of the ridges to incorporate this structure in an E-plane filter, with this convergence analysis we want to cover all the range of possible values of T. In this case the gaps are wider than in the previous case so a higher number of expansion terms is expected for these regions.

A=22.86	
B=20.32	
C1=C2=2	
S1=S2=6.16	
T=10	
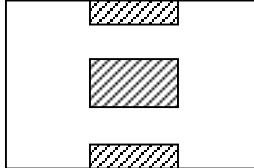
Table 5-4: Dimensions of the RCWG in mm

TE			
M1	**M2**	**M3**	**Kc (mode 1)**
4	1	1	0.1160672
8	2	2	0.1125561
12	3	3	0.1126907
16	4	4	0.1126218
20	5	5	0.1126148
24	6	6	0.1126142
28	7	7	0.1126224
32	8	8	0.1126081

(a)
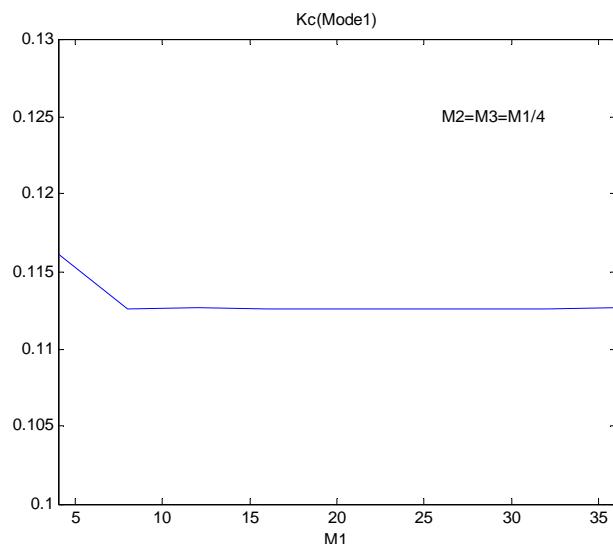
TM			
M1	M2	M3	Kc (mode 1)
4	1	1	0.4315221
8	2	2	0.4452796
12	3	3	0.4435193
16	4	4	0.4447320
20	5	5	0.4442496
24	6	6	0.4444737
28	7	7	0.4443219
32	8	8	0.4443823
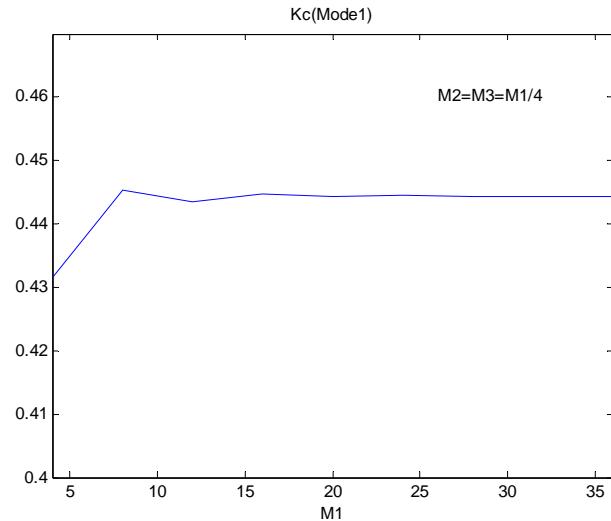
(b)

Figure 5-4: Convergence analysis for fundamental mode of ridge coaxial waveguide for TE (a) and TM (b) with dimensions as in Table 5-4

As was to be expected, the number of expansion terms for the gap regions which allows a fine convergence is higher than in the previous case. Good results are observed for M1=20 and M2=M3=5. As it was pointed out before, for an asymmetric structure a suitable number of expansion terms for each gap region must be chosen according to their areas.

Chapter VI

Cutoff frequency and modes distributions

The first parameter to compare with commercial software in order to validate the accuracy of the developed program and to validate the chosen number of expansion terms is the cutoff frequency. This section presents the results obtained by the field matching method based on Generalized Transverse Resonance (GTR) in comparison with cutoff frequencies given by a commercial software based on Finite Elements Method (FEM) (Ansoft HFSS). Comparison between the found cutoff wavenumber (rad/mm) for the first four modes of the ridged waveguide, coaxial waveguide and ridge coaxial waveguide are going to be presented. As it will be shown below, the very good agreement of the developed code with the commercial software validates the accuracy of the former.

In this section it is also shown the electric and magnetic field distribution for the first four TE and TM modes. It is interesting to make some remarks concerning these representations. The components along the x-y plane are the only ones which are depicted here. That is to say that for the TE modes, due to the electric field has no components along z this field is completely defined in this plane but for the magnetic field the z-component of the field should be taken into account even though this component is not represented in the following figures. For the TM modes the z-component of the electric field is omitted.

We will start showing the study for Ridge WG and CWG since they are known structures and then we will focus on the structure under study in this project, Ridge Coaxial WG.

6.1. SYMMETRIC CASE

In this subsection, symmetrical structures of Ridge WG, Coaxial WG and Ridge Coaxial WG will be studied in order to show results easier to understand due to the fact that the knowledge of symmetry properties can be applied for a better explanation of them.

6.1.1. RIDGE WAVEGUIDE

The dimensions (in mm) of the structure under study are given in Table 6-1.

A=22.86	
B=20.32	
C1=2	
S1=6.16	
T=10	
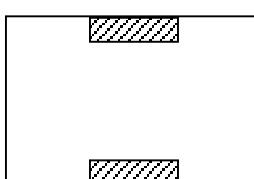
Table 6-1: Dimensions of the RIDGE WG in mm

Table 6-2 gives the comparison between the four first cutoff wavenumbers (rad/mm) as obtained with GTR and commercial FEM software. 10 expansion terms are used for the transverse dependence of the vector potentials in region 1, while 5 expansion terms are used in region 2. Very good agreement is observed and the relative error between the two methods is less than $.8.37 \cdot 10^{-4}$.

TE			TM		
GTR	FEM	Relative error	GTR	FEM	Relative error
0.1126148	0.1125263	7.86E-04	0.4734103	0.4734610	1.07E-04
0.3293108	0.3295866	8.37E-04	0.5913421	0.5913071	5.92E-05
0.4239568	0.4239807	5.64E-05	0.7661710	0.7655540	8.06E-04
0.5823001	0.5824866	3.20E-04	0.8117262	0.8120421	3.89E-04

Table 6-2: Comparison between the four first cutoff wavenumbers (rad/mm) as obtained with GTR and commercial FEM software.

In the following figure it is outlined the Electric and Magnetic fields for the first four TE modes showing the value of the wavenumber in each case.

*TE modes: Electric and Magnetic Fields*

MODE 1 (Kc= 0.1126148)	MODE 2 (Kc= 0.3293108)
MODE 3 (Kc= 0.4239568)	MODE 4 (Kc= 0.5823001)

Figure 6-1: Electric and Magnetic fields distribution for the four first TE modes at cutoff

TM modes: Electric and Magnetic Fields

MODE 1 (Kc=0.4734103)	MODE 2 (Kc= 0.5913421)

MODE 3 (Kc= 0.7661710)	MODE 4 (Kc= 0.8117262)

Figure 6-2: Electric and Magnetic fields for the four first TM modes at cutoff
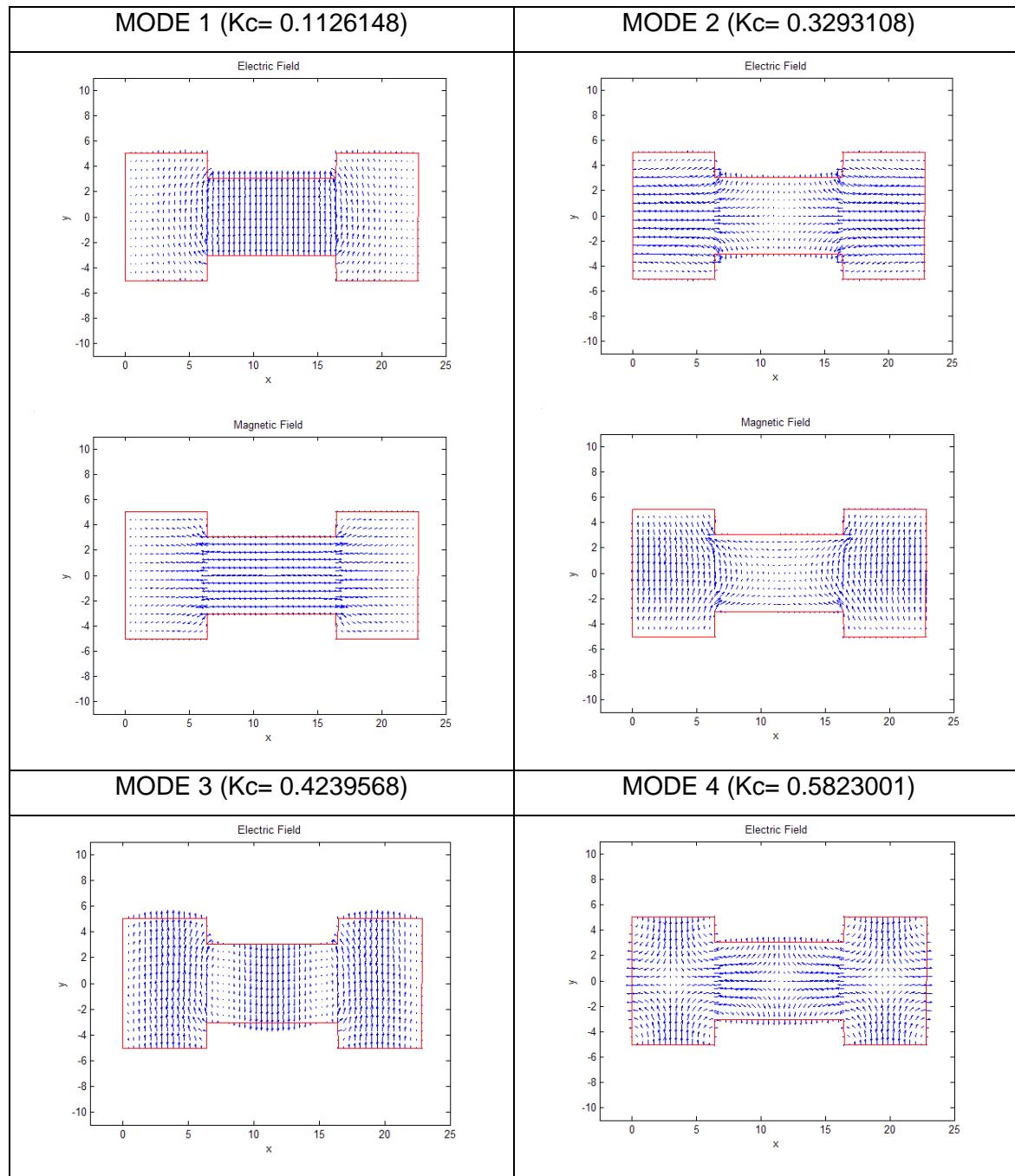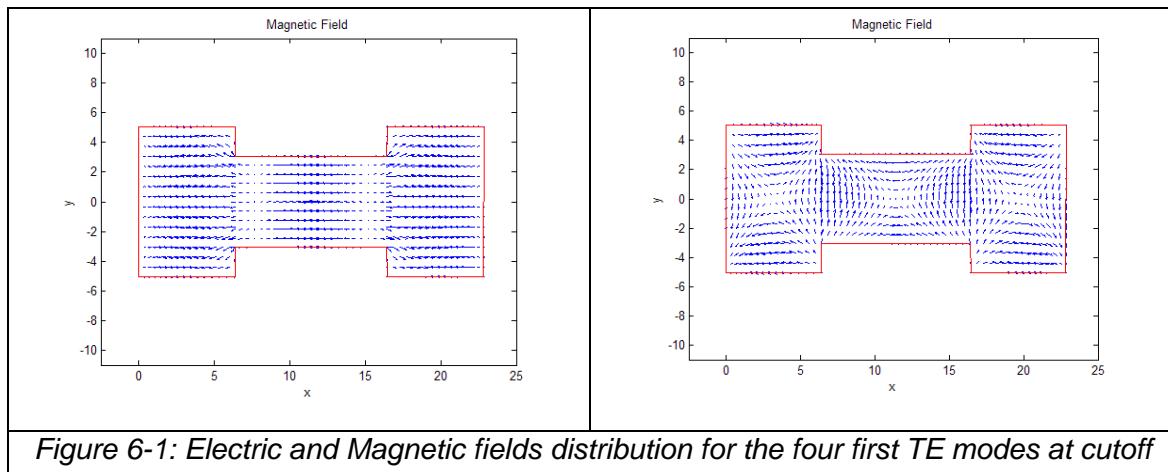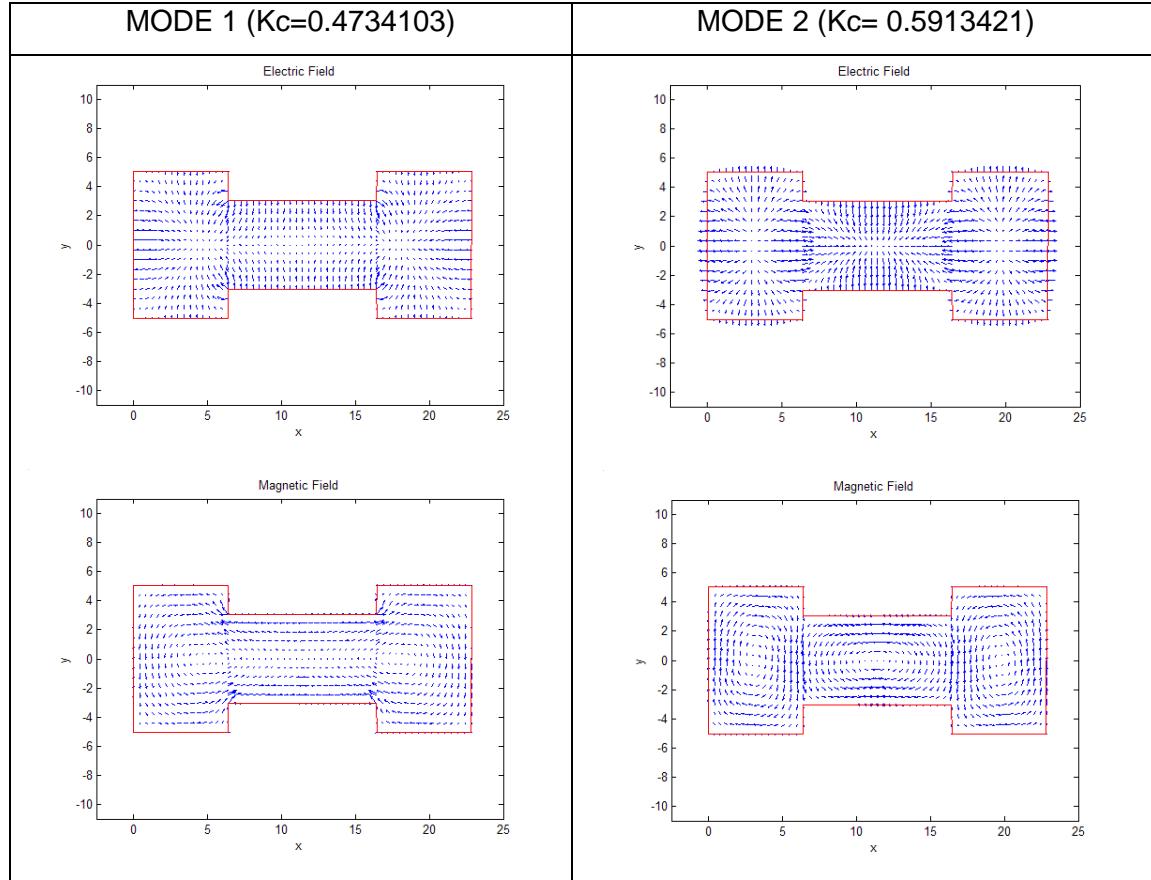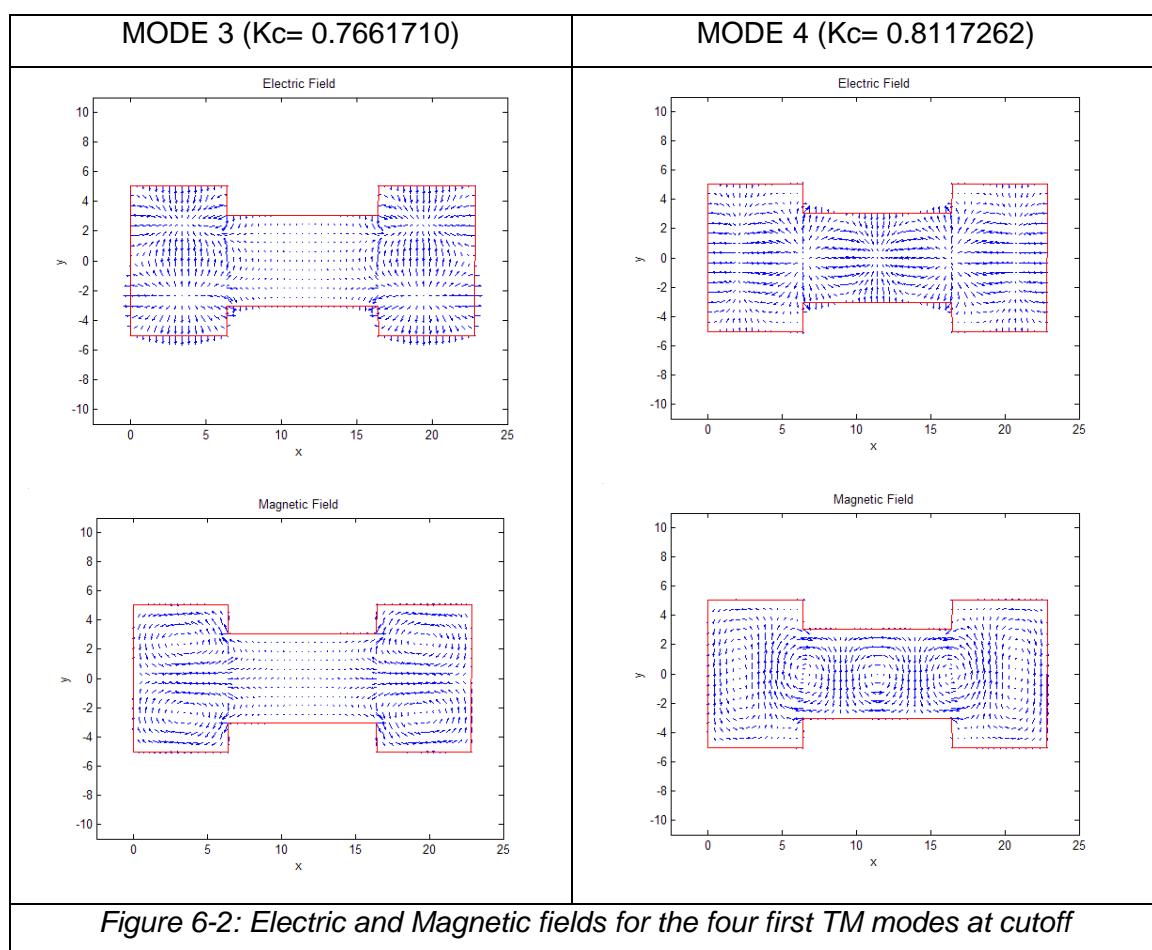
6.1.2. COAXIAL WAVEGUIDE

Table 6-4 gives the comparison between the found cutoff wavenumber (rad/mm) for the first four modes of the coaxial waveguide. The dimensions of the structure (in mm) are given in Table 6-3. 20 expansion terms are used for the transverse dependence of the vector potentials in region 1, while 5 expansion terms are used in region 2 and 3. Very good agreement is observed and the relative error between the two methods is less than $7.10 \cdot 10^{-4}$.

A=22.86	
B=20.32	
S1=8.16	
S2=8.16	
T=10	
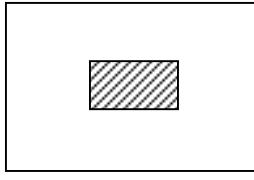
Table 6-3: Dimensions of the CWG in mm

TE			TM		
GTR	FEM	Relative Error	GTR	FEM	Relative Error
0.1253606	0.1253083	4.17E-04	0.3894359	0.3892427	4.96E-04
0.2008842	0.2009105	1.31E-04	0.3979667	0.3978852	2.05E-04
0.3334922	0.3336862	5.81E-04	0.5016423	0.5012863	7.10E-04
0.4182422	0.4182636	5.12E-05	0.5368520	0.5367572	1.77E-04

Table 6-4: Comparison between the four first cutoff wavenumbers (rad/mm) as obtained with GTR and commercial FEM software.

The electric and magnetic field distribution is outlined below. As it was pointed out before, it is important to keep in mind that in coaxial line the first mode is the fundamental TEM whose cutoff frequency is zero. This mode is not study in this project so it is not included in the following figure.

## TE modes: Electric and Magnetic Fields

MODE 1 (Kc= 0.1253606)	MODE 2 (Kc= 0.2008842)
MODE 3 (Kc= 0.3334922)	MODE 4 (Kc= 0.4182422)

Figure 6-3: Electric and Magnetic fields for the four first TE modes

TM modes: Electric and Magnetic Fields

MODE 1 (Kc= 0.3894359)	MODE 2 (Kc= 0.3979667)

MODE 3 (Kc= 0.5016423)	MODE 4 (Kc= 0.5368520)
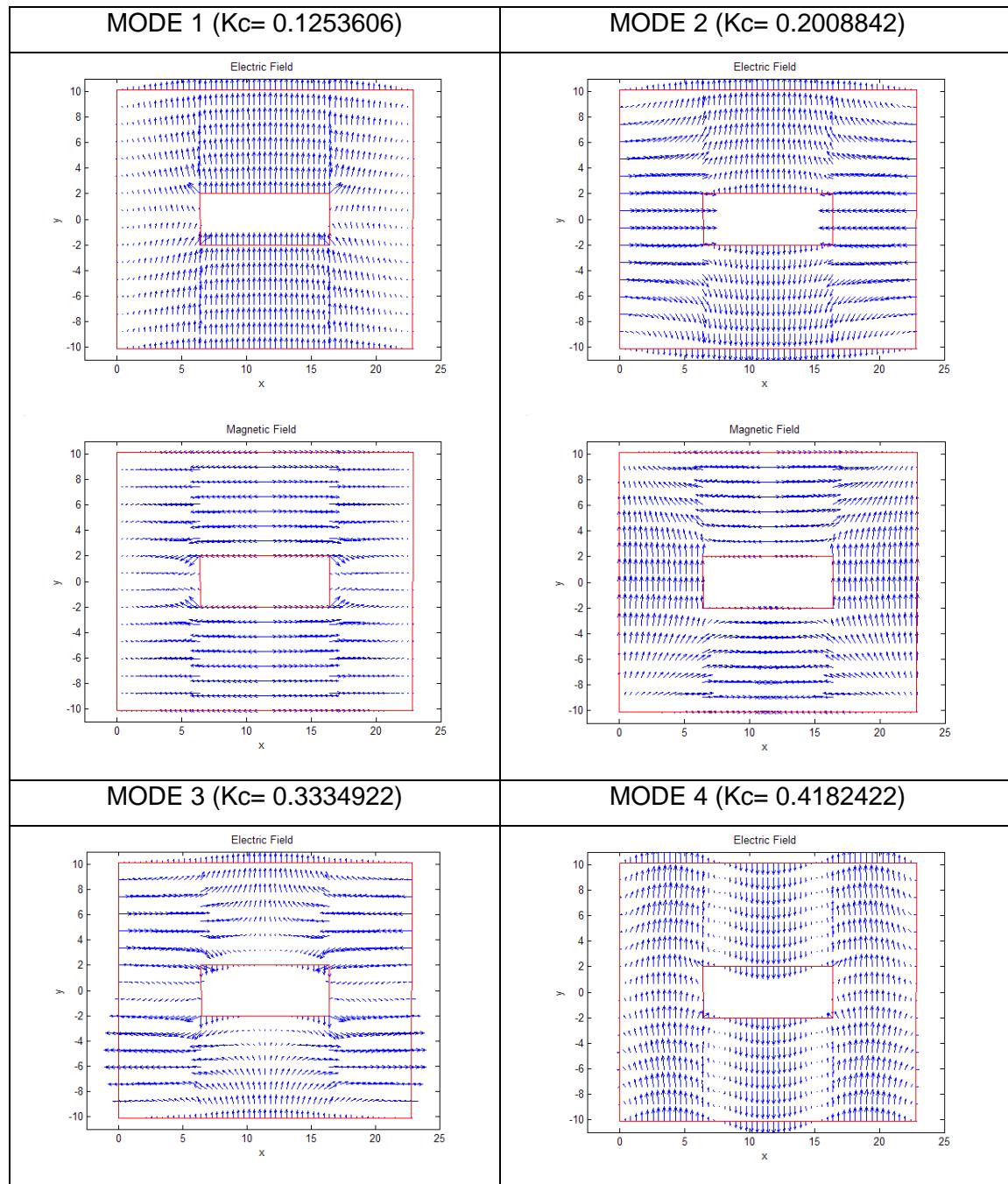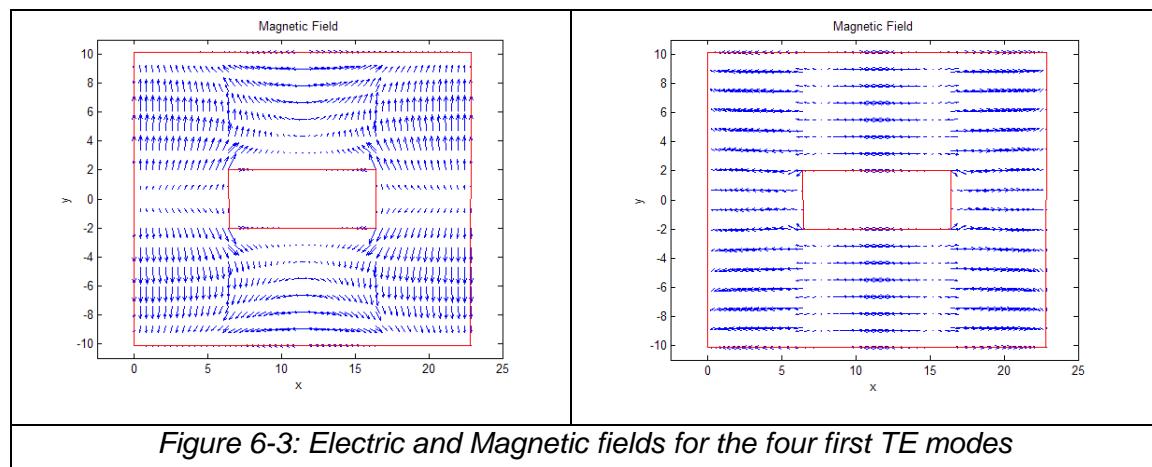
Figure 6-4: Electric and Magnetic fields for the four first TM modes
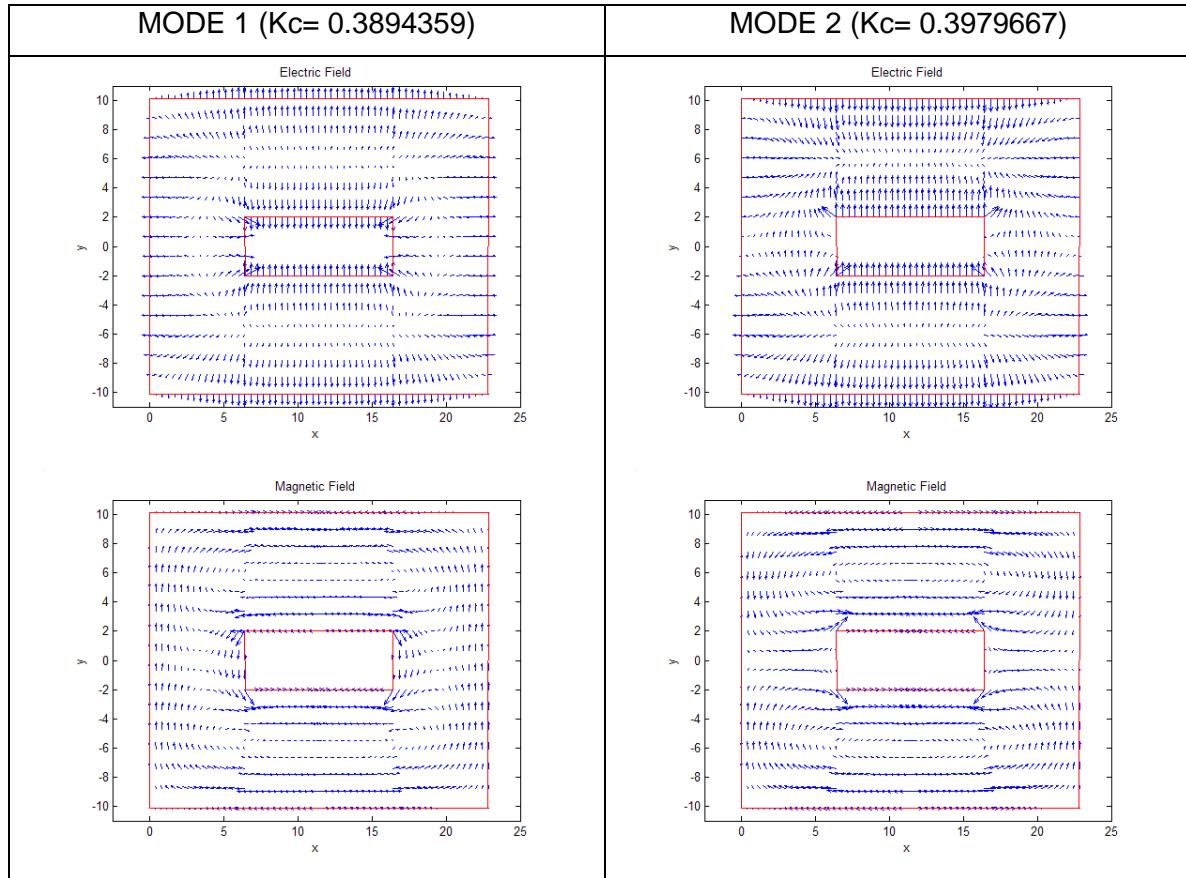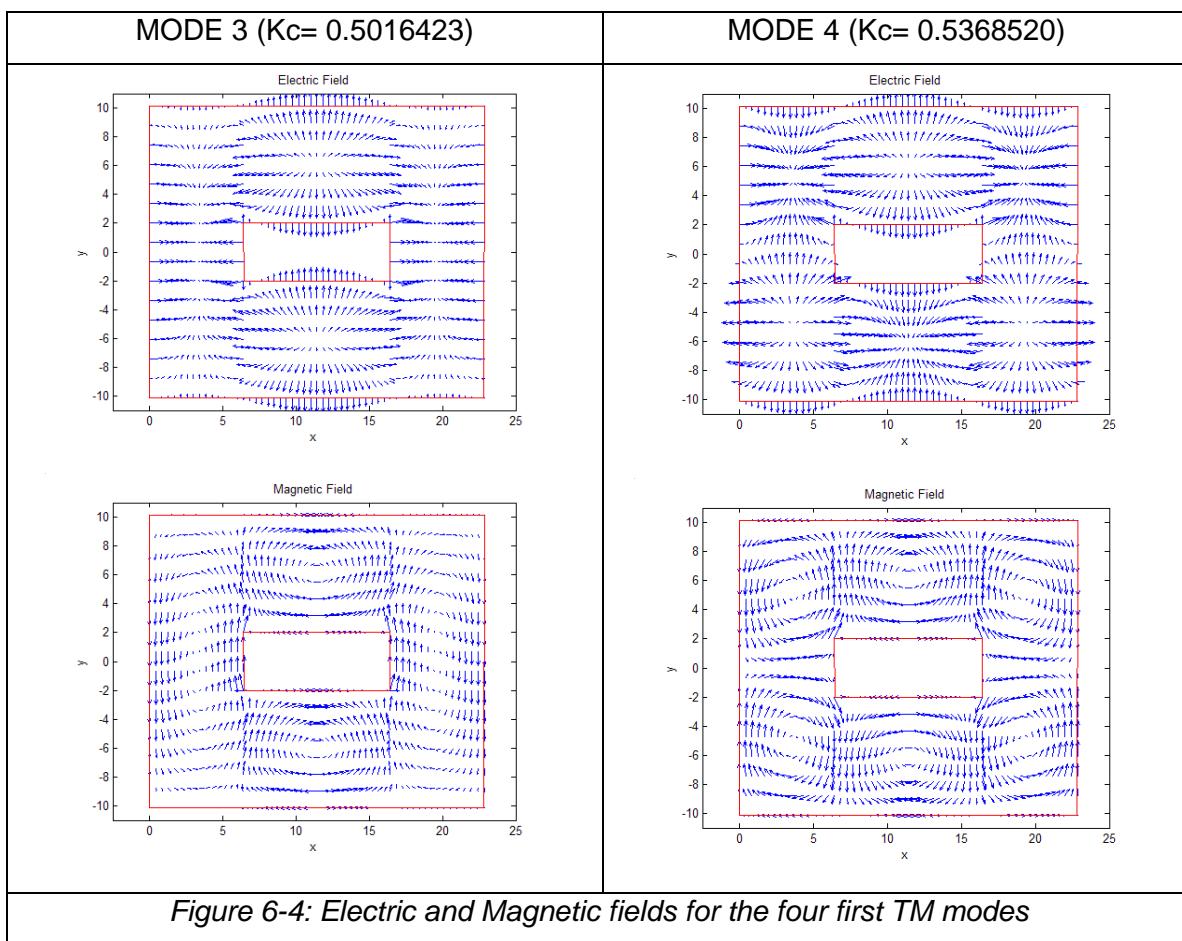
6.1.3. RIDGE COAXIAL WAVEGUIDE

Once Ridge WG and Coaxial WG have been analysed the Ridge Coaxial WG will be studied. As it was done before, the results obtained by the field matching method in comparison with cutoff wavenumber given by Finite Elements Method will be presented. The dimensions of the structure under study are given in Table 6-5. In this case, 20 expansion terms are used for the transverse dependence of the vector potentials in trough region, while 5 expansion terms are used in gap regions. Very good agreement is observed and the relative error between the two methods is less than $8.80 \cdot 10^{-4}$.
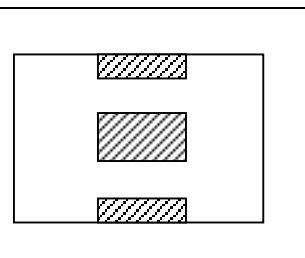
A=22.86	
B=20.32	
C1=C2=2	
S1=S2=6.16	
T=10	

Table 6-5: Dimensions of the RCWG in mm

TE			TM		
GTR	FEM	Relative Error	GTR	FEM	Relative Error
0.11261	0.11252	8.00E-04	0.44424	0.44419	1.13E-04
0.18847	0.18852	2.65E-04	0.47341	0.47354	2.75E-04
0.32931	0.32960	8.80E-04	0.56622	0.56623	1.77E-05
0.42395	0.42397	4.72E-05	0.59134	0.59139	8.45E-05

Table 6-6: Comparison between the four first cutoff wavenumbers (rad/mm) as obtained with GTR and commercial FEM software.

Below it is shown the Electric and Magnetic fields distribution for the four first TE and TM modes.

TE modes: Electric and Magnetic Fields

MODE 1 (Kc=0.1126148)	MODE 2 (Kc= 0.1884709)

MODE 3 (Kc=0.3293108)

MODE 4 (Kc= 0.4239568)

Figure 6-5: Electric and Magnetic fields for the four first TE modes

TM modes: Electric and Magnetic Fields
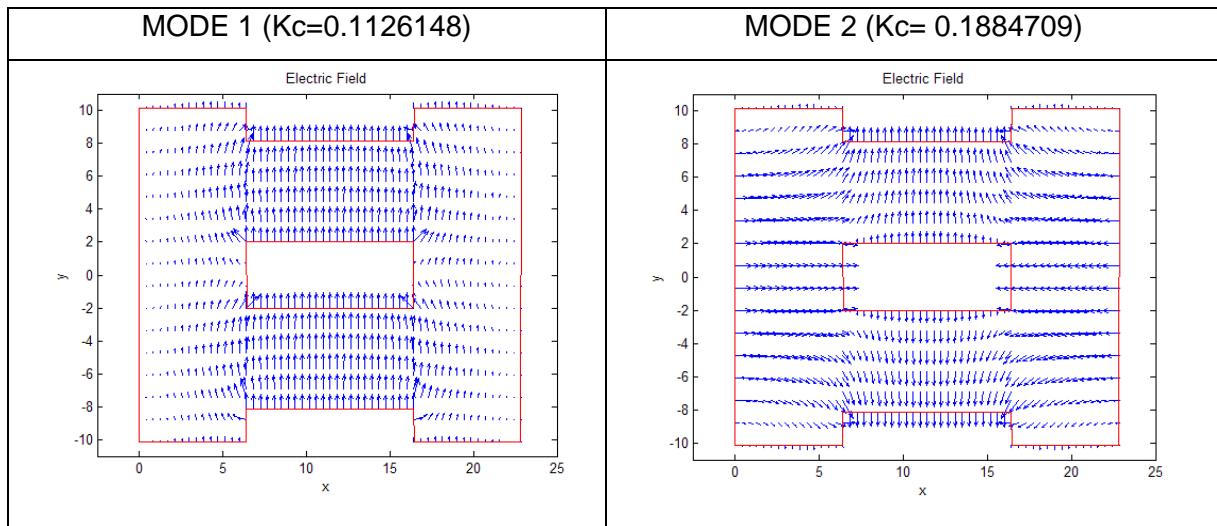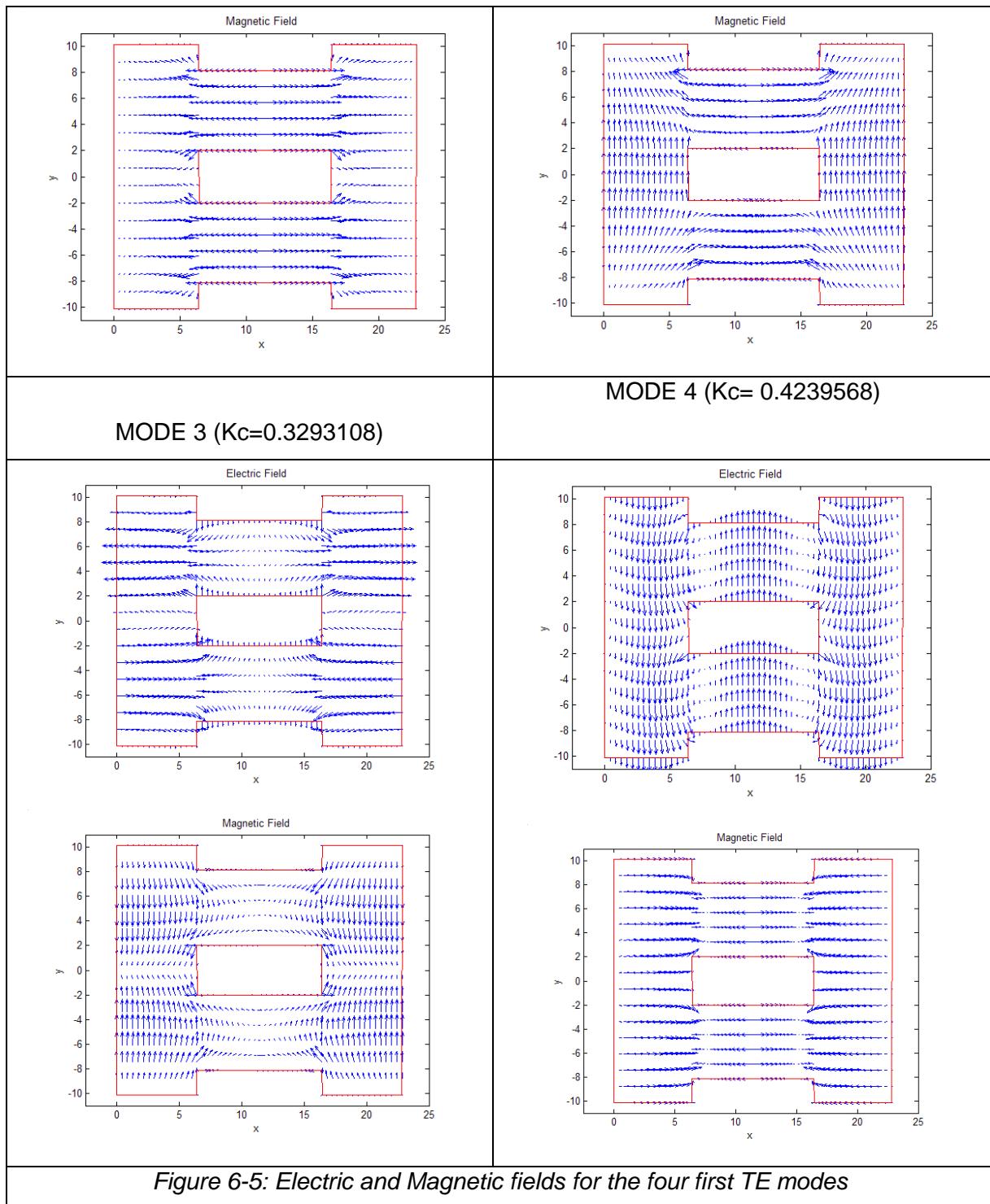
Figure 6-6: Electric and Magnetic fields for the four first TM modes
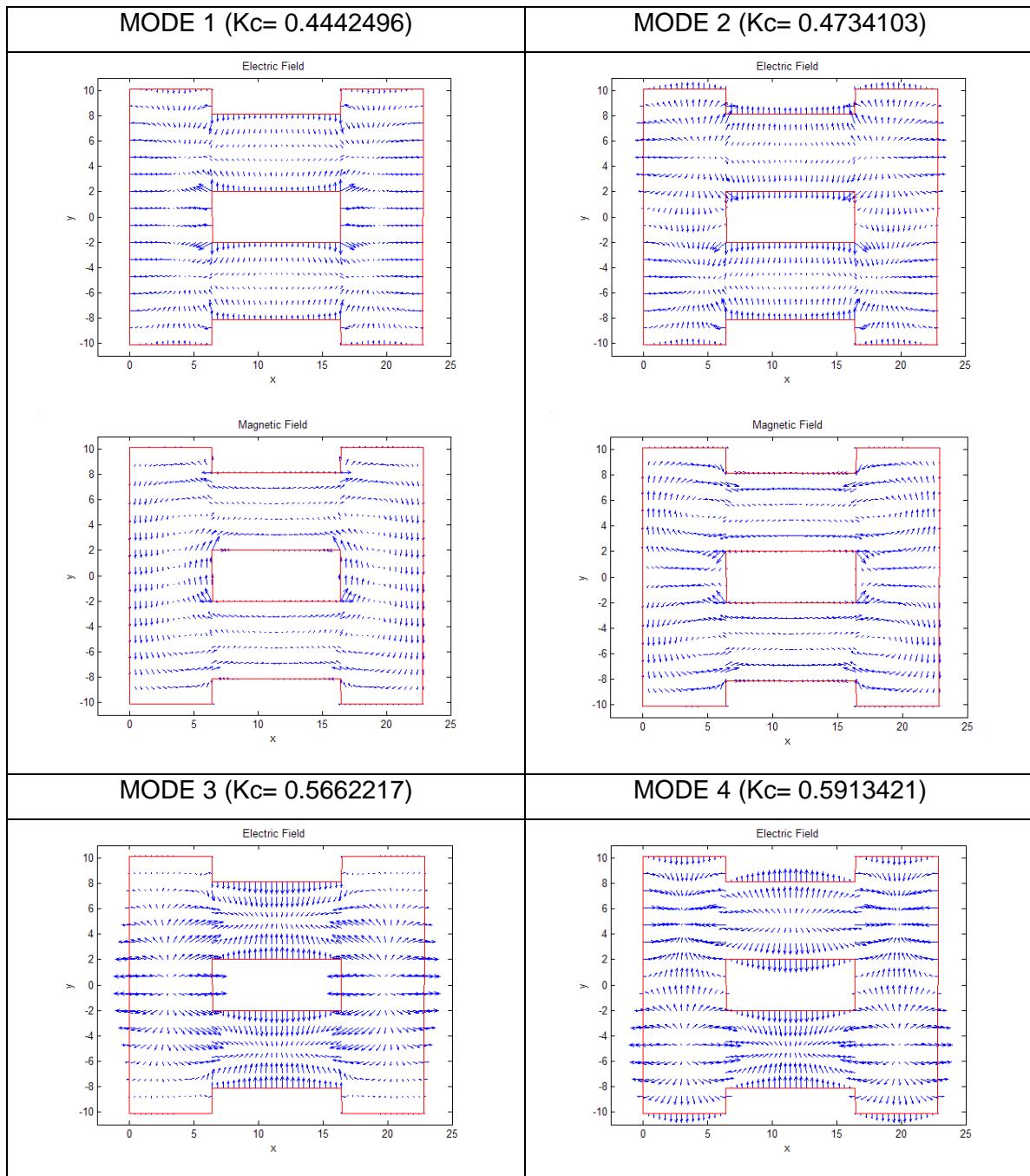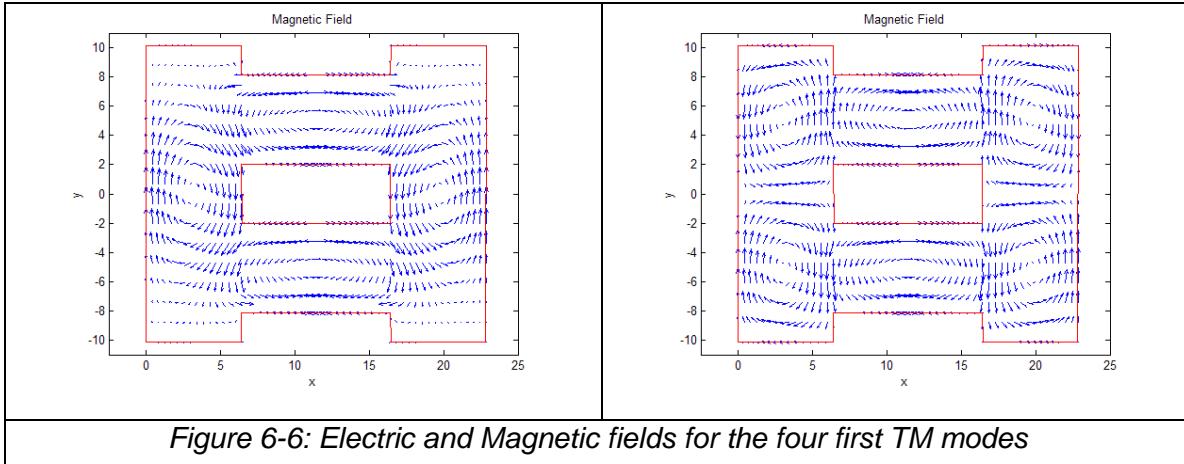
6.1.4. COMPARATION

After presenting the cutoff wavenumber and the field distribution for the three different structures, we will try to compare the results obtained for the Ridge Coaxial WG with the Ridge WG and Coaxial WG in order to find some relationships between them and also to show how the introduction of the ridges modifies the propagation characteristic of the structure. With this study a better understanding of the Ridge Coaxial WG will be achieved.

6.1.4.1. RIDGE WG-RIDGE COAXIAL WG

Beginning from the electric field distribution of Ridge Coaxial Waveguide, as shown in Figure 6-7, in both gaps the field distribution of the first mode resembles that of the double ridge waveguide. However, for the second mode, the field distribution does not obey this rule.

To try to explain this, some remarks have to be taken into account. These considerations derive from the symmetry of the structure. In this symmetric case the structure has the symmetric shape not only in both sides of axis y but also in both sides of axis x. To study all the possible cases, an electric and a magnetic wall have to be considered at y=0. If we think about the mode which appears when a PEC at y=0 is studied, it is easy to realise that this structure consists of two Ridge WG. So the field distribution must be the same to the double ridge waveguide and both modes must have the same value of Kc. When a PMC lies at y=0 this consideration is not true any more so we can not find a relationship between Ridge Coaxial WG and Ridge WG for this mode.

Kc(Mode1)=0.1126148

(a)

Kc(Mode1)=0.1126148

(b)

Kc(Mode2)=0.1884709

(c)
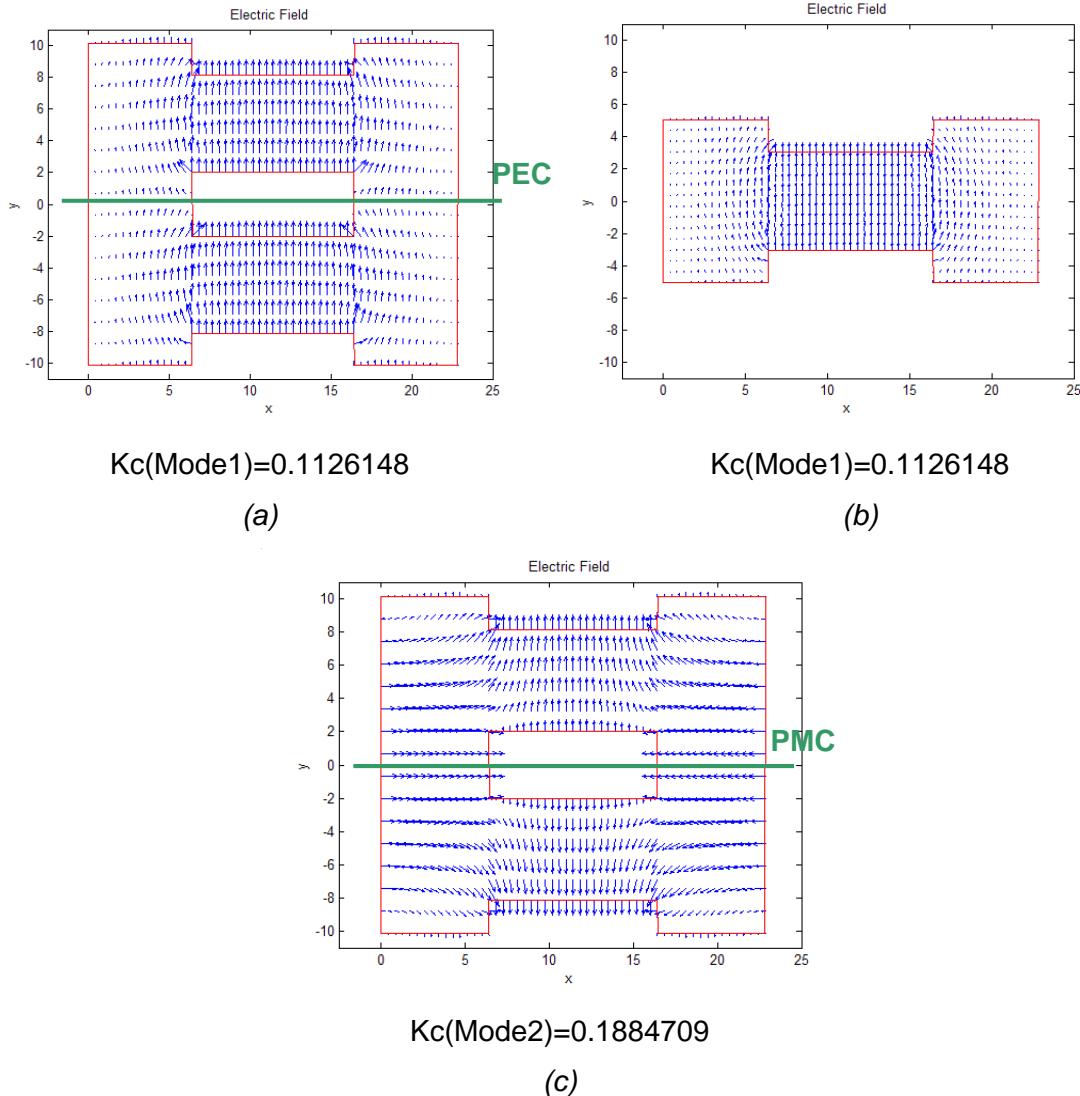
Figure 6-7: Electric field distribution for the first (a) and second (c) TE mode in RCWG and the first TE mode in RCW (b)

Figure 6-7 shows the Electric field distribution for the first and second TE modes in a Ridge Coaxial WG. From these field distributions it is easy to detect when a PMC or a PEC is lied at y=0. For the first mode of a Ridge Coaxial WG, the Electric field passes through the symmetry plane perpendicularly so we can be sure that it is a PEC and therefore we can compare this first mode with the first mode in a Ridge WG obtaining the same field distribution and the same value of Kc, as it is shown above. For the second mode, the Electric field is parallel to the symmetry plane so we can affirm that it is a PMC.

In Table 6-7 it is shown the equivalence of the wavenumbers for the TE and TM modes of each structure.

74

TE		TM	
RCWG	**RIDGE WG**	**RCWG**	**RIDGE WG**
0.1126148 (mode=1)	0.1126148 (mode=1)	0.4442496 (mode=1)	
0.1884709 (mode=2)		0.4734103 (mode=2)	0.4734103 (mode=1)
0.3293108 (mode=3)	0.3293108 (mode=2)	0.5662217 (mode=3)	
0.4239568 (mode=4)	0.4239568 (mode=3)	0.5913421 (mode=4)	0.5913421 (mode=2)
0.4267797 (mode=5)		0.6505550 (mode=5)	
0.4862749 (mode=6)		0.7661710 (mode=6)	0.7661710 (mode=3)
0.5823001 (mode=7)	0.5823001 (mode=4)	0.8050348 (mode=7)	

Table 6-7: Equivalence of the wavenumbers (rad/mm) for the TE and TM modes in RCWG and RIDGE WG.

From Figure 6-4 and Figure 6-6 we can check that for these TE modes with the same value of Kc (in blue) the field distribution in Ridge Coaxial Waveguide is the double of the corresponding mode field in a Ridge waveguide. For the TM modes, Figure 6-5 and Figure 6-7 help us to check it.

6.1.4.2. COAXIAL WG-RIDGE COAXIAL WG

As it is shown in Figure 6-8, the field distribution of the first TE and TM mode in a Coaxial WG and a Ridge Coaxial WG are quite similar, but the cutoff wavenumbers are different, without any relationship between them.

It is noted that the field distribution of each mode in Ridge Coaxial WG seems to be a modification of the corresponding mode field in a CoaxialWG, due to the presence of the ridges.

Loading the ridges, the wavenumbers of the TE mode decrease with respect to the case without ridges. The opposite behaviour is found for the wavenumbers of the TM modes.

| Mode 1 Kc= 0.1253606 | Mode 1 Kc=0.1126148 |

(a)

| Kc= 0.3894359 | Kc= 0.4442496 |

(b)
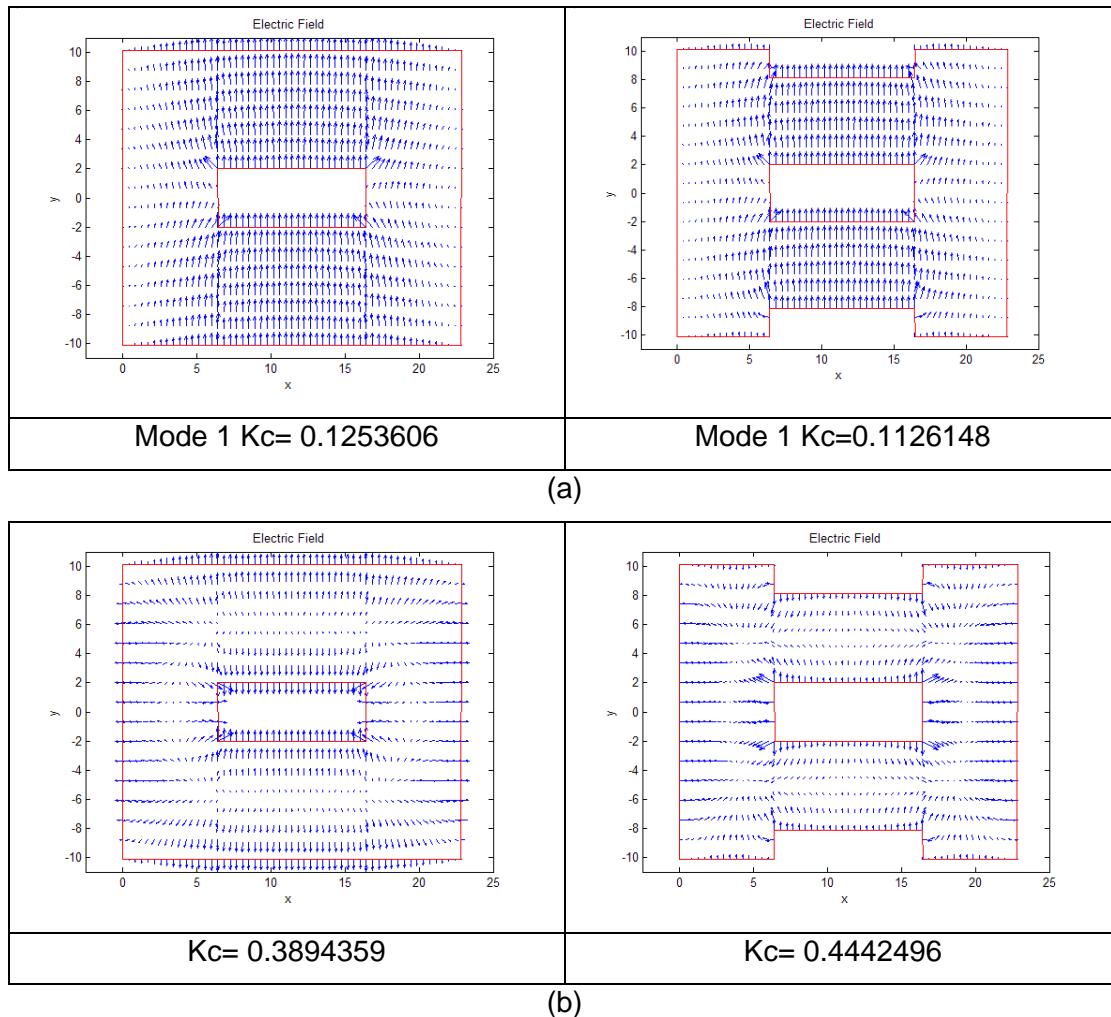
Figure 6-8: Representation of the Electric field for the first TE (a) and TM (b) modes in a Coaxial WG and RCWG

76

6.2.   ASYMMETRIC CASE

In this subsection, asymmetrical structures of Ridge WG, Coaxial WG and Ridge Coaxial WG will be studied. As it will be shown, in this asymmetric case it is very difficult to explain the relationship among them because no symmetric consideration can be taken into account.

However this study is interesting for many reasons. On one hand, because among the several geometries reported in the literature, the asymmetric structures have received little attention. On the other hand, to demonstrate that the variation of the dimensions of the structures modifies the propagation characteristic of the waveguides. It will be in section 7 where the parametric studies will be achieved.

6.2.1.   RIDGE WG

The dimensions (in mm) of the asymmetric structure under study are given in Table 6-8.

| A=22.86 |
| B=10.16 |
| C1=2 |
| C2=6.16 |
| S1 =2 |
| T=10 |
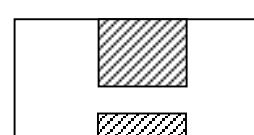
Table 6-8-: Dimensions of the RIDGE WG in mm

Table 6-9 gives the comparison between the two methods for each mode in the waveguide. 10 expansion terms are used for the transverse dependence of the vector potentials in region 1, while 5 expansion terms are used in region 2. Very good agreement is observed and the relative error between the two methods is less than $5.46 \cdot 10^{-3}$.

TE			TM		
GTR	**FEM**	**Relative Error**	**GTR**	**FEM**	**Relative Error**
0.0682961	0.0681310	2.42E-03	0.5722390	0.5725895	6.12E-04
0.3112128	0.3112817	2.21E-04	0.7818098	0.7822001	4.99E-04
0.4530046	0.4554894	5.46E-03	1.007327	1.0080592	7.26E-04
0.5455799	0.5449203	1.21E-03	1.047498	1.0476637	1.58E-04

Table 6-9: Comparison between the four first cutoff wavenumbers (rad/mm) as obtained with GTR and commercial FEM software.

Below it is shown the Electric and Magnetic fields distribution for the four first TE and TM modes.

TE modes: Electric and Magnetic Fields

MODE 3 (Kc= 0.4530046)	MODE 4 (Kc= 0.5455799)

Figure 6-9: Electric and Magnetic fields for the four first TE modes

TM modes: Electric and Magnetic Fields
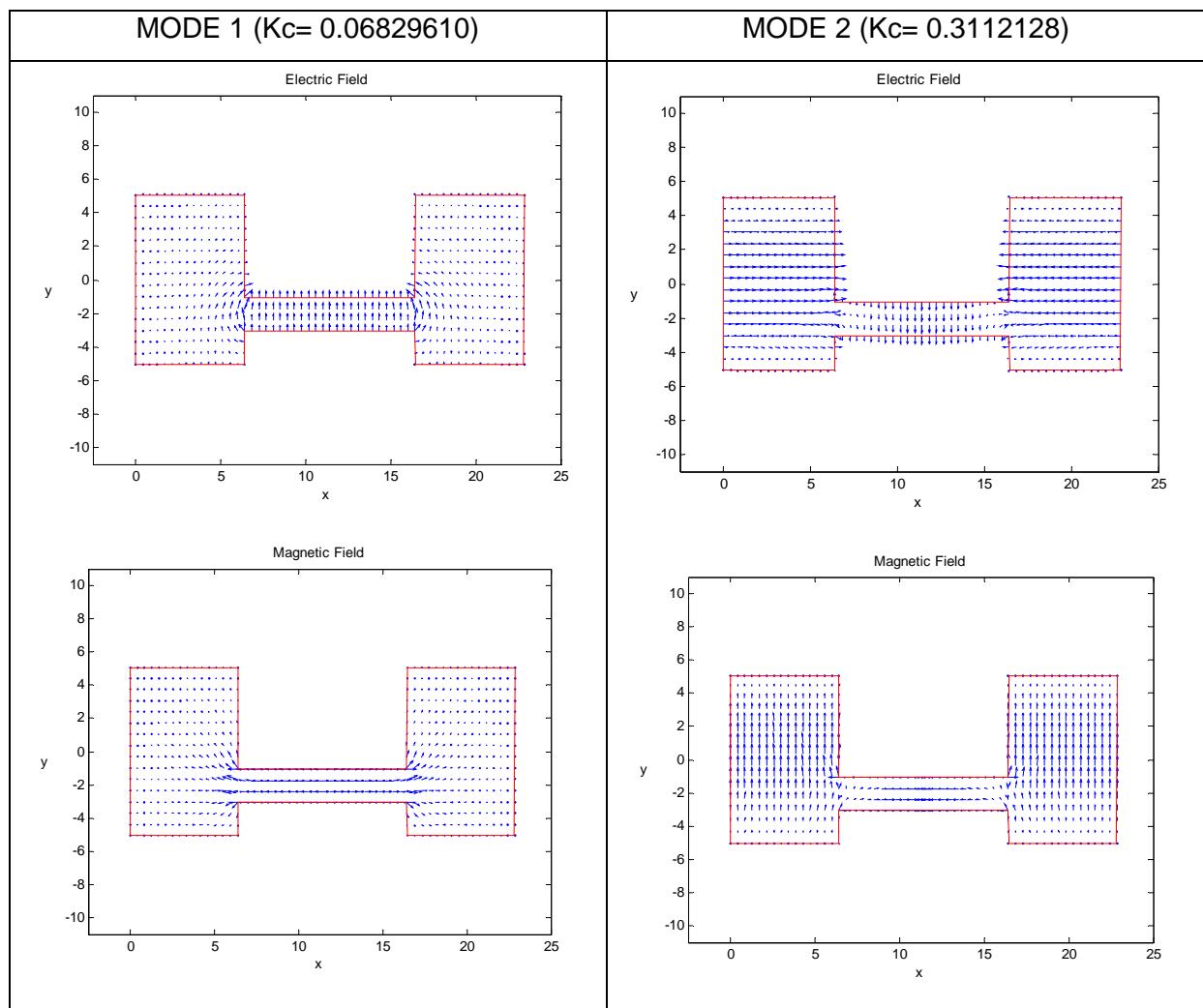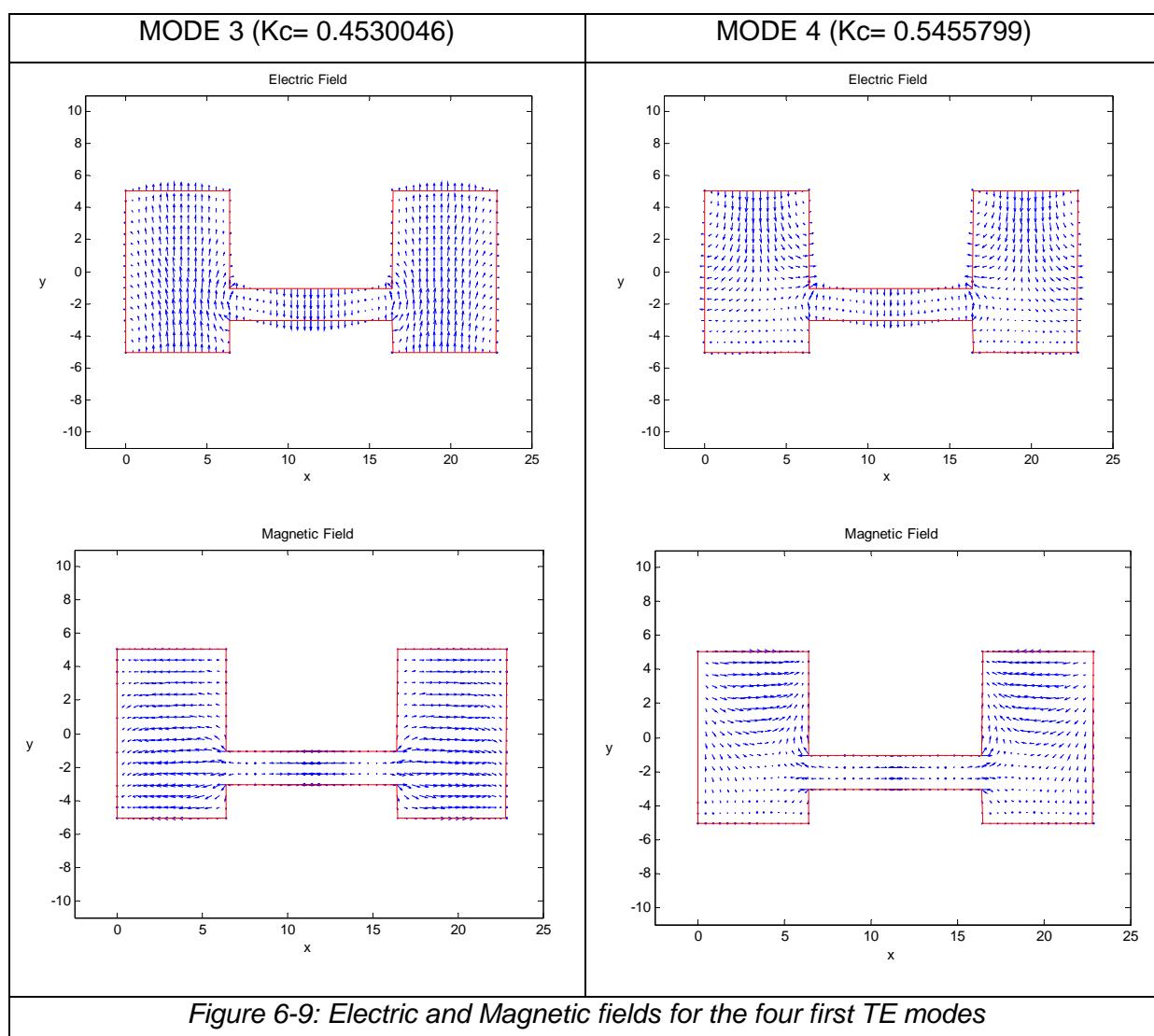
Figure 6-10: Electric and Magnetic fields for the four first TM modes
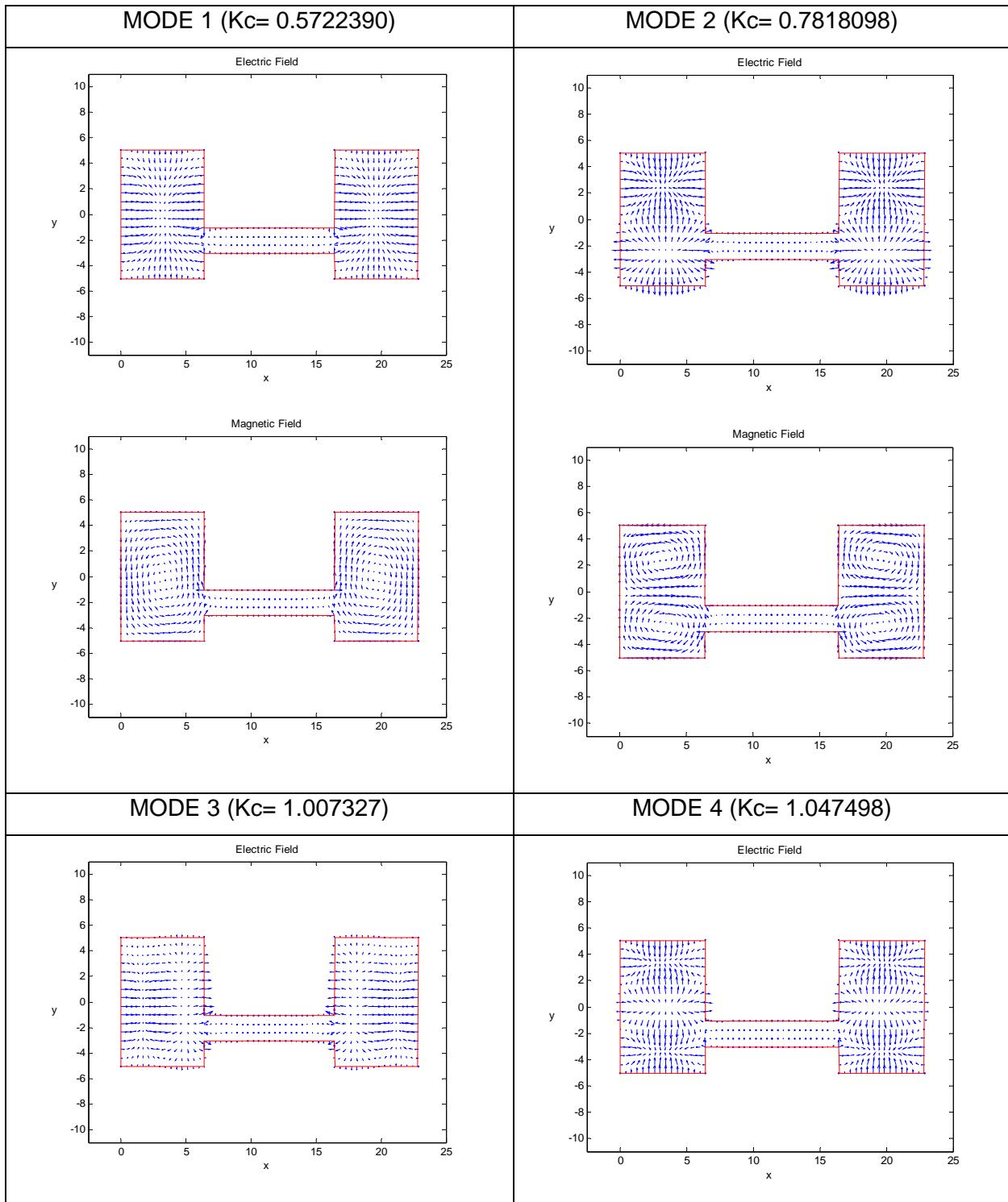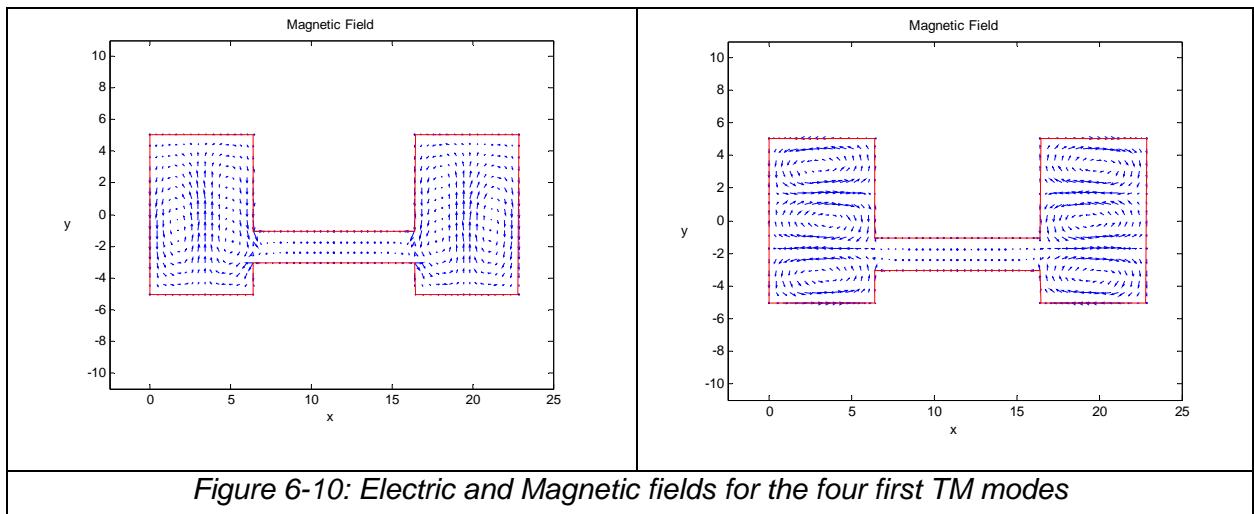
6.2.2. COAXIAL WG

The dimensions (in mm) of the asymmetric structure under study are given in Table 6-10.

A=22.86	
B=20.32	
C1= C2=0	
S1 =5	
S2 =11.32	
T=10	
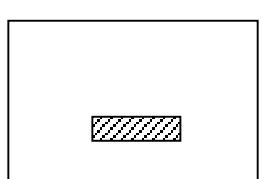
Table 6-10: Dimensions of the RIDGE WG in mm

Table 6-11 gives the comparison between the two methods for each mode in the waveguide. 20 expansion terms are used for the transverse dependence of the vector potentials in region 1, while 5 expansion terms are used in region 2 and 3. Very good agreement is observed and the relative error between the two methods is less than $8.26 \cdot 10^{-4}$.

	TE			TM	
GTR	FEM	Relative Error	GTR	FEM	Relative Error
0.1249899	0.1249464	3.48E-04	0.3038475	0.3037163	4.32E-04
0.1997385	0.1998278	4.47E-04	0.470595	0.4702067	8.26E-04
0.3284109	0.3284498	1.18E-04	0.5263630	0.5262634	1.89E-04
0.4160471	0.4161276	1.93E-04	0.5645219	0.5645436	3.84E-05

Table 6-11: Comparison between the four first cutoff wavenumbers (rad/mm) as obtained with GTR and commercial FEM software.

Below it is shown the Electric and Magnetic fields distribution for the four first TE and TM modes.

TE modes: Electric and Magnetic Field
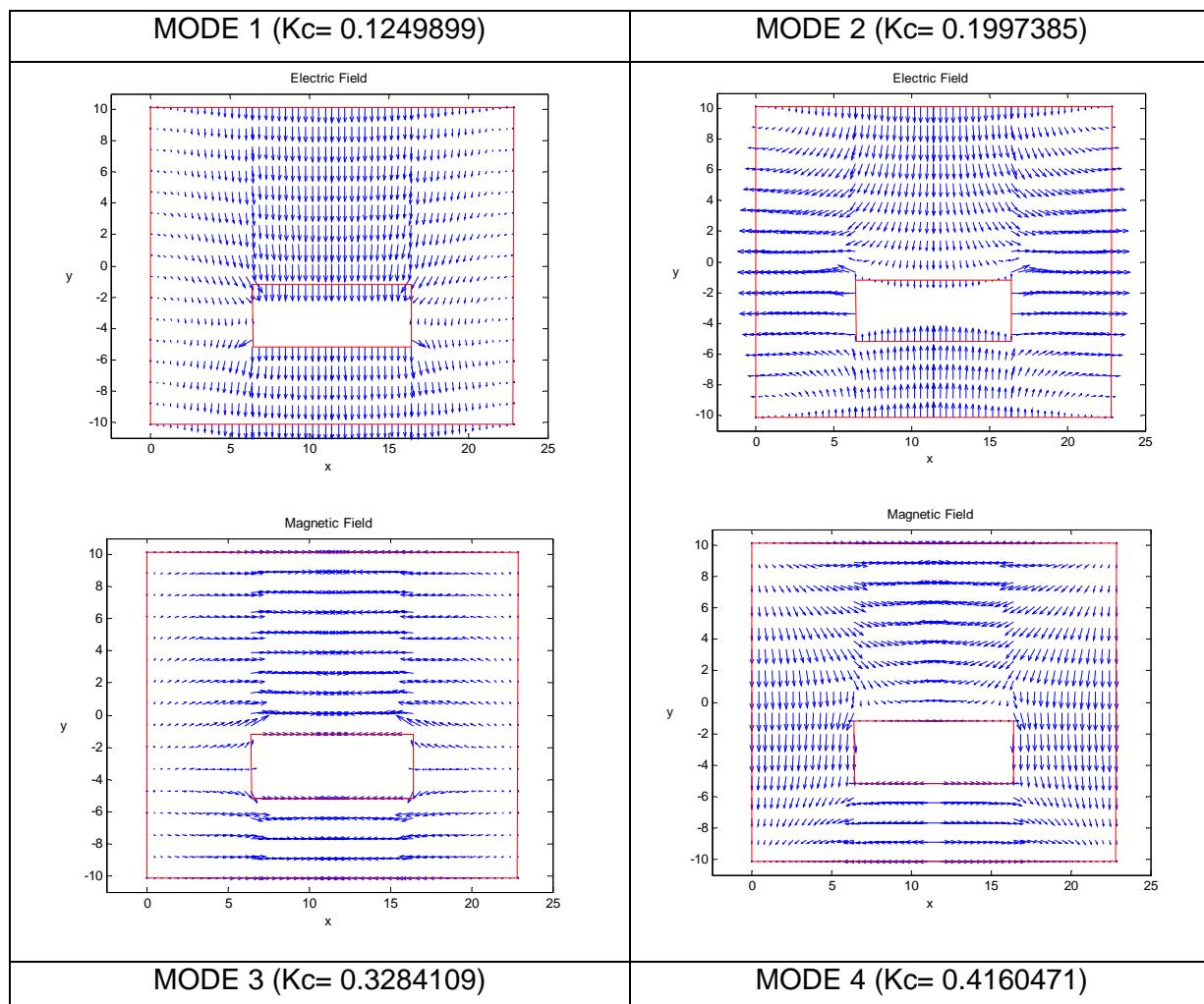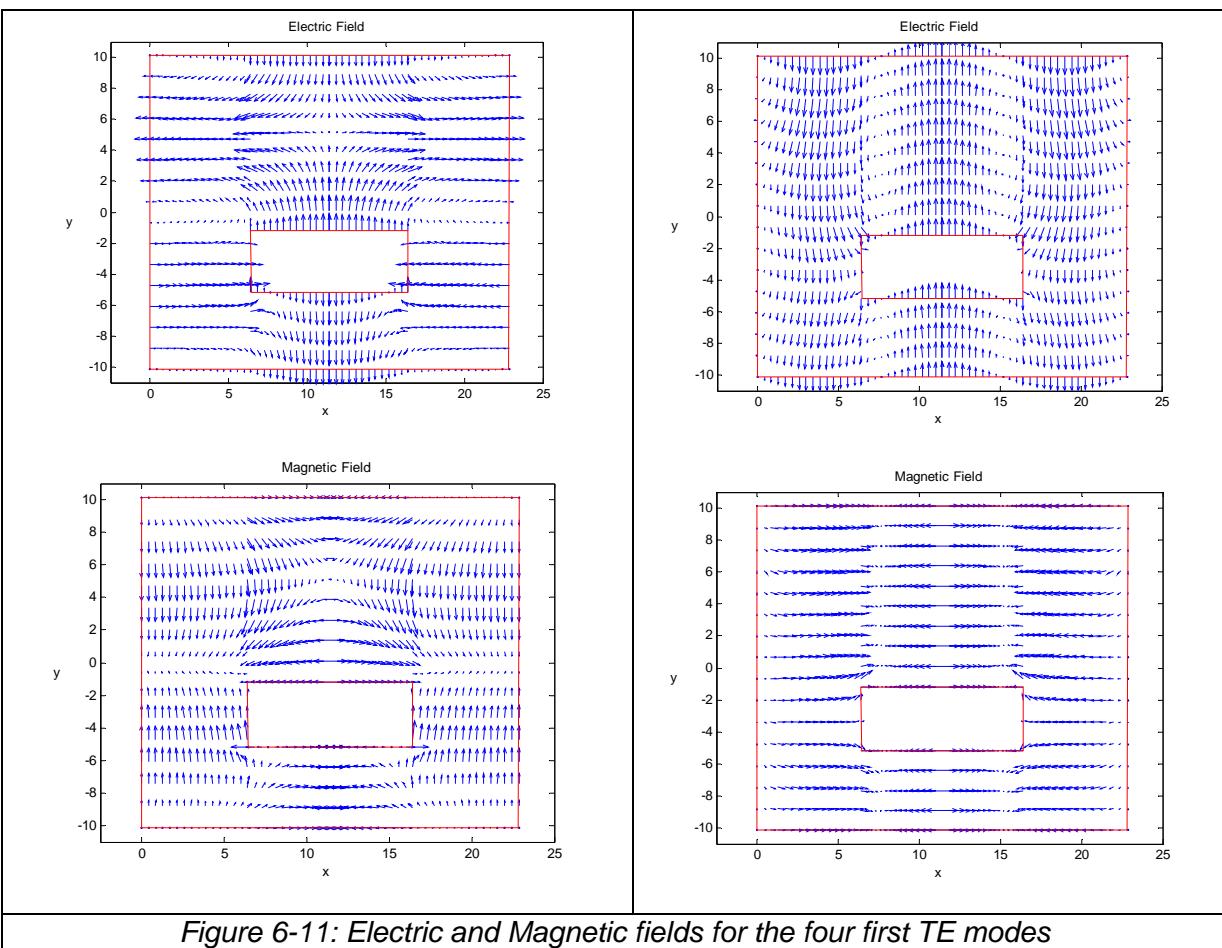
Figure 6-11: Electric and Magnetic fields for the four first TE modes

TM modes: Electric and Magnetic Fields

Figure 6-12: Electric and Magnetic fields for the four first TM modes
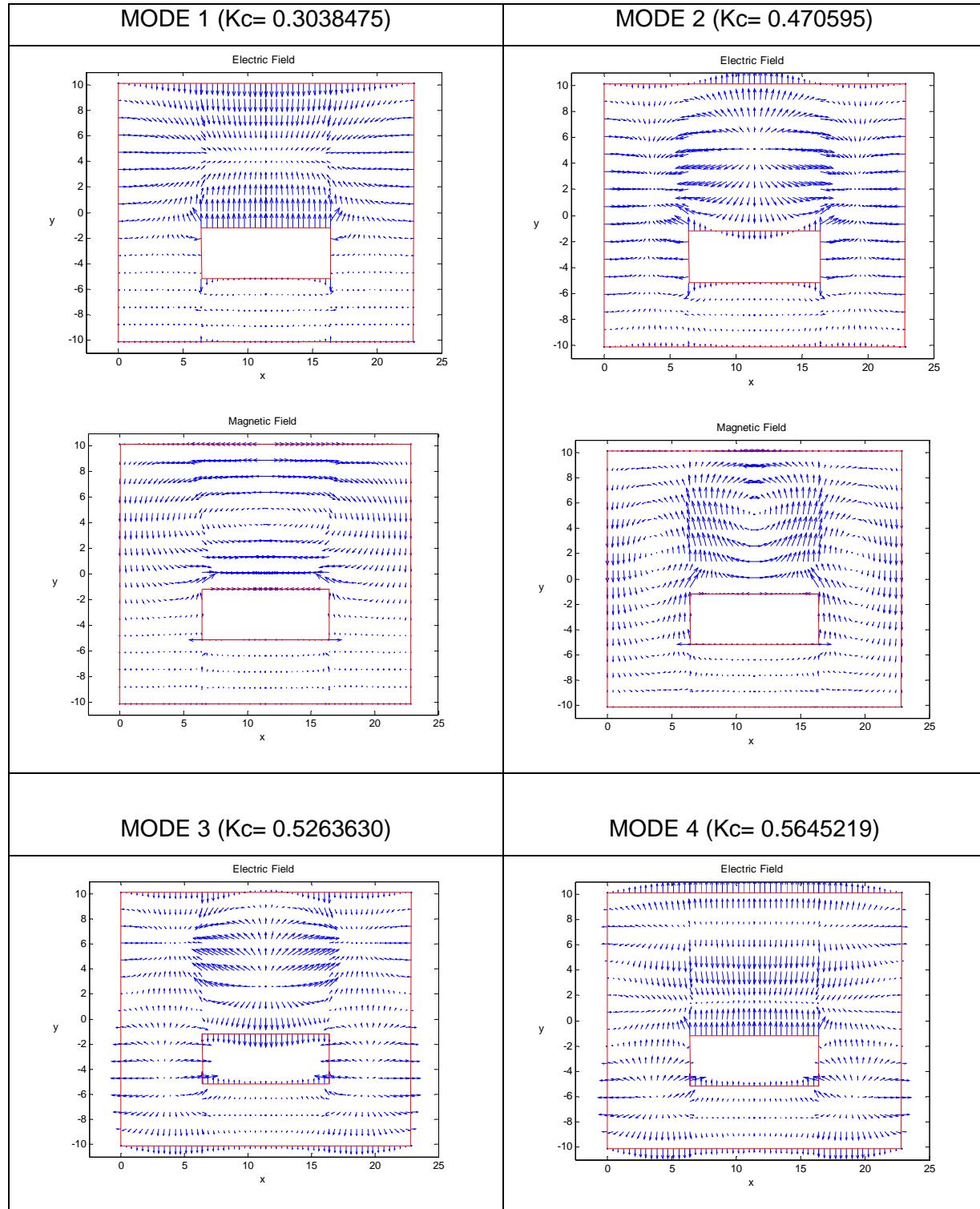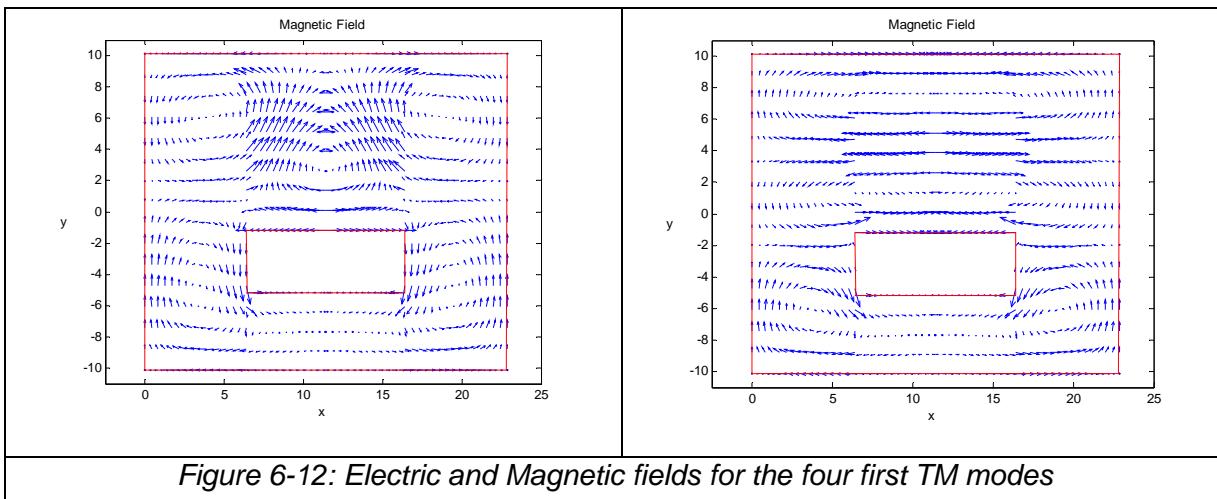
6.2.3. RIDGE COAXIAL WG. SAME GAPS, DIFFERENT HEIGHT OF THE RIDGES

The dimensions (in mm) of the asymmetric structure under study are given in Table 6-12.
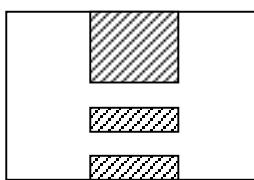
A=22.86	
B=20.32	
C1=2	
C2=8.32	
S1= S2=3	
T=10	

Table 12-: Dimensions of the RIDGE WG in mm

Table 6-13 gives the comparison between the two methods for each mode in the waveguide. 20 expansion terms are used for the transverse dependence of the vector potentials in region 1, while 5 expansion terms are used in region 2 and 3. Very good agreement is observed and the relative error between the two methods is less than $1.09 \cdot 10^{-3}$.

TE			TM		
GTR	FEM	Relative Error	GTR	FEM	Relative Error
0.0784111	0.0783712	5.09E-04	0.4970196	0.4975634	1.09E-03
0.1702451	0.1701124	7.80E-04	0.5686203	0.5690778	8.04E-04
0.3120729	0.3119686	3.34E-04	0.6563966	0.6569782	8.85E-04
0.4392262	0.4389903	5.37E-04	0.7808745	0.7813710	6.35E-04

Table 6-13: Comparison between the four first cutoff wavenumbers (rad/mm) as obtained with GTR and commercial FEM software.

Below it is shown the Electric and Magnetic fields distribution for the four first TE and TM modes.


TE modes: Electric and Magnetic Fields

MODE 1 (Kc= 0.0784111)	MODE 2 (Kc= 0.1702451)

MODE 3 (Kc= 0.3120729)	MODE 4 (Kc= 0.4392262)

Figure 6-13: Electric and Magnetic fields for the four first TE modes

TM modes: Electric and Magnetic Fields

MODE 1 (Kc= 0.4970196)	MODE 2 (Kc= 0.5686203)

87

| MODE 3 (Kc= 0.6563966) | MODE 4 (Kc= 0.7808745) |

Figure 6-14: Electric and Magnetic fields for the four first TM modes

88
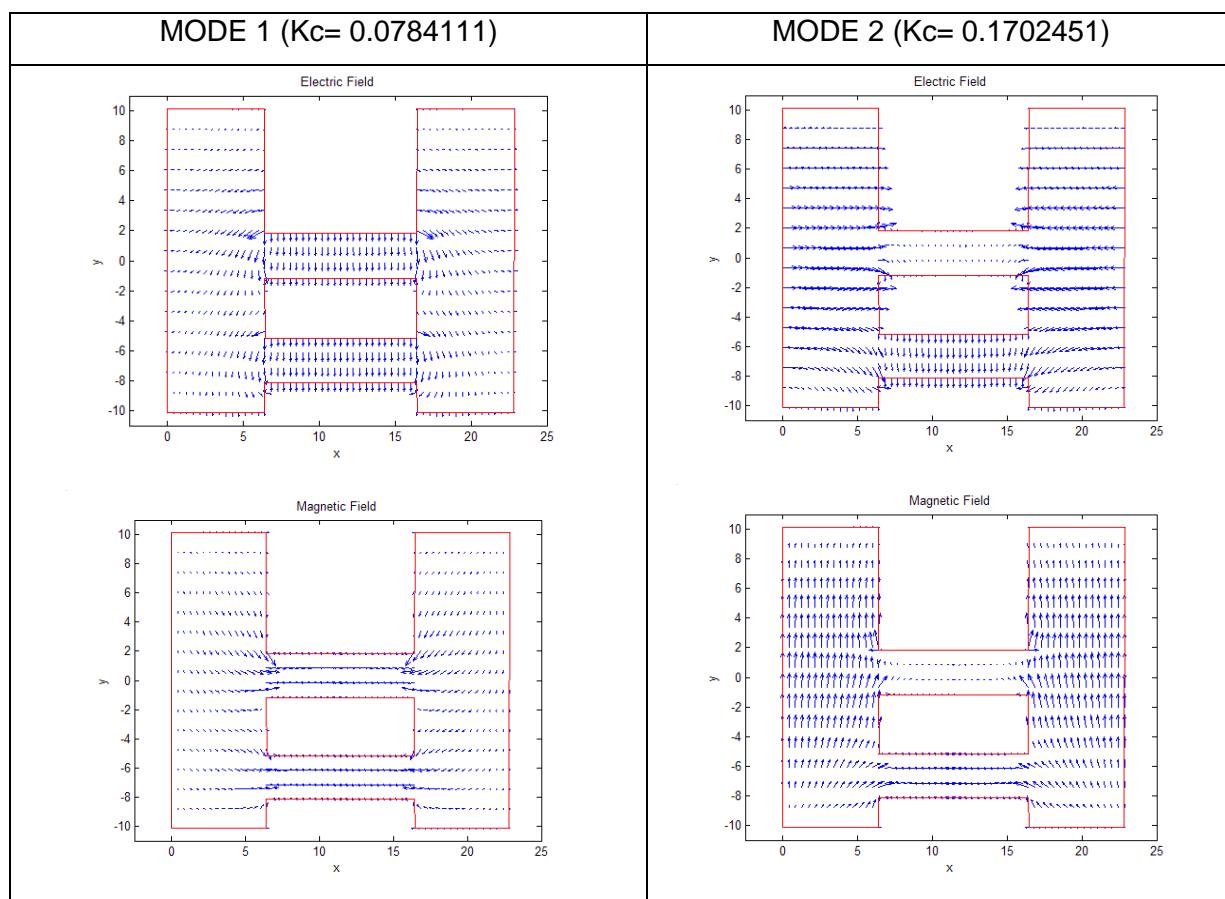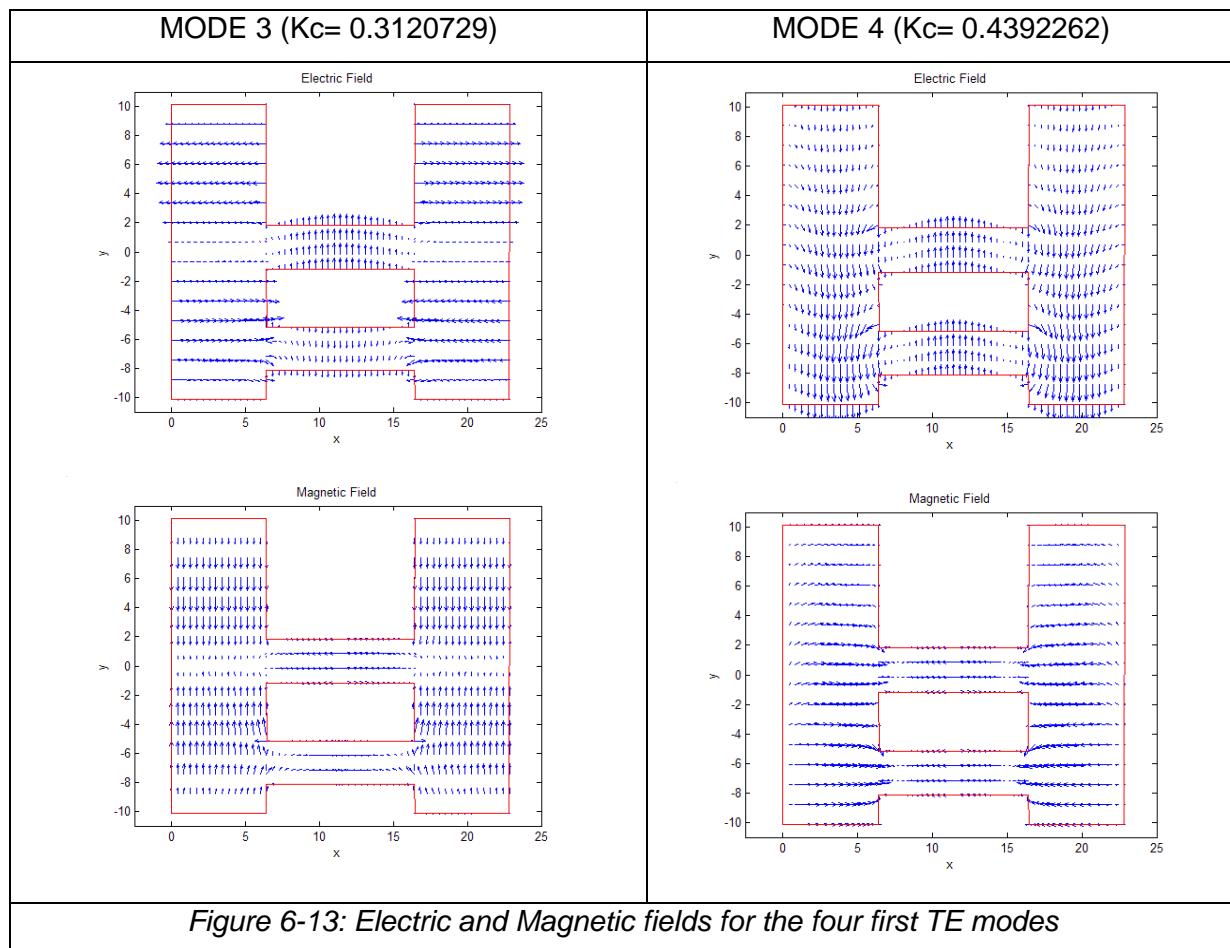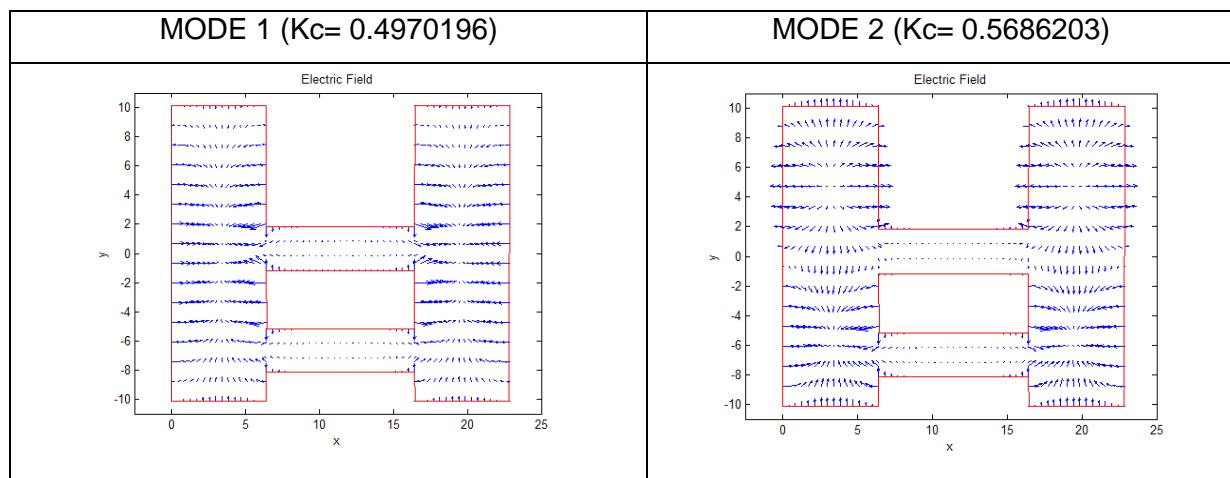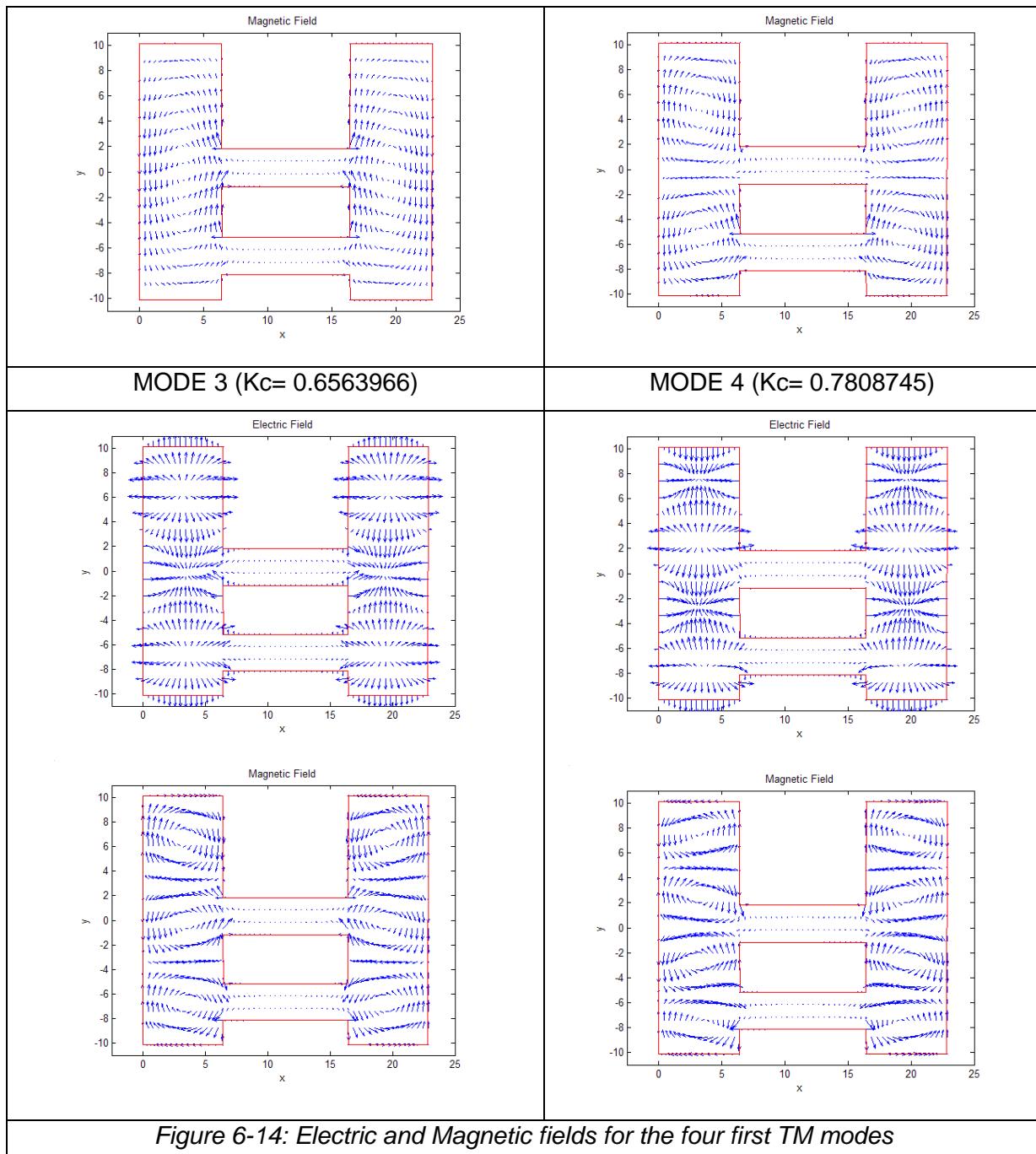
6.2.4. RIDGE COAXIAL WG. SAME HEIGHT OF THE RIDGES, DIFFERENT GAPS

The dimensions (in mm) of the asymmetric structure under study are given in Table 6-14.
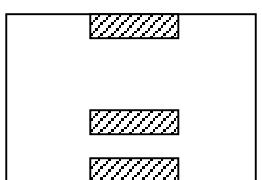
A=22.86	
B=20.32	
C1=C2=2	
S1=3.16	
S2=9.16	
T=10	

Table 6-14: Dimensions of the RIDGE WG in mm

Table 6-15 gives the comparison between the two methods for each mode in the waveguide. In this case, 20 expansion terms are used for the transverse dependence of the vector potentials in region 1, while 3 expansion terms are used in region 2 and 5 expansion terms are used in region 3. Very good agreement is observed and the relative error between the two methods is less than $8.19 \cdot 10^{-4}$.

TE			TM		
GTR	**FEM**	**Relative Error**	**GTR**	**FEM**	**Relative Error**
0.1115929	0.1115029	8.07E-04	0.3509337	0.3507440	5.41E-04
0.1870706	0.1871900	6.38E-04	0.4888783	0.4886350	4.98E-04
0.3253941	0.3254495	1.70E-04	0.5435874	0.5436235	6.64E-05
0.4216279	0.4217941	3.94E-04	0.6246037	0.6240923	8.19E-04

Table 6-15: Comparison between the four first cutoff wavenumbers (rad/mm) as obtained with GTR and commercial FEM software.

Below it is shown the Electric and Magnetic fields distribution for the four first TE and TM modes.

*TE modes: Electric and Magnetic Fields*

MODE 1 (Kc= 0.1115929)	MODE 2 (Kc= 0.1870706)
MODE 3 (Kc= 0.3253941)	**MODE 4 (Kc= 0.4216279)**

90

Figure 6-15: Electric and Magnetic fields for the four first TE modes

TM modes: Electric and Magnetic Fields

MODE 1 (Kc= 0.3509337)	MODE 2 (Kc= 0.4888783)

MODE 3 (Kc= 0.5435874)	MODE 4 (Kc= 0.6246037)
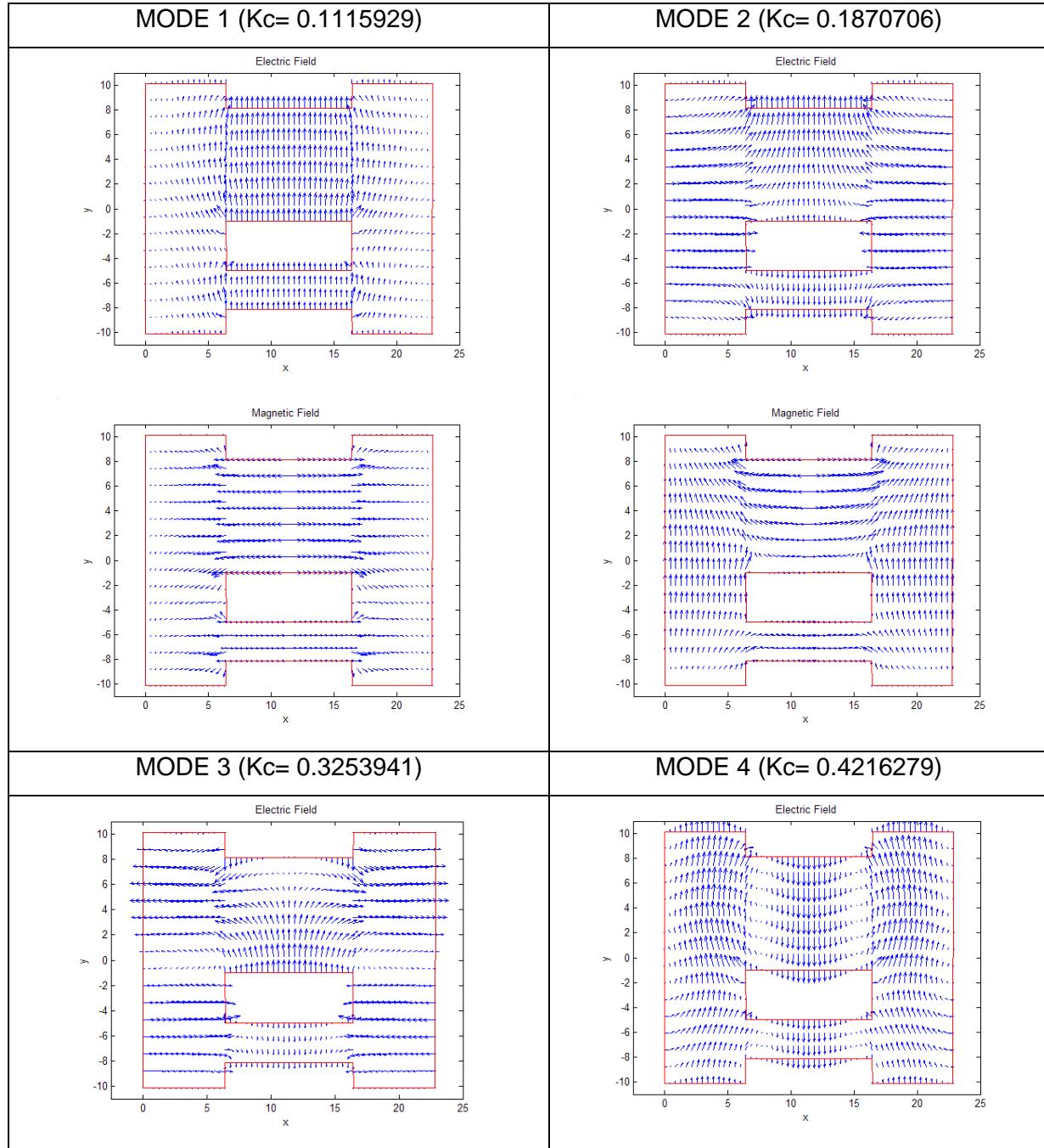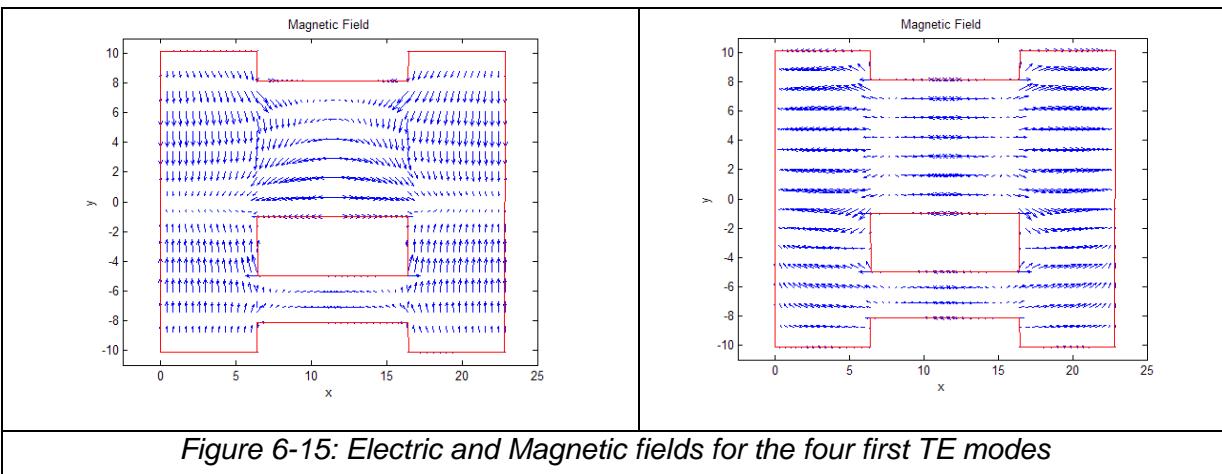
Figure 6-15: Electric and Magnetic fields for the four first TM modes

<div align="right">
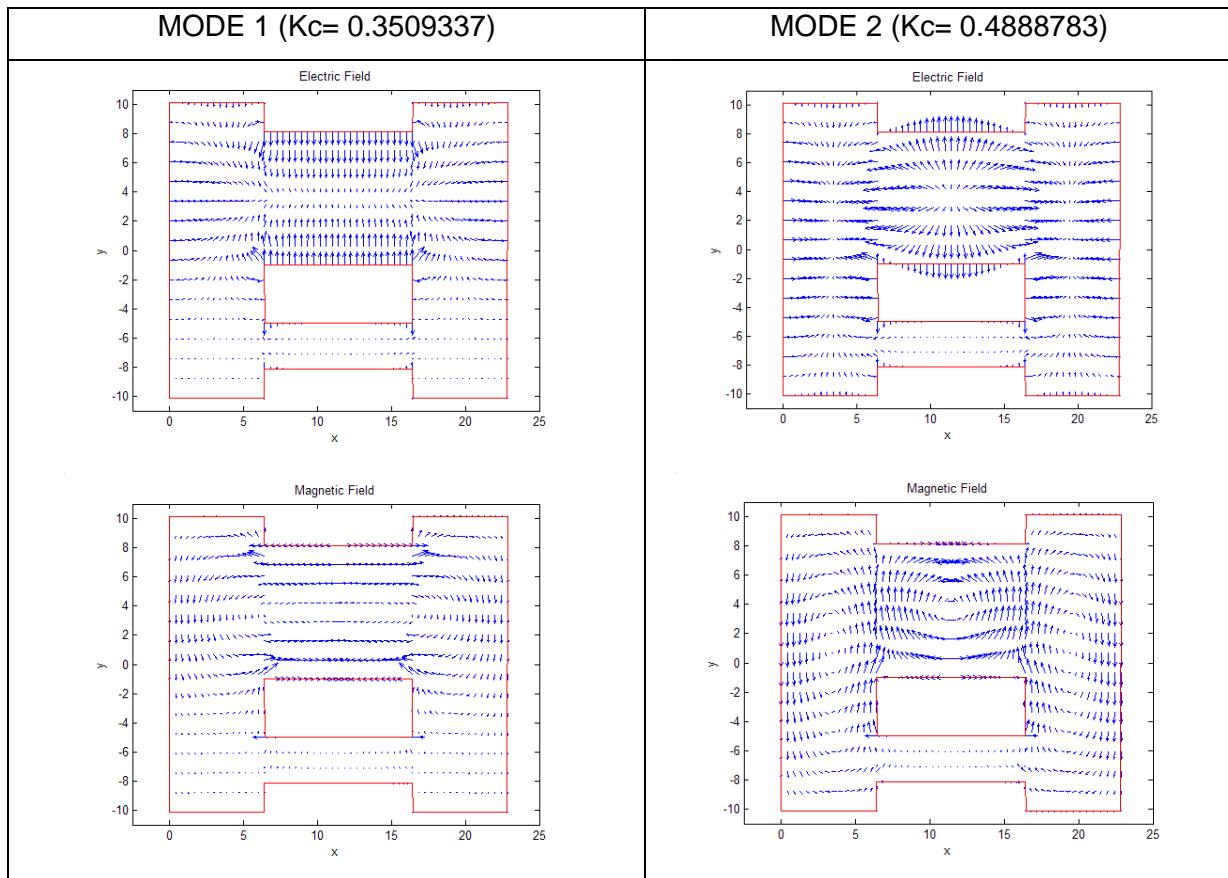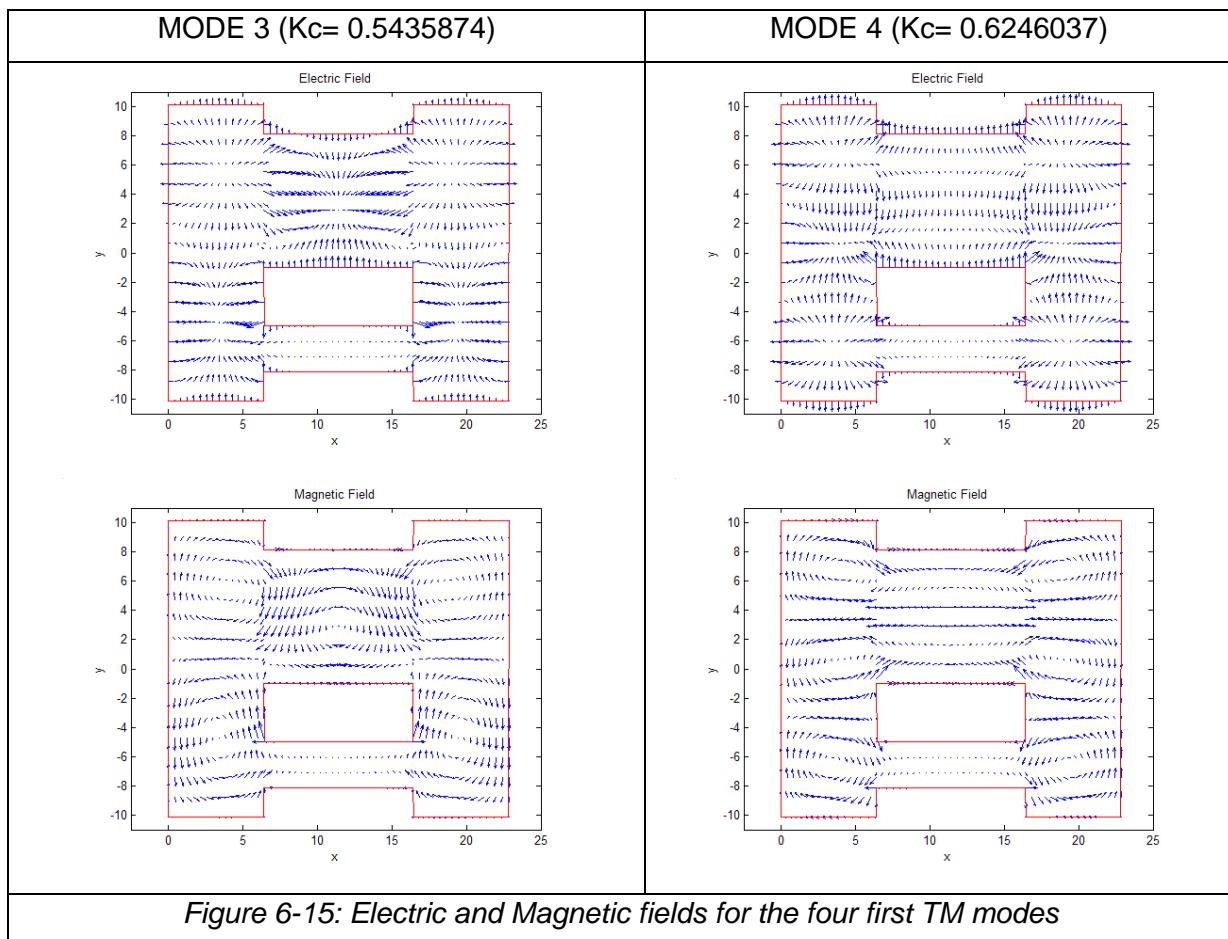
Chapter VII

Parametric studies

</div>

In this section parametric studies of the variation of the dimensions of the waveguide will be presented to demonstrate the dependence of the cutoff wavenumber on the geometry of the structure. Firstly, parametric curves for the ridge waveguide will be studied since this is a known structure but we will pay special attention to the asymmetric case which has not been deeply studied up to now. Then we will focus on the parametric studies of the ridge coaxial waveguide. Furthermore, with all these studies, we will be able to know how the variation of each parameter affects to the propagation of the modes in the waveguide and it will be also shown a physical explanation of the variation with the geometry by studying the field distribution of each mode.

7.1. RIDGE WG

For the Ridge WG, the parameters to be taken into account are, T S, C1 and C2 which allow us to vary the width, the height and the position of the GAP. In the following subsections it is shown the variation of the wavenumber for the first four TE and TM modes when these parameters are varied in all the range of possible values.

7.1.1. VARIATION OF KC VS. THE WIDTH OF THE GAP (T)

In this case the width of the GAP or which is the same, the width of the ridges will be varied. Two parametric studies will be achieved. The first one consists of a symmetric case where the GAP is located in a symmetrical position in the centre of the structure. In

the second one the GAP is located in an asymmetric position. As a remark, it is important to note that the value of T will be incremented from 0.0001 mm up to 15 mm in order to cover all the range of possible values. To be able to represent this T variation correctly two curves are needed. One of them where T parameter varies from 0.0001 up to 1 mm in a logarithmic scale and another one varying T from 1 up to 15 mm in a lineal scale.

7.1.1.1.   SYMMETRIC CASE (C1=C2)

In this case the width of the GAP which is located in a symmetrical position in the centre of the structure will be varied. The dimensions (in mm) are given in Table 7-1.

DIMENSIONS	
A=22.86	
B=10.16	
C1=C2=2	
S=6.16	
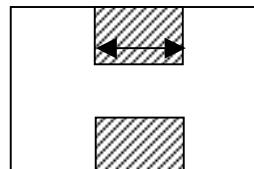
Table 7-1: Dimensions of the structure in mm

Figure 7-1 shows the cutoff wavenumber for a fixed GAP height S, as its width T is incremented. Small variation is observed in both TE and TM modes for values of T below 1 mm. When T is incremented above 1 mm the value of kc increases slightly, being this increment more pronounce for the TM modes as it can be observed in the figure.


(a)

(b)
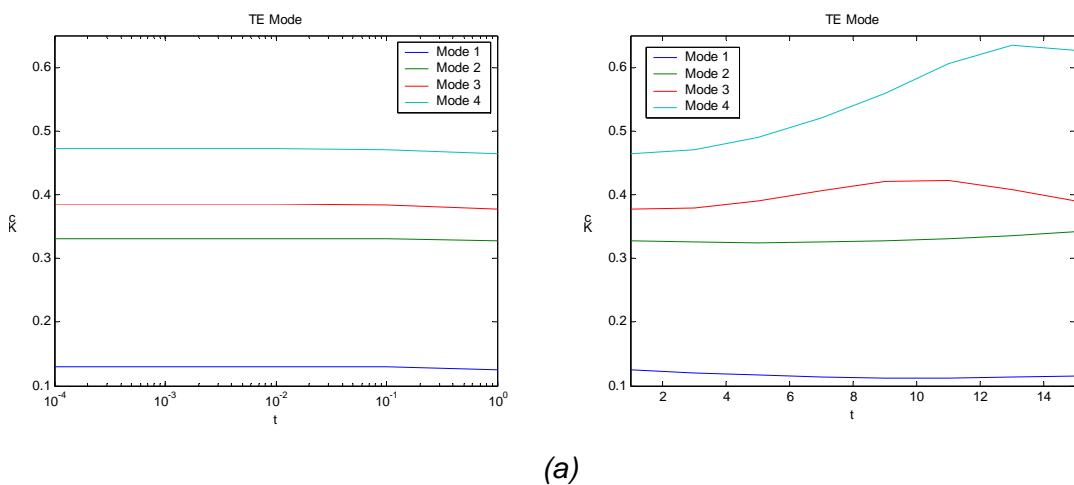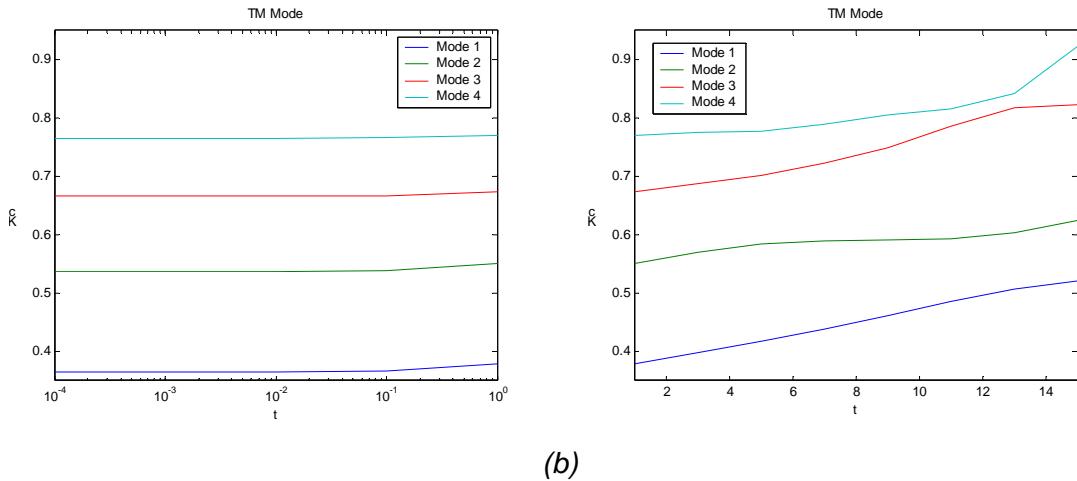
Figure 7-1: K_c vs. t for the first four TE (a) and TM (b) modes

It is important to point out that for the incorporation of this structure in a E-plane Filter, a practical values of T must be very small, around 0.1mm and as we can see in Figure 7-1 for these values of T, the variation of Kc versus T is almost imperceptible.

In order to give a physical explanation of the dependence of kc with T we will start analysing the electric field distribution of the first TE mode shown in Figure 7-2. As can be seen, the field concentration under the ridges is not heavier when T is incremented but it is wider.


(a)   *(b)*
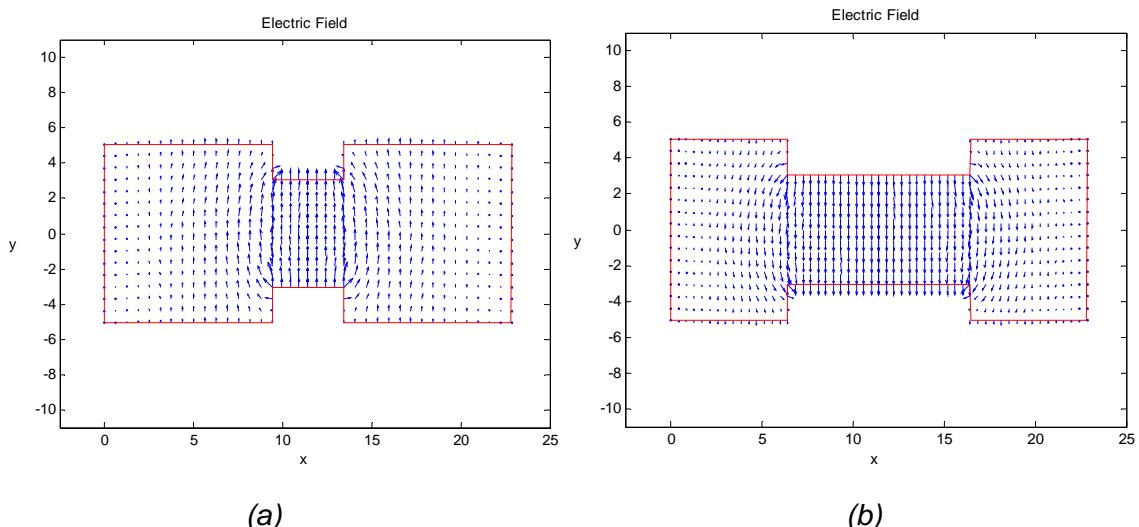
Figure 7-2:Field distribution in a RIDGE WG with thin ridges (a) and with wide ridges (b) for the TE10

In Figure 7-5 it is shown a graphical depiction of the E field variation of the TE_{10} in a Ridge WG with thin ridges and in a Ridge WG with wide ridges. As it was said above

since the field concentration under the ridges is wider when T is incremented it means that the effective distance from the centre of the structure to the electric wall is smaller.


(a)   (b)
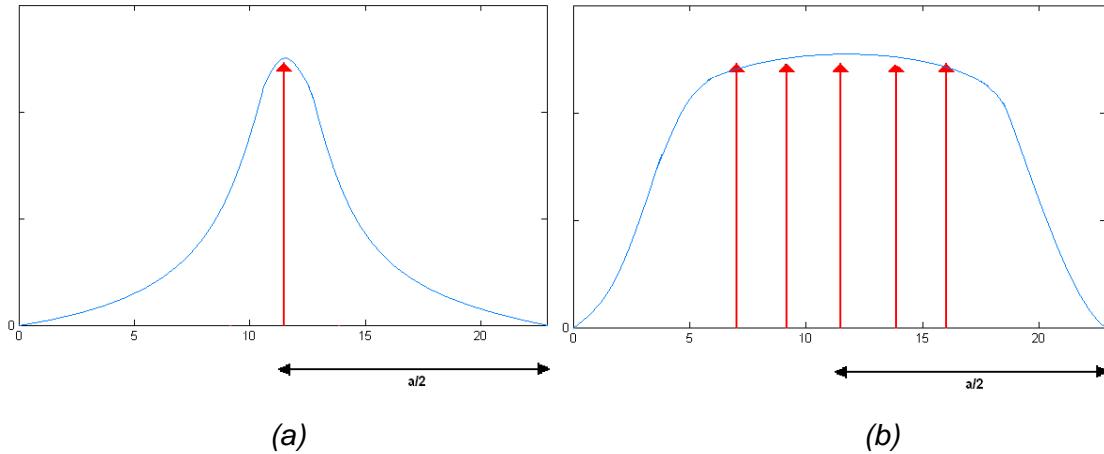
Figure 7-3: Graphical depiction of the E field variation in a RIDGE WG with thin ridges (a) and with wide ridges (b) for the TE10

The lower cutoff frequency for a particular mode in rectangular waveguide is determined by the following equation:

$$\left(f_c\right)_{mn} = \frac{1}{2\pi\sqrt{\mu\varepsilon}}\sqrt{\left(\frac{m\pi}{a}\right)^2 + \left(\frac{n\pi}{b}\right)^2}$$

As it can be observed in the previous equation, the cutoff frequency is inversely proportional to the dimension *a* of the waveguide so if *a* is decreed the cutoff frequency will be incremented and vice versa. Therefore as it was said before, since the effective distance is smaller for bigger values of T, then the cutoff frequency will increase when T will be incremented. As can be seen the difference between the effective distance is not too much pronounce so the variation of Kc will be slight.

7.1.1.2. ASYMMETRIC CASE (C1≠C2)

In this case the width of the GAP which is located in an asymmetrical position in the centre of the structure will be varied. The dimensions (in mm) are given in Table 7-2.

| DIMENSIONS	
A=22.86	
B=10.16	
C1= 6.16	
C2=2	
S=2	
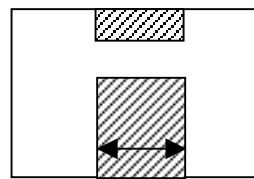
Table 7-2: Dimensions of the structure in mm

Figure 7-4 shows the cutoff wavenumber for a fixed GAP height S, as its width T is incremented. In this case the GAP is located in an asymmetrical position and similar behaviour to the symmetric case has been found. As a conclusion it can be said that the influence of the variation of T is independent of the symmetry of the structure. The physical explanation given in the symmetric case can be also considered now.

(a)

(b)
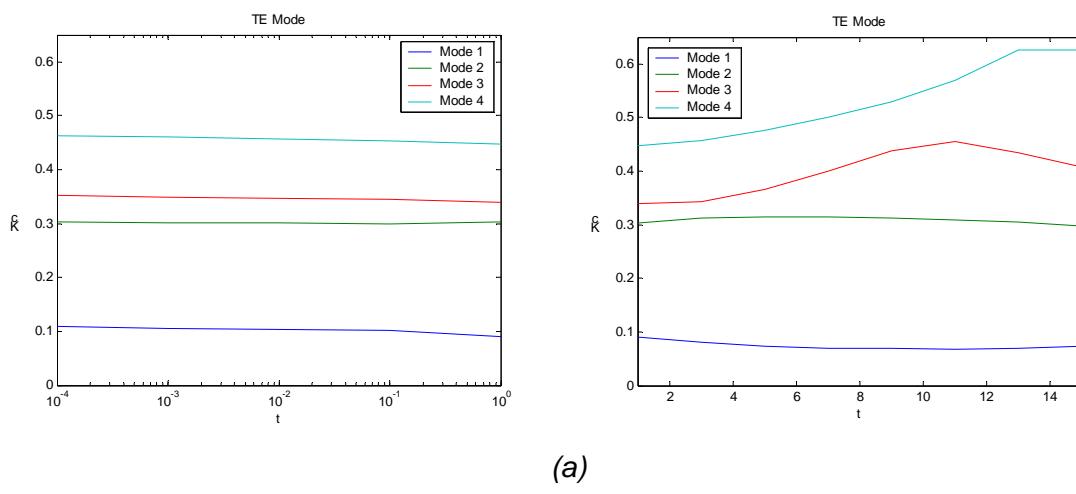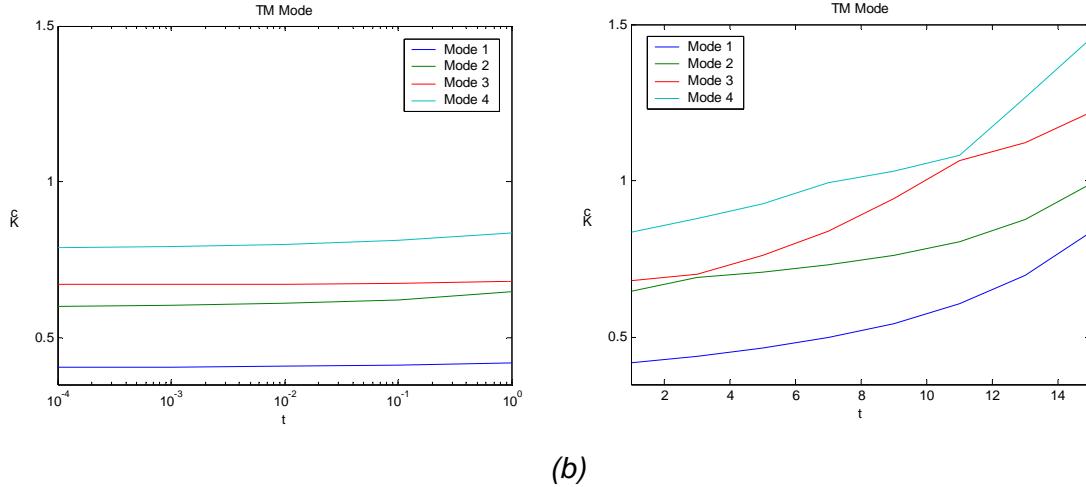
Figure 7-4: K_c vs. t for the first four TE (a) and TM (b) modes

7.1.2. VARIATION KC VS. THE HEIGHT OF THE GAP (S1)

In this case the height of the GAP or which is the same, the height of the ridges will be varied. Two parametric studies will be achieved. The first one consists of a symmetric case where the GAP is always located in a symmetrical position in the centre of the structure. In the second one the GAP is located in an asymmetric position. As a remark, it is important to note that the value of T for this parametric study is 0.1mm in order to obtain practical results which can be useful to design E-plane filter incorporating Ridge WG.

7.1.2.1. SYMMETRIC CASE (C1=C2)

In this case the height of the GAP is varied but it is maintained in a symmetrical position in the centre of the structure. The dimensions (in mm) are given in Table 7-3.

DIMENSIONS	
A=22.86	
B=10.16	
T=0.1	
C1=C2=0-5	
S=B-C1-C2	
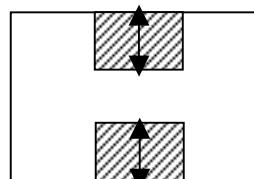
Table 7-3: Dimensions of the structure in mm

Figure 7-5 shows how Kc changes for a symmetric variation of the height of the GAP (S1) for the first four TE and TM modes.

(a)   (b)
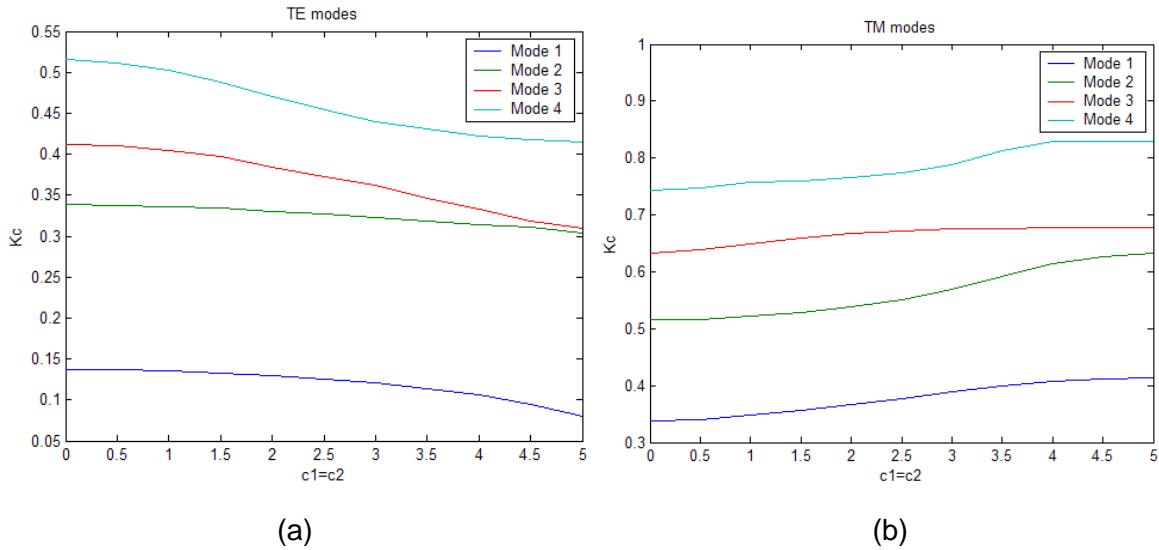
Figure 7-5: Kc for a symmetric variation of S1 for TE modes (a) and TM modes (b)

It is noted that for TE modes Kc decreases when the height of both lower and upper ridges increases, doing the GAP smaller. It can be seen that the kc of each TE or TM mode in the Ridge waveguide approaches the value of a rectangular waveguide of the same dimensions as the ridges approach a value of zero. Therefore, the hollow rectangular waveguide may be viewed as a special case in the Ridge waveguide modelling.

Hence, in absence of ridges, the higher value of Kc is obtained so, as a conclusion, it can be said that loading a rectangular waveguide with ridges the modes start to propagate before. The opposite behaviour is observed for TM modes.

We will try to give a physical explanation of this behaviour. The introduction of the ridges mainly lowers the cutoff frequency of the TE modes from that of the unloaded guide. The reason for this can easily be explained when the field configuration in the guide at cutoff is investigated.

(a)   (b)
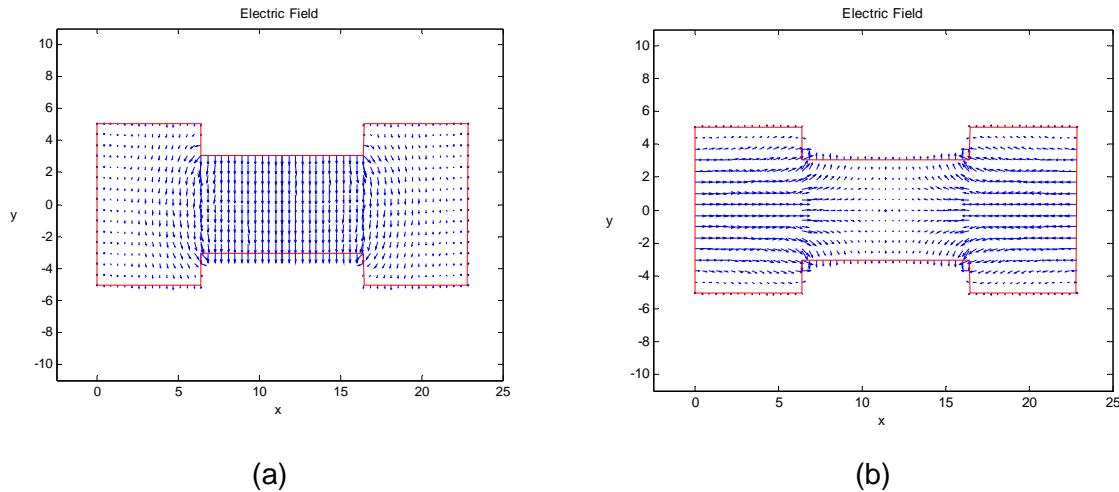
Figure 7-6: Field distribution in a RIDGE WG for the first (a) and the second (b) TE mode

The first TE mode cutoff occurs when there is only one E field maximum across the guide which occurs at the center for a symmetrical ridge as it is shown in Figure 7-6 (a). Because of the reduced height of the guide under the ridge, the effective first TE mode resonator is heavily loaded as though a shunt capacitor were placed across it. The cutoff frequency is thus lowered considerably. For the second TE mode the fields in the center of the guide will be at a minimum as can be seen in Figure 7-6 (b). Therefore the loading will have a negligible effect.

Once again we can make use to the explanation given in section 7.1.1 for a better understanding of the above explanation. In Figure 7-7 it is shown a graphical depiction of the E field variation of the TE_{10} in a rectangular WG and in a Ridge WG. As it was said above since the field concentration at the centre of the structure is more pronounce in the Ridge WG it means that the effective distance from the centre to the electric wall is bigger than a/2. Therefore the cutoff frequency decrees.
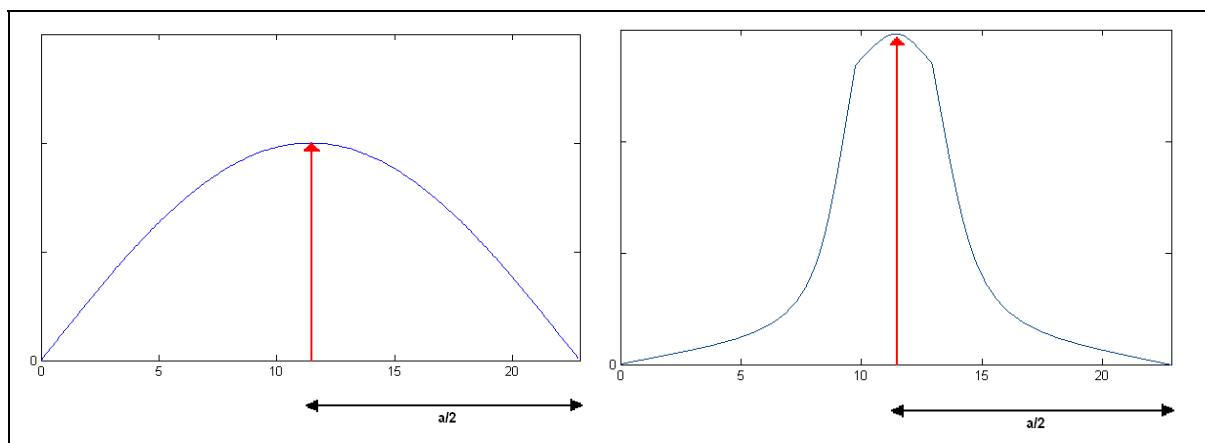
(a)	(b)
Figure 7-7: Graphical depiction of the E field variation in a rectangular WG (a) and in a Ridge WG (b) for the TE10	

As a conclusion it can be said that the first TE mode cutoff can be lowered substantially at the same time the second TE mode cutoff is varied slightly.

7.1.2.2. ASYMMETRIC CASE (C1≠C2)

Now, the height of the GAP is also varied but it is maintained in an asymmetrical position due to the lower ridge height, c1, is only increases in this case. The dimensions of the structure (in mm) are given in Table 7-4.

DIMENSIONS	
A=22.86	
B=10.16	
T=0.1	
C1=0-9.5	
C2=0.5	
S=B-C1-C2	
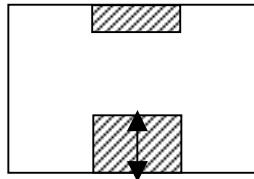
Table 7-4: Dimensions of the structure in mm


(a)   (b)
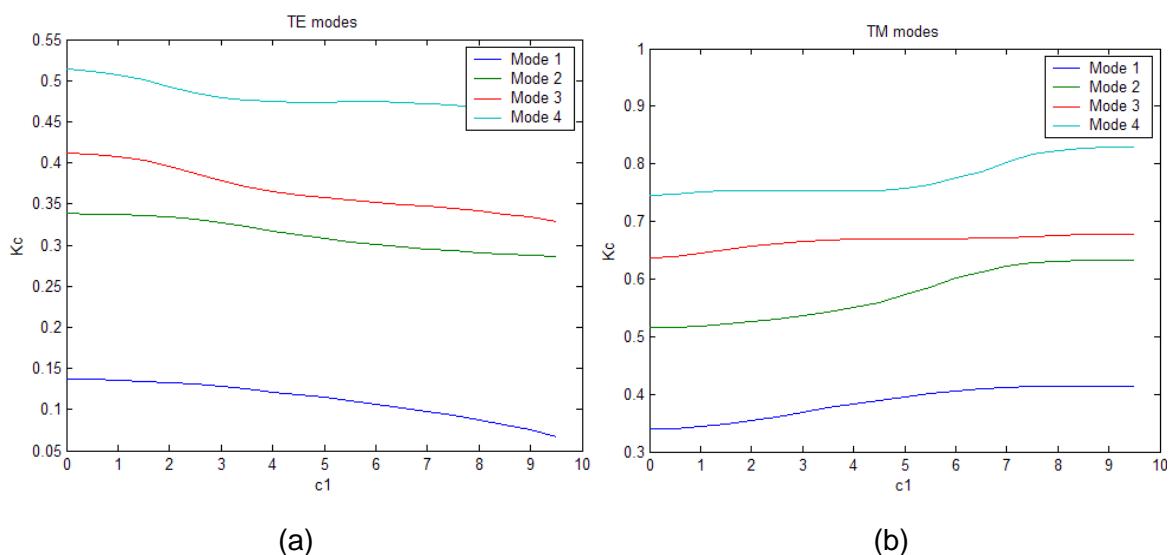
Figure 7-8:Kc(rad/mm) for an asymmetric variation of the GAP for TE modes (a) and TM modes (b)

Figure 7-8 shows how Kc changes for an asymmetric variation of the height of the GAP. In this asymmetrical case, the behaviour of kc is quite similar to the symmetrical case. As a remark it can be said that the variation of kc for TE modes is a little bit more pronounce in this asymmetric case but for TM modes the variation is almost the same to in the previous case. The physical explanation given in the symmetric case can be also considered now.

7.1.3. VARIATION KC VS. C1 (FIXED GAP UP AND DOWN)

For this study, on the contrary to what was done in the previous sections the value of the gap is fixed and it is shifted along the y-axis moving it up and down. The dimensions for this case are shown in Table 7-5.

DIMENSIONS
A=22.86
B=10.16
T=0.1
C1=0-8
C2=B-S-C1
S=2
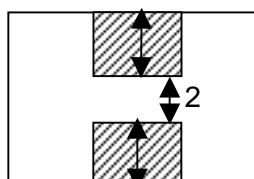
Table 7-5: Dimensions of the structure in mm

(a)   (b)
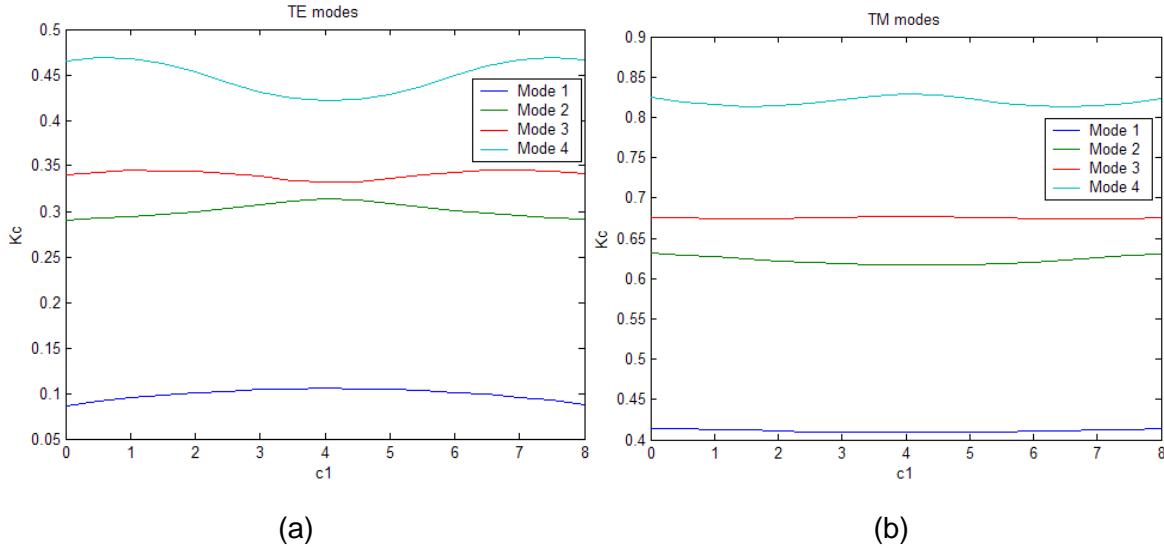
*Figure 7-9: Kc moving the GAP up and down for TE modes (a) and TM modes (b)*

Figure 7-9 shows how Kc changes for a fixed value of the GAP as it shifts along the y-axis. It is noted that for the two first TE modes the Kc has a maximum when the GAP is in the centre of the structure, in a symmetric position. For the third and fourth TE modes Kc has a minimum at the same position. An opposite behaviour is found for TM modes. As a remark it is important to point out that the position of the GAP varies substantially the value of Kc so it is a critical parameter to take into account for the design of E-Plane filter.

It is important to note that this variation depends on the field distribution of each mode as it is shown in Figure 7-10. We can note that when the field distribution under the ridges presents a change of direction, a minimum of the value of kc is obtained.

Mode 1   *Mode 2*

Mode 3   *Mode 4*
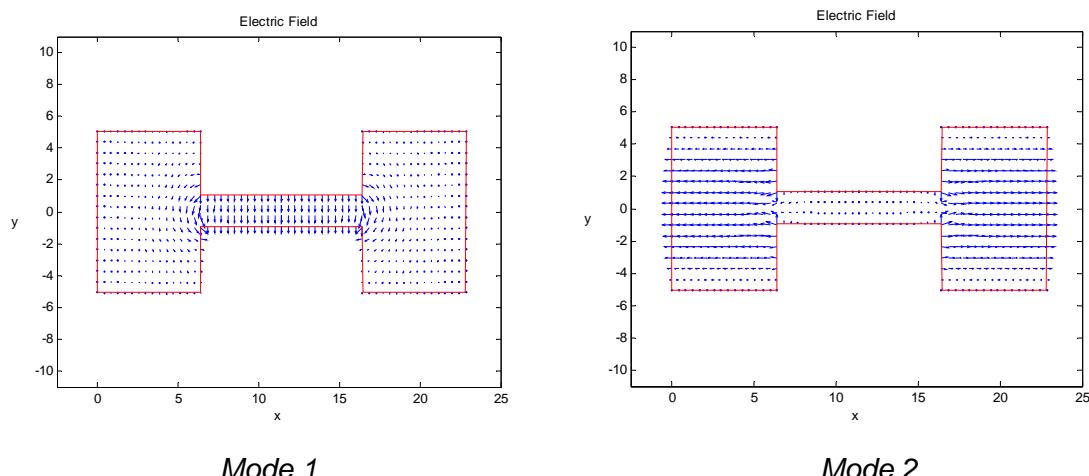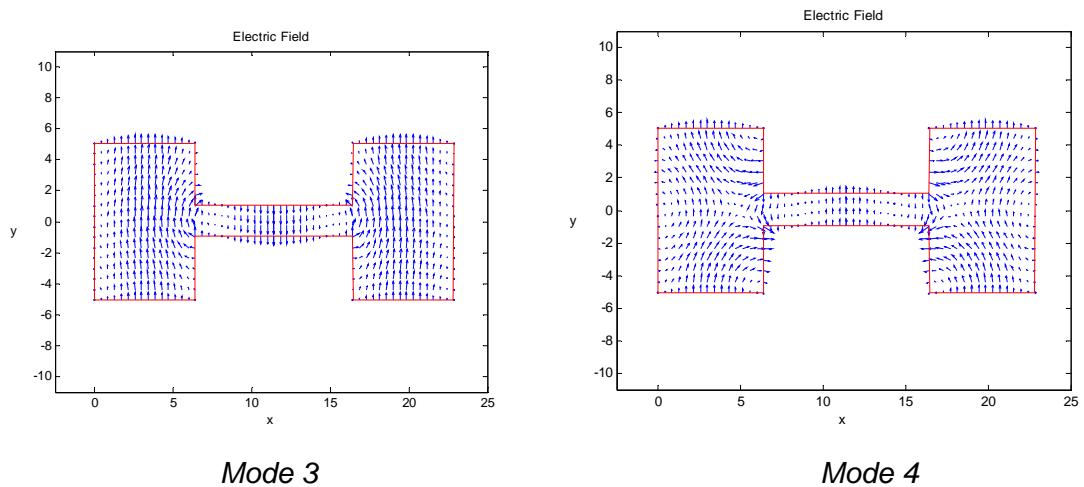
Figure 7-10: Electric field distribution for the first four TE modes in a RidgeWG

7.1.4. CONCLUSIONS OF THE PARAMETRIC STUDY OF THE RIDGE WG.

This section summarizes all the conclusions extracted from the parametric study of the RIDGE WG presented above. These conclusions are important to demonstrate the dependence of the cutoff wavenumber on the geometry of the structure.

The parameters which have been varied to achieve the parametric studies have been T, S1, C1 and C2 which allow to vary the width, the height and the position of the GAP.

The conclusions to be taken into account for further works are:

- About the width of the GAP (T parameter) very small variation of the Kc is observed in both TE and TM modes for values of T below 1 mm. When T is incremented above 1 mm the value of kc increases slightly, being this increment more pronounce for the TM modes. As a remark it is important to keep in mind that a practical value of T must be very small, around 0.1mm and for these values of T, the variation of Kc is almost imperceptible. Therefore the value of T is not a critical parameter for the design of E-plane filter.

- In relation to the height of the gap (S1 parameter) for TE modes Kc increases when the height of the GAP increases. The opposite behaviour is observed for TM modes. This variation is more pronounce that in the previous case. Hence, It is important to point out that this parameter is interesting to be considered for the design of E-plane filter.

- With regard to the position of the GAP (C1 and C2 parameters) it can be said that the position of the GAP varies substantially the value of Kc so it is a critical parameter to take into account for the design of E-Plane filter. This variation follows a different pattern for each mode and there is not a constant tendency.

7.2. RIDGE COAXIAL WG

To achieve parametric studies for Ridge Coaxial WG, the parameters to be taken into account are, T S1, S2, C1 and C2 which allow us to vary the width, the height and the position of the GAPs and the inner conductor. In the following subsections it is shown the variation of the wavenumber for the firsts TE and TM modes when these parameters are varied in all the range of possible values.

7.2.1. VARIATION KC VS. THE WIDTH OF THE INNER CONDUTOR (T)

In this case the width of the inner conductor (and at the same time the width of the ridges) will be varied. Two parametric studies will be achieved. The first one consists of a symmetric case where the inner conductor is located in a symmetrical position in the centre of the structure. The second one has de inner conductor in an asymmetric position. As it was done in section 7.1.1 the value of T will be incremented from 0.0001 mm up to 15 mm in two curves with different scales.

7.2.1.1. SYMMETRIC CASE

This parametric study has been performed for the dimensions given in Table 7-6:
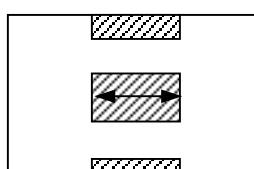
A=22.86	
B=20.32	
C1=C2=2	
S1=S2=6.16	

Table 7-6: Dimensions of the structure in mm

Figure 7-11 shows the cutoff wavenumber for a fixed inner conductor height g, as its width T is incremented. The variation in both Ridge WG and Ridge Coaxial WG follows a similar pattern with the width of the ridges. Small variation is observed in both TE and TM modes for values of T below 1 mm. When T is incremented above 1 mm the value of kc increases slightly, being this increment more pronounce for the TM modes as it can be observed below.

(a)

(b)
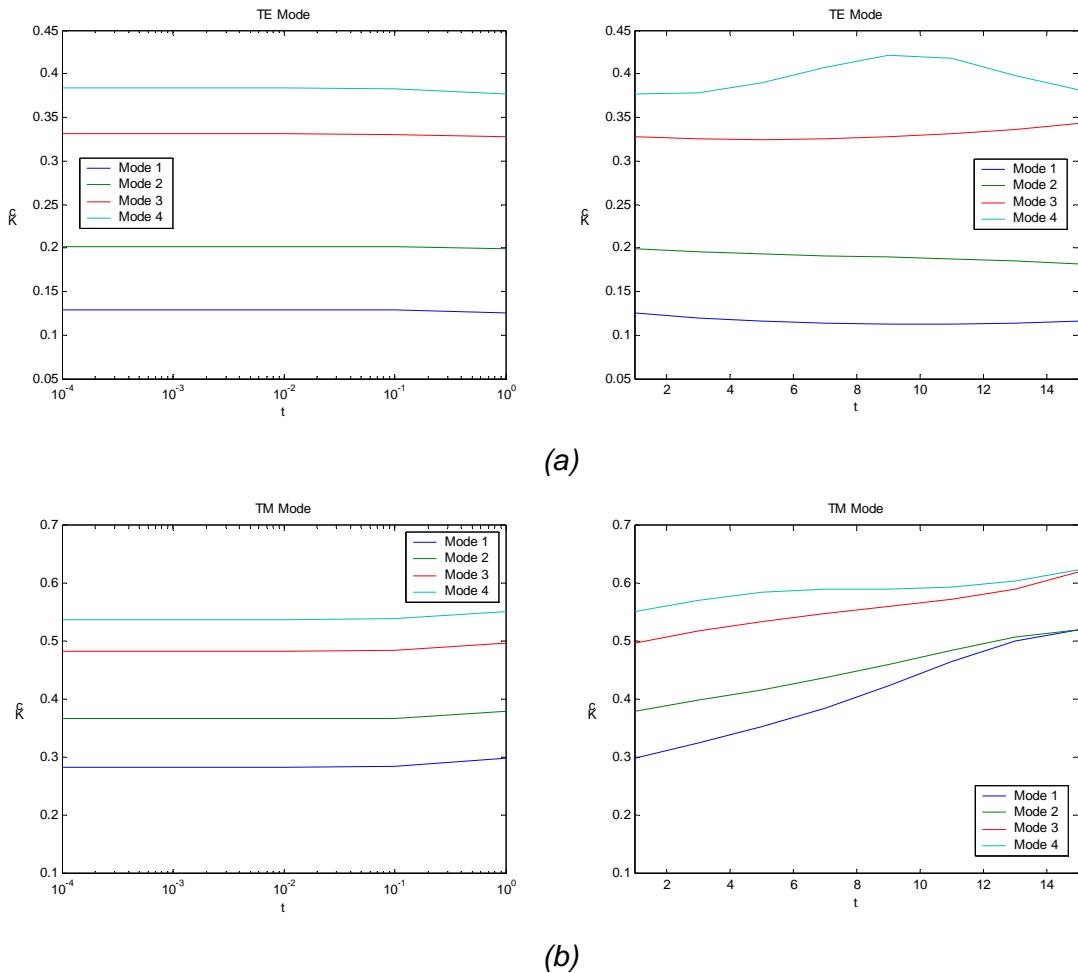
Figure 7-11: K_c vs. t for the first four TE (a) and TM (b) modes

The physical explanation given in Section 7.1.1.1 which explains the variation of Kc versus T in a Ridge WG is also valid for this case due to, as it was commented in Section 6.1.4.1, the Ridge Coaxial WG and Ridge CW have the same behaviour for many of their modes.

7.2.1.2. ASYMMETRIC CASE: C1=C2

This parametric study has been made for the dimensions given in Table 7.7:
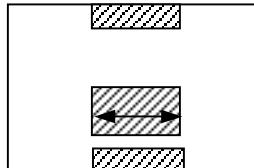
A=22.86	
B=20.32	
C1=C2=2	
S1=3.16	
S2=9.16	

Table 7-7: Dimensions of the structure in mm


(a)

(b)
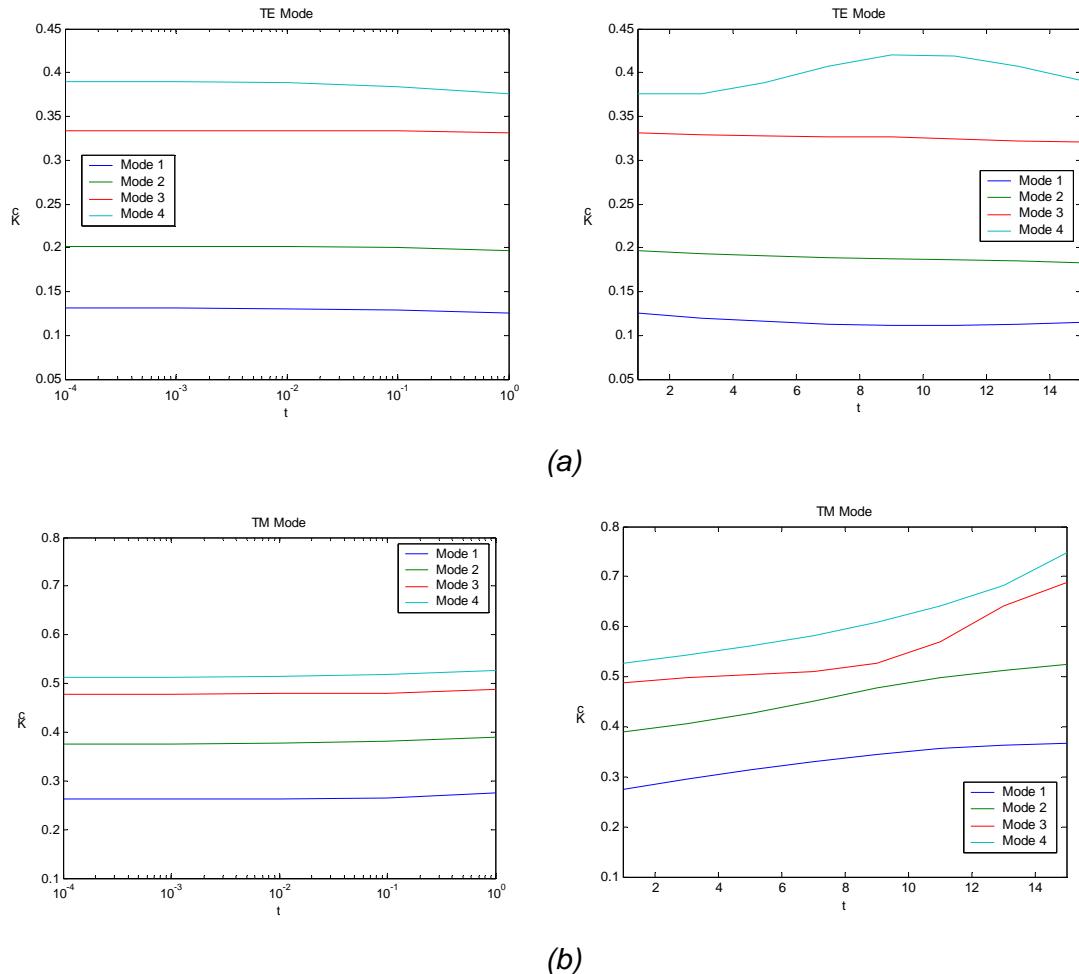
Figure 7-12: K_c vs. t for the first four TE (a) and TM (b) modes

Figure 7-12 shows the cutoff wavenumber for a fixed inner conductor height G, as its width T is incremented. In this case the inner conductor is located in an asymmetrical position and similar behaviour to the symmetric case has been found.

This parametric study has been also achieved for other asymmetric structures but the results have not been represented because very similar behaviours to this one were found.

As a conclusion it can be said that the influence of the variation of T is independent of the symmetry of the structure.

7.2.2. VARIATION OF KC VS. POSITION OF THE INNER CONDUCTOR (CHANGING S1 AND S2)

For this study, the height of the inner conductor is fixed and it is shifted along the y-axis moving it up and down. The dimensions for this case are shown in Table 7-9.
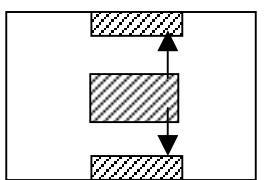
A=22.86	
B=20.32	
S1+S2=12.32	
C1=C2=2	
G=4	
T=10	

Table 7-9: Dimensions of the structure in mm


| (a) | (b) |
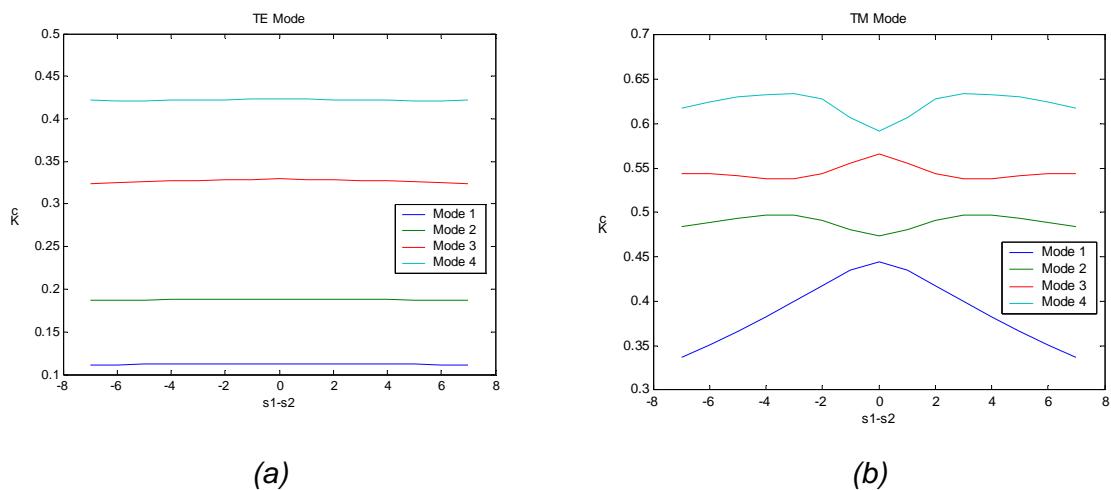
Figure 7-14: K_c vs. s1-s2 for the first four TE (a) and TM (b) modes

Figure 7-14 shows the cutoff wavenumber for a fixed inner conductor height g, as it shifts along the y-axis. Small variation is observed in the TE modes, as the overall equivalent capacitance remains approximately constant. The variation of the TM modes is more pronounce. As can be observed, for the first and third TM modes the value of Kc has a maximum when the inner conductor is in the centre of the structure, in a symmetric position. For the second and fourth TM modes Kc presents a minimum at the same position.

As a remark, it is important to point out that this variation depends on the field distribution of each mode, as it is shown in Figure 7-15. We can note that when the electric field distribution in both GAPs has the same direction, a maximum of the value of kc is obtained. On the contrary, if the field distribution in both GAPs has opposite directions, a minimum of kc is obtained.

.

MODE 1 (Kc= 0.4442496)   MODE 2 (Kc= 0.4734103)

MODE 3 (Kc= 0.5662217)   MODE 4 (Kc= 0.5913421)
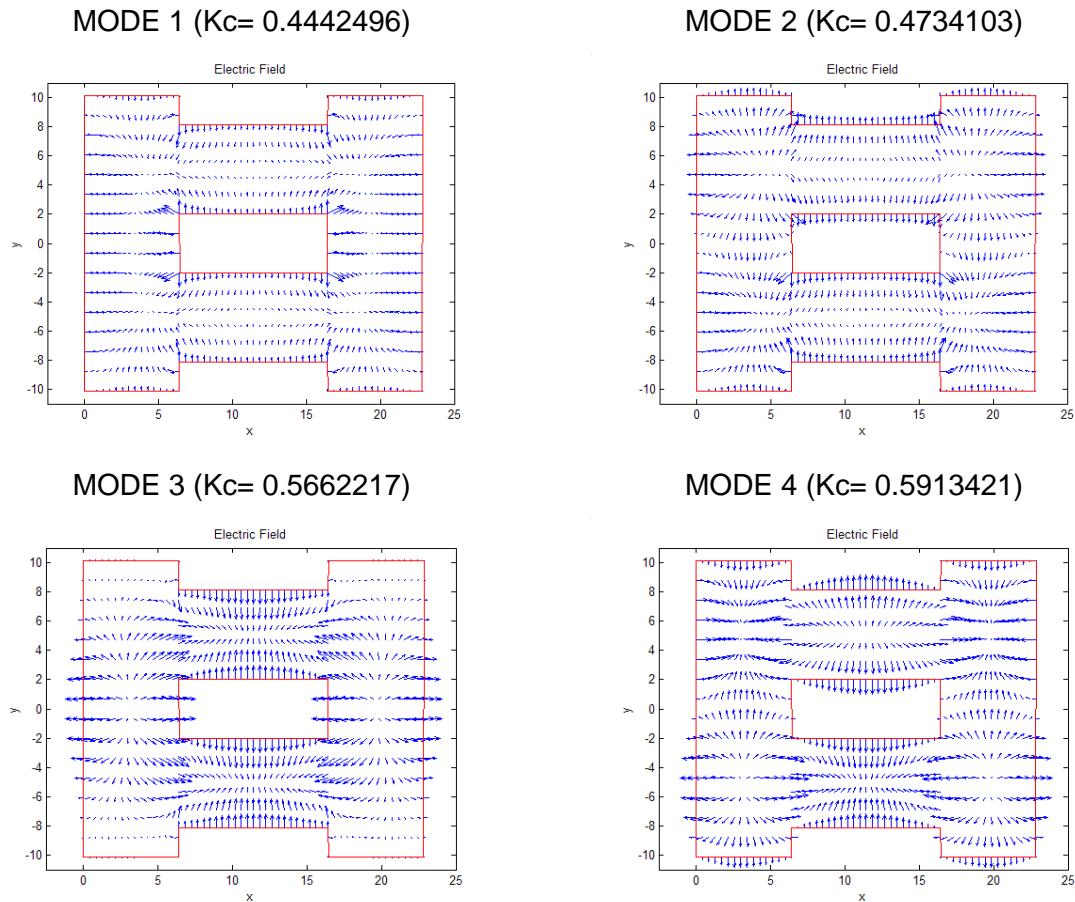
Figure 7-15: Electric and Magnetic fields for the four first TM modes

7.2.3.   VARIATION KC VS. S1 (CENTRAL CONDUCTOR INCREASING IN HEIGHT)

Figure 7-16 shows the variation of the wavenumbers for a fixed upper ridge (C2) and the lower ridge (C1) varying by changing the height of the central conductor g and at the same time, the height of the lower gap is also varied. This parametric study has been achieved for the dimensions given in Table 7-10:

A=22.86	
B=20.32	
G+S1=12.16	
C1=C2=2	
S2=4.16	
T=10	
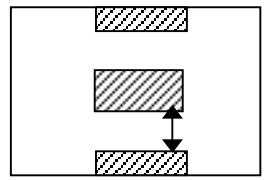
Table 7-10: Dimensions of the structure in mm

(a)   (b)
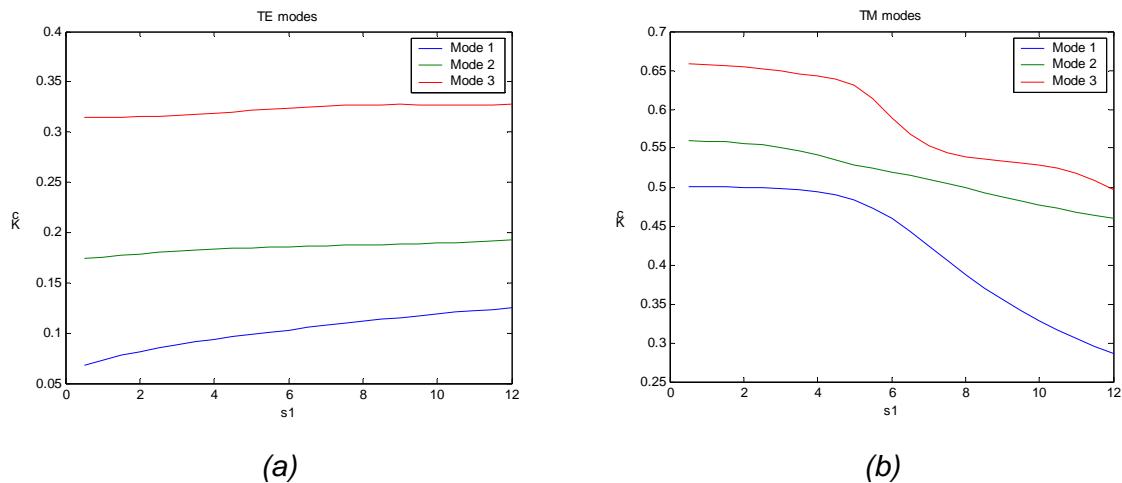
Figure 7-16: K_c vs. s1 for the first four TE (a) and TM (b) modes

As it was expected, the results are in good agreement with the ones obtained for the Ridge WG. As it was said in Section 7.1.2, when the height of the GAP is incremented the value of kc is also incremented. An opposite behaviour is found for the TM modes but in this case the variation is more pronounce.

Loughborough University

The physical explanation given in section 7.1.2.1 for RIDGE WG can be adapted to explain this behaviour.

7.2.4. VARIATION KC VS. C1 (FIXED INNER CONDUCTOR)

Figure 7-17 shows the variation of the wavenumbers for a fixed upper ridge (C2) and fixed central conductor varying by changing the lower ridge height C1. In this case, as in the previous one, the height of the GAP is being changed so the same conclusion extracted for that case can be valid for this one, This parametric study has been made for the dimensions given in Table 7-11:
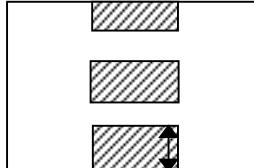
A=22.86	
B=20.32	
C1+S1=8.16	
C2=2	
S2=4.16	
G=6	
T=10	

Table 7-11: Dimensions of the structure in mm


(a)   *(b)*
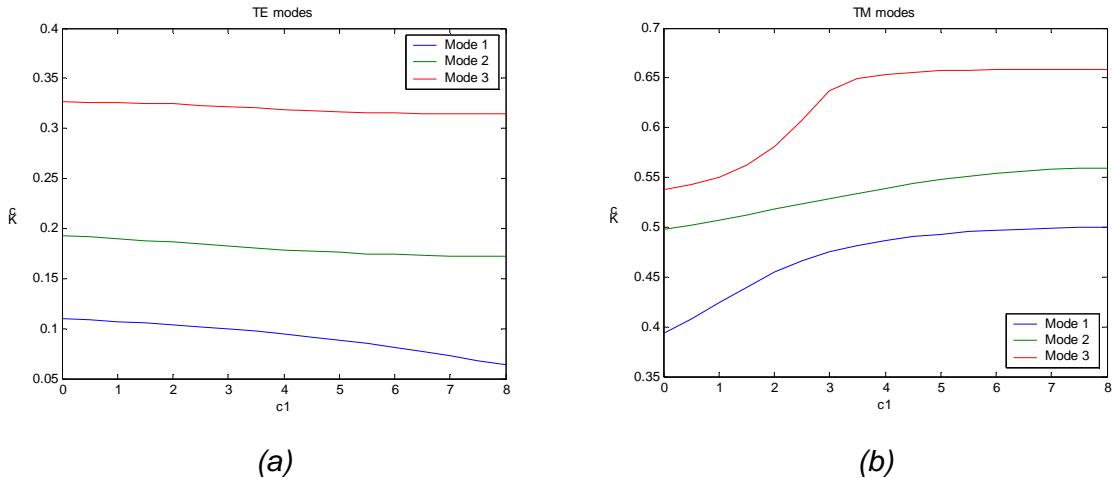
Figure 7-17: K_c vs. c1 for the first four TE (a) and TM (b) modes

7.2.5.   CONCLUSIONS OF THE PARAMETRIC STUDY OF THE RIDGE WG.

This section summarizes all the conclusions extracted from the parametric study of the Ridge Coaxial WG presented above. These conclusions are important to demonstrate the dependence of the cutoff wavenumber on the geometry of the structure.

The parameters which have been varied to achieve the parametric studies have been, T S1, S2, C1 and C2 which allow to vary the width, the height and the position of the GAPs and the inner conductor.

The conclusions to be taken into account for further works are:

- About the width of the GAPs and the inner conductor (T parameter) very small variation of the Kc is observed in both TE and TM modes for values of T below 1 mm. When T is incremented above 1 mm the value of kc increases slightly, being this increment more pronounce for the TM modes. As a remark it is important to keep in mind that a practical value of T must be very small, around 0.1mm and for these values of T, the variation of Kc is almost imperceptible. Therefore the value of T is not a critical parameter for the design of E-plane filter.

- In relation to the height of the GAPs (S1 and S2 parameter) for TE modes Kc increases when the height of the GAPs increases. The opposite behaviour is observed for TM modes. The variation of Kc for these parameters is more pronounce that in the previous case. Hence, it is important to point out that these parameter are interesting to be considered for the design of E-plane filter.

- With regard to the position of the inner conductor, small variation is observed in the TE modes. However, the variation of the TM modes is more pronounce. This variation follows a different pattern for each mode and there is not a constant tendency.

- In relation to the height of the inner conductor it is important to note that when it is incremented the GAPs are smaller and therefore the value of Kc decreases for the TE modes. An opposite behaviour is observed for the TM modes.

Chapter VIII

Conclusions of the

parametric studies for Ridge Coaxial WG

and Ridge WG useful for the design of E-plane filter

Sections 7.1.4 and 7.2.5 summarize all the conclusions extracted from the parametric studies of the Ridge WG and Ridge Coaxial WG respectively. However only the conclusions for the first TE mode suffices in order to know which parameters are more influential to obtain the required response of an E-plane Filter which incorporates the Ridge WG or Ridge Coaxial WG.

The E-Plane filters are going to operate in the X-Band, therefore the lowest central frequency will be 8 GHz and the highest will be 12 GHz. Moreover, they are excited with the first TE mode of a rectangular waveguide, the TE_{10} mode.

If the frequency of the impressed signal is above the cutoff frequency for a given mode, the electromagnetic energy can be transmitted through the guide for that particular mode with minimal attenuation. Otherwise the electromagnetic energy with a frequency below cutoff for that particular mode can not be propagated. They are evanescent modes.

Table 8-1 presents the cutoff frequencies for the two first modes in different sections of waveguides which are included in a E plane filter. These sections are WG, Reduced WG, Ridge WG and Ridge Coaxial WG.

Apart from the case of the Reduced WG, the cutoff frequencies for the first modes in each section are lower than the possible central operation frequency of the filter at the X

band. Therefore, the first mode always satisfies the propagation condition and will be propagated. As a remark, if the Reduced WG is seen as a WG with half width, the first mode of the Reduced WG will have roughly a double cutoff frequency than the cutoff frequency of the WG. For the second mode of the sections, the cutoff frequencies are higher than the possible central operation frequency of the filter at the X band. For that reason the second mode and higher modes will not be propagated.

	fc 1st mode (GHz)	fc 2nd mode (GHz)
WG	6,561679615	16,1562629
Reduced WG	13,18101898	14,7637797
Ridge WG	4,53617877	14,0478872
Ridge Coaxial WG	6,143415621	15,982071

Table 1-1: Cutoff frequencies for the first and the second modes of

different waveguides

Dimensions of the WG in mm: a=22.86, b=10.16

Dimensions of the Reduced WG in mm: a=22.86, b=10.16, t=0.1

Dimensions of the Ridge WG in mm: a=22.86, b=10.16, t=0.1, s=2, c=1

Dimensions of the Ridge Coaxial WG in mm: a=22.86, b=10.16, t=0.1, s1=s2=2, c1=c2=1

However, it is important to keep in mind that for the modelling of the discontinuities by using the mode matching method all the higher order modes are needed even though only the first one will be transmitted.

As a remark, it is interesting to point out that for the Ridge Coaxial Waveguide, the total energy that is propagated will be a combination of both modes above cutoff. These two modes are the fundamental quasi-static mode TEM (having zero cutoff frequency) and the first TE mode. As it was commented before, this TEM mode has rigorously solved in [1-20] and it is not included in this project.

Therefore, the conclusions of the variation of the cutoff frequency of the first TE modes will be presented below and it is important to keep in mind that these conclusions suffice in order to know which parameter have a stronger influence in the final response of an E-Plane filter.

The parameters which have been varied to achieve the parametric studies have been, T S1, S2, C1 and C2 which allow us to vary the width, the height and the position of the GAPs and the inner conductor.

The conclusions to be taken into account for further works are:

- About the width of the GAPs and the inner conductor (T parameter) very small variation of the Kc is observed for the first TE mode in all the range of possible

value of T. Therefore the value of T is not a critical parameter for the design of E-plane filter. As a remark it is important to keep in mind that a practical value of T useful for the design of E-plane filter must be very small, around 0.1mm.

- In relation to the height of the GAPs (S1 and S2 parameter) for the first TE mode Kc increases when the height of the GAPs increases. The variation of Kc for these parameters is more pronounce that in the previous case. Hence, it is important to point out that these parameters are interesting to be considered for the design of E-plane filter.

- With regard to the position of the inner conductor, small variation is observed in the TE modes so it is not a critical parameter for the design of E-plane filter.

- In relation to the height of the inner conductor it is important to note that when it is incremented the GAPs are smaller and therefore the value of Kc decreases for the first TE mode. This behaviour is identical to the one when the height of the GAPs is varied.

Chapter XI

Conclusion

This section summarises the work presented in this project, comments in relation with the aims and objectives set in the introduction. Furthermore it points out the contributions made in this work and reiterates the potential for future work.

9.1.   PROGRESS OF THE WORK

As it was pointed out in the introduction, the first main aim has been to develop a fast and accurate simulation tool for ridge coaxial waveguide for the incorporation of this structure in an all metal E-plane insert in order to investigate the possibilities of stopband performance improvement and size reduction of all metal E-plane filter. Furthermore, this novel E-plane filter configuration allows for a transmission zero at finite frequencies to address sharp cutoff specifications. As a remark, it is important to keep in mind that this configuration maintains the fabrication simplicity and mass-productivity of standard E-plane filters.

Following some literature review, the transverse resonance field matching method was chosen as most appropriate. Several formulations of the problem have been considered [9-1], [9-2] and finally as optimal routine was decided to follow [9-2]. By expressing the transverse dependence of the vector potentials in each region of the structure as sum of series respecting the boundary condition and applying the field matching at the interfaces, we form the eigenvalue problem, whose solutions are the unknown cutoff wavenumbers. The field distributions were then obtained.

FORTRAN code has been developed in order to realize this solution of the eigenvalue problem. The developed program was thoroughly compared with published results, other available softwares and their validity was confirmed.

A time comparison between this implemented code and a commercial software based on FEM was achieved and a considerable reduction of time is attained with our implemented code.

Parametric studies of the variation of the dimensions of the waveguide were presented to demonstrate the dependence of the cutoff wavenumber on the geometry of the structure. Interesting conclusions were extracted from these parametric studies which were focused on the determination of which parameters are more influential to obtain the required response of an E-plane Filter which incorporates the Ridge WG or Ridge Coaxial WG.

9.2.   SUGGESTIONS FOR FURTHER WORKS

A suggestion for further works is to investigate the possibilities of stopband performance improvement of all metal E-plane inserts incorporating ridge coaxial waveguide and also asymmetric ridge waveguide as a particular case. In order to reach the point where investigation is feasible, a fast and accurate simulation tool for the filter is needed. Hence to achieve this work it will be necessary the formulation and computer realisation of the mode matching method. The solutions for the surface discontinuities of Asymmetric ridge-to-rectangular and Ridge coaxial-to-Ridge waveguide have to be combined with the propagation along the finite length sections in order to obtain a 3D structure simulator for E-plane filters.

With this simulation tool we will be able to demonstrate the improvement of the novel configuration and also get the ability to control the appearance frequency of the transmission zero.

Furthermore, since the main object of this study is microwave filters, a design procedure for this type of distributed electrical filters would be interesting. Together with the simulation tool, this would complete a CAD software package. An efficient CAD tool for E-plane configuration therefore would complete the study.

9.3.   REFERENCES

[9-1] Montgomery J., "On the complete eigenvalue solution of ridged waveguide", IEEE Trans. Microwave Theory and Techniques, MTT-19, 457-555 (1971)

[9-2] J. Bornemann, "Comparison between different formulations of the Transverse Resonance Field-Matching Technique for the three-dimensional analysis of metal-finned waveguide resonators", International Journal of Numerical Networks, Devices and Fields, Vol. 4, 63-73 (1991)

APPENDICES

Appendix 1. The transverse dependence for the magnetic type of vector potential (TE modes).

REGION 1:

The magnetic type of vector potential for this region is:

$$T_{hq}{}^1(x, y) = \sum_{m=0}^{M1} \left[A_{qm}{}^1 e^{+j \cdot K_{xqm}{}^1 \cdot x} + B_{qm}{}^1 e^{-j \cdot K_{xqm}{}^1 \cdot x} \right] \frac{\cos\left(\frac{m\pi}{b} \left(y + \frac{b}{2} \right) \right)}{\sqrt{1 + \delta_{om}}}$$

The boundary condition to be satisfied in this case is:

$$E_y(x = 0) = 0 \Rightarrow -\frac{\partial A_h}{\partial x} = 0 \Rightarrow \frac{\partial T_{hq}(x, y)}{\partial x} = 0 \Rightarrow$$

$$\Rightarrow \frac{\partial}{\partial x} \left[\sum_{m=0}^{M1} \left[A_{qm}{}^1 e^{+j \cdot K_{xqm}{}^1 \cdot x} + B_{qm}{}^1 e^{-j \cdot K_{xqm}{}^1 \cdot x} \right] \frac{\cos\left(\frac{m\pi}{b} \left(y + \frac{b}{2} \right) \right)}{\sqrt{1 + \delta_{om}}} \right] = 0 \Rightarrow$$

$$\Rightarrow \sum_{m=0}^{M1} \left[A_{qm}{}^1 j \cdot K_{xqm}{}^1 e^{+j \cdot K_{xqm}{}^1 \cdot 0} - B_{qm}{}^1 j \cdot K_{xqm}{}^1 e^{+j \cdot K_{xqm}{}^1 \cdot 0} \right] \frac{\cos\left(\frac{m\pi}{b} \left(y + \frac{b}{2} \right) \right)}{\sqrt{1 + \delta_{om}}} = 0 \Rightarrow$$

$$\Rightarrow \sum_{m=0}^{M1} \left[A_{qm}{}^1 j \cdot K_{xqm}{}^1 - B_{qm}{}^1 j \cdot K_{xqm}{}^1 \right] \frac{\cos\left(\frac{m\pi}{b} \left(y + \frac{b}{2} \right) \right)}{\sqrt{1 + \delta_{om}}} = 0$$

Due to the orthogonality of $\cos\left(\frac{m\pi}{b} \left(y + \frac{b}{2} \right) \right) \Rightarrow A_{qm}{}^1 = B_{qm}{}^1$

So
$$T_{hq}{}^1(x, y) = \sum_{m=0}^{M1} \left[e^{+j \cdot K_{xqm}{}^1 \cdot x} + e^{-j \cdot K_{xqm}{}^1 \cdot x} \right] A_{qm}{}^1 \cdot \frac{\cos\left(\frac{m\pi}{b} \left(y + \frac{b}{2} \right) \right)}{\sqrt{1 + \delta_{om}}}$$

or

$$\boxed{T_{hq}{}^1(x, y) = \sum_{m=0}^{M1} A_{qm}{}^1 \cos\left(K_{xqm}{}^1 x \right) \frac{\cos\left(\frac{m\pi}{b} \left(y + \frac{b}{2} \right) \right)}{\sqrt{1 + \delta_{om}}}}$$

REGION 2

The magnetic type of vector potential for this region is:

$$T_{hq}{}^2(x,y) = \sum_{m=0}^{M2}\left[A_{qm}{}^2 e^{+j\cdot K_{xqm}{}^2\cdot x} + B_{qm}{}^2 e^{-j\cdot K_{xqm}{}^2\cdot x}\right]\frac{\cos\left(\frac{m\pi}{s1}\left(y+\frac{b}{2}-c1\right)\right)}{\sqrt{1+\delta_{om}}}$$

The boundary Condition in this case:

$$H_z\left(x=\frac{a}{2}\right) = H_y\left(x=\frac{a}{2}\right) = 0 \Rightarrow H_z = -\frac{1}{j\omega\mu_0}\cdot\left[K_0^2\cdot A_h + \frac{\partial^2 A_h}{\partial z^2}\right] = -\frac{1}{j\omega\mu}\cdot K_0^2\cdot A_h = 0 \Rightarrow A_h = 0$$

These are satisfied if:

$$T_{hq}{}^2\left(x=\frac{a}{2},y\right) = 0 \Rightarrow \sum_{m=0}^{M2}\left[A_{qm}{}^2 e^{+j\cdot K_{xqm}{}^2\cdot\frac{a}{2}} + B_{qm}{}^2 e^{-j\cdot K_{xqm}{}^2\cdot\frac{a}{2}}\right]\cdot\frac{\cos\left(\frac{m\pi}{s1}\left(y+\frac{b}{2}-c1\right)\right)}{\sqrt{1+\delta_{om}}} = 0 \Rightarrow$$

$$\Rightarrow A_{qm}{}^2 e^{+j\cdot K_{xqm}{}^2\cdot\frac{a}{2}} + B_{qm}{}^2 e^{-j\cdot K_{xqm}{}^2\cdot\frac{a}{2}} = 0 \Rightarrow B_{qm}{}^2 = -A_{qm}{}^2 e^{+j\cdot K_{xqm}{}^2\cdot a}$$

so

$$T_{hq}{}^2(x,y) = \sum_{m=0}^{M2}A_{qm}{}^2\left[e^{+j\cdot K_{xqm}{}^2\cdot x} - e^{-j\cdot K_{xqm}{}^2\cdot(x-a)}\right]\frac{\cos\left(\frac{m\pi}{s1}\left(y+\frac{b}{2}-c1\right)\right)}{\sqrt{1+\delta_{om}}} =$$

$$= \sum_{m=0}^{M2}A_{qm}{}^2\cdot e^{+j\cdot K_{xqm}{}^2\cdot\frac{a}{2}}\left[e^{+j\cdot K_{xqm}{}^2\cdot(x-\frac{a}{2})} - e^{-j\cdot K_{xqm}{}^2\cdot(x-\frac{a}{2})}\right]\cdot\frac{\cos\left(\frac{m\pi}{s1}\left(y+\frac{b}{2}-c1\right)\right)}{\sqrt{1+\delta_{om}}} =$$

$$= \sum_{m=0}^{M2}A_{qm}{}^2\left[\cos\left(K_{xqm}{}^2\cdot\frac{a}{2}\right) + j\sin\left(K_{xqm}{}^2\cdot\frac{a}{2}\right)\right]\left[j2\sin\left(K_{xqm}{}^2\cdot(x-\frac{a}{2})\right)\right]\cdot\frac{\cos\left(\frac{m\pi}{s1}\left(y+\frac{b}{2}-c1\right)\right)}{\sqrt{1+\delta_{om}}}$$

Since we are interested in the real part only

$$\Re\left[T_{hq}{}^2\right] = \sum_{m=0}^{M2}-A_{qm}{}^2\left[2\sin\left(K_{xqm}{}^2\cdot\frac{a}{2}\right)\sin\left(K_{xqm}{}^2\cdot(x-\frac{a}{2})\right)\right]\cdot\frac{\cos\left(\frac{m\pi}{s1}\left(y+\frac{b}{2}-c1\right)\right)}{\sqrt{1+\delta_{om}}}$$

The function $A_{qm}{}^2$ is still undetermined so we can introduce $\sin\left(K_{xqm}{}^2\cdot\frac{a}{2}\right)$ into it and write:

$$T_{hq}{}^2 = \sum_{m=0}^{M2}A_{qm}{}^2\frac{1}{K_{xqm}{}^2}\sin\left(K_{xqm}{}^2\cdot(x-\frac{a}{2})\right)\cdot\frac{\cos\left(\frac{m\pi}{s1}\left(y+\frac{b}{2}-c1\right)\right)}{\sqrt{1+\delta_{om}}}$$

Appendix 2. Electric Field Matching for TE Modes.

From **A1** and **A2** it is obtained:

$$\frac{\partial T_{hq}{}^1}{\partial x}\bigg|_{x=e} = \frac{\partial T_{hq}{}^2}{\partial x}\bigg|_{x=e} + \frac{\partial T_{hq}{}^3}{\partial x}\bigg|_{x=e} \quad \frac{\partial T_{hq}{}^1}{\partial x}\bigg|_{x=e} = -\sum_{m=0}^{M1} A_{qm}{}^1 \cdot K_{xhm}{}^{q1} \sin\left(K_{xhm}{}^{q1}\cdot e\right)\frac{\cos\left(\dfrac{m\pi}{b}(y+\dfrac{b}{2})\right)}{\sqrt{1+\delta_{om}}}$$

$$\frac{\partial T_{hq}{}^2}{\partial x}\bigg|_{x=e} = \sum_{m=0}^{M2} A_{qm}{}^2 \cos\left(K_{xhm}{}^{q2}(e-\frac{a}{2})\right)\cdot\frac{\cos\left(\dfrac{m\pi}{s1}(y+\dfrac{b}{2}-c1)\right)}{\sqrt{1+\delta_{om}}}$$

$$\frac{\partial T_{hq}{}^3}{\partial x}\bigg|_{x=e} = \sum_{m=0}^{M3} A_{qm}{}^3 \cos\left(K_{xhm}{}^{q3}(e-\frac{a}{2})\right)\cdot\frac{\cos\left(\dfrac{m\pi}{s2}(y-\dfrac{b}{2}+c2+s2)\right)}{\sqrt{1+\delta_{om}}}$$

$$e-\frac{a}{2} = -\frac{t}{2} \text{ and } \cos(-x)=\cos(x)$$

$$\frac{\partial T_{hq}{}^2}{\partial x}\bigg|_{x=e} = \sum_{m=0}^{M2} A_{qm}{}^2 \cos\left(K_{xhm}{}^{q2}\frac{t}{2}\right)\cdot\frac{\cos\left(\dfrac{m\pi}{s1}(y+\dfrac{b}{2}-c1)\right)}{\sqrt{1+\delta_{om}}}$$

$$\frac{\partial T_{hq}{}^3}{\partial x}\bigg|_{x=e} = \sum_{m=0}^{M3} A_{qm}{}^3 \cos\left(K_{xhm}{}^{q3}\frac{t}{2}\right)\cdot\frac{\cos\left(\dfrac{m\pi}{s2}(y-\dfrac{b}{2}+c2+s2)\right)}{\sqrt{1+\delta_{om}}}$$

The orthogonality property of the cosine function is now to be used; we multiply both sides

of the relation (2.6-51) with the appropriate cosine function $\dfrac{\cos\left(\dfrac{n\pi}{b}(y+\dfrac{b}{2})\right)}{\sqrt{1+\delta_{on}}}$ and integrate

over its period $y \in \left[-\dfrac{b}{2}, \dfrac{b}{2}\right]$.

$$-\sum_{m=0}^{M1} A_{qm}{}^1 \cdot K_{xqm}{}^1 \sin\left(K_{xqm}{}^1\cdot e\right)J_1 = \sum_{m=0}^{M2} A_{qm}{}^2 \cos\left(K_{xqm}{}^2\frac{t}{2}\right)\cdot J_2 + \sum_{m=0}^{M3} A_{qm}{}^3 \cos\left(K_{xqm}{}^3\frac{t}{2}\right)\cdot J_3$$

The resolve of every J_i is shown bellow:

$$J_1 = \int_{-\frac{b}{2}}^{\frac{b}{2}} \frac{\cos\left(\frac{m\pi}{b}(y+\frac{b}{2})\right)}{\sqrt{1+\delta_{om}}} \cdot \frac{\cos\left(\frac{n\pi}{b}(y+\frac{b}{2})\right)}{\sqrt{1+\delta_{on}}} dy = \frac{b}{2} \cdot \delta_{mn}$$

We have solved J_2 for different cases of m and n:

$$J_2 = \int_{-\left(\frac{b}{2}-c1\right)}^{-\left(\frac{b}{2}-c1-s1\right)} \frac{\cos\left(\frac{m\pi}{s1}(y+\frac{b}{2}-c1)\right)}{\sqrt{1+\delta_{om}}} \cdot \frac{\cos\left(\frac{n\pi}{b}(y+\frac{b}{2})\right)}{\sqrt{1+\delta_{on}}} dy$$

- m=0: $$J_2 = \frac{b}{n\cdot\pi\cdot\sqrt{2}}\left[\sin\left(\frac{n\cdot\pi}{b}(c1+s1)\right) - \sin\left(\frac{n\cdot\pi}{b}c1\right)\right]$$

- n=0: $$J_2 = 0$$

- Other case: $$J_2 = \frac{s1^2 \cdot b \cdot n}{\pi\cdot\left((m\cdot b)^2 - (n\cdot s1)^2\right)}\left[\sin\left(\frac{n\cdot\pi}{b}c1\right) - \cos(m\cdot\pi)\cdot\sin\left(\frac{n\cdot\pi}{b}(c1+s1)\right)\right]$$

-

We have solved J_3 for different cases of m and n:

$$J_3 = \int_{\frac{b}{2}-c2-s2}^{\frac{b}{2}-c2} \frac{\cos\left(\frac{m\pi}{s2}\left(y-\frac{b}{2}+c2+s2\right)\right)}{\sqrt{1+\delta_{om}}} \cdot \frac{\cos\left(\frac{n\pi}{b}\left(y+\frac{b}{2}\right)\right)}{\sqrt{1+\delta_{on}}} dy$$

- m=0: $$J_3 = \frac{b}{n\cdot\pi\cdot\sqrt{2}}\cdot\cos(n\cdot\pi)\cdot\left[\sin\left(\frac{n\cdot\pi}{b}(c2+s2)\right) - \sin\left(\frac{n\cdot\pi}{b}c2\right)\right]$$

- n=0: $$J_3 = 0$$

- Other case:

$$J_3 = \frac{s2^2 \cdot b \cdot n}{\pi\cdot\left((m\cdot b)^2 - (n\cdot s2)^2\right)}\cdot\cos(n\cdot\pi)\cdot\left[\cos(m\cdot\pi)\cdot\sin\left(\frac{n\cdot\pi}{b}c2\right) - \sin\left(\frac{n\cdot\pi}{b}(c2+s2)\right)\right]$$

Appendix 3. Resolve of J_i for the Field Matching for TM Modes.

$$J_1 = \int_{-\frac{b}{2}}^{\frac{b}{2}} \sin\left(\frac{l\cdot\pi}{b}(y+\frac{b}{2})\right)\sin\left(\frac{n\pi}{b}(y+\frac{b}{2})\right)dy = \frac{b}{2}\cdot\delta_{ln}$$

$$J_2 = \int_{-\left(\frac{b}{2}-c1\right)}^{-\left(\frac{b}{2}-c1-s1\right)} \sin\left(\frac{l\cdot\pi}{s1}(y+\frac{b}{2}-c1)\right)\cdot\sin\left(\frac{n\pi}{b}(y+\frac{b}{2})\right)dy$$

$$= \frac{s1\cdot b^2\cdot l}{\pi\cdot\left((l\cdot b)^2-(n\cdot s1)^2\right)}\cdot\left[\sin\left(\frac{n\cdot\pi}{b}c1\right)-\cos(l\cdot\pi)\cdot\sin\left(\frac{n\cdot\pi}{b}(c1+s1)\right)\right]$$

$$J_3 = \int_{\frac{b}{2}-c2-s2}^{\frac{b}{2}-c2} \sin\left(\frac{l\cdot\pi}{s2}\left(y-\frac{b}{2}+c2+s2\right)\right)\cdot\sin\left(\frac{n\pi}{b}\left(y+\frac{b}{2}\right)\right)dy$$

$$= \frac{s2\cdot b^2\cdot n}{\pi\cdot\left((l\cdot b)^2-(n\cdot s2)^2\right)}\cdot\cos(n\cdot\pi)\cdot\left[\cos(l\cdot\pi)\cdot\sin\left(\frac{n\cdot\pi}{b}c2\right)-\sin\left(\frac{n\cdot\pi}{b}(c2+s2)\right)\right]$$